

VALIDATION OF THE CHARGE EQUILIBRATION LIPID FORCE
FIELD FOR SIMULATIONS OF PHOSPHOLIPID MEMBRANES
WITH AN APPLICATION TO THE STUDY OF THE FREE
ENERGETICS OF METHYL GUANIDINIUM PERMEATION ACROSS
A DPPC BILAYER

by

Timothy R. Lucas

A thesis submitted to the Faculty of the University of Delaware in partial fulfillment of the requirements for the degree of Master of Science in Chemistry and Biochemistry

Summer 2012

© 2012 Timothy R. Lucas
All Rights Reserved

VALIDATION OF THE CHARGE EQUILIBRATION LIPID FORCE
FIELD FOR SIMULATIONS OF PHOSPHOLIPID MEMBRANES
WITH AN APPLICATION TO THE STUDY OF THE FREE
ENERGETICS OF METHYL GUANIDINIUM PERMEATION ACROSS
A DPPC BILAYER

by

Timothy R. Lucas

Approved: _____
Sandeep Patel, Ph.D.
Professor in charge of thesis on behalf of the Advisory Committee

Approved: _____
Klaus H. Theopold, Ph.D.
Chairman of the Department of Chemistry and Biochemistry

Approved: _____
George H. Watson, Ph.D.
Dean of the College of Arts and Sciences

Approved: _____
Charles G. Riordan, Ph.D.
Vice Provost for Graduate and Professional Education

ABSTRACT

Previous work in our group focused on the development and refinement of polarizable charge equilibration (CHEQ) force fields for use in molecular dynamics (MD) simulations of phospholipid bilayers. We present results to further validate these force fields by extending to simulations of a model DPPC-water monolayer. Several physical and electrostatic properties have been calculated for comparison with previously reported experimental and computational studies including component density profiles, deuterium order parameters, surface pressure and tension, and the monolayer-water potential difference relative to a pure water-air interface. Having validated the CHEQ force field for use with both lipid bilayer and monolayer systems, as well as having identified areas where improvement is needed, we apply an intermediate, revised version of the force field to study the energetics of an arginine side-chain analog, methyl guanidinium, as it crosses a DPPC lipid bilayer. Combining umbrella sampling MD simulations with the Weighted Histogram Analysis Method (WHAM) for unbiasing probabilities, we compute a potential of mean force (PMF) for the reversible transfer of methyl guanidinium from bulk solution to bilayer center. Decomposition of the PMF in component contributions allows us to investigate the role of lipid and solvent to the energetics of permeation. Finally, through a series of simulations in which water is first prevented from entering the bilayer center where methyl guanidinium is restrained and then, after equilibration, allowed to enter the bilayer, we find that water permeation into the bilayer is required for the deformation of individual lipid molecules and permeation of ions into the membrane.

TABLE OF CONTENTS

ABSTRACT	iii
LIST OF TABLES	vi
LIST OF FIGURES	viii
 Chapter	
1 INTRODUCTION	1
1.1 Background	1
1.2 Charge Equilibration Model	6
2 MOLECULAR DYNAMICS SIMULATION OF HYDRATED DPPC MONOLAYERS USING CHARGE EQUILIBRATION FORCE FIELDS	10
2.1 Simulation Protocol	10
2.2 Results and Discussion	11
2.2.1 Atomic and Electron Density Profiles	11
2.2.2 Lipid Orientation and Ordering	17
2.2.3 Dielectric Permittivity and Water Dipole Moment Variation	20
2.2.4 Surface Tension and Pressure	25
2.2.5 Monolayer Dipole Potential	26
3 FREE ENERGETICS AND THE ROLE OF WATER IN THE PERMEATION OF METHYL GUANIDINIUM ACROSS THE BILAYER-WATER INTERFACE	36
3.1 Simulation Setup	37
3.1.1 Methyl Guanidinium Hydration Free Energy via Thermodynamic Integration	39

3.1.2	Potential of Mean Force	42
3.2	Results and Discussion	44
3.2.1	Hydration Free Energies	44
3.2.2	Salt PMF	45
3.2.3	No Salt PMF	47
3.2.4	Water Excluded PMF	50
3.2.5	Water Contribution to Total PMFs	51
3.2.5.1	Asymmetric Water Solvation	51
3.2.5.2	Position Dependent Forces	54
3.2.5.3	Density and Density-Weighted Force Differences between Salt and No Salt Systems	57
3.2.6	Core Lipid and Water Contributions	61
3.2.7	Water Defect Mediated Lipid Deformation	64
4	CONCLUSION	69
	BIBLIOGRAPHY	73
	Appendix	
A	88
B	89
B.1	Lipid Force Field Reparameterization	89
B.2	Unrestrained Methyl Guanidinium	93
B.3	Lipid Structure	93
B.4	Chloride Ion Position and Forces	96
B.5	Asymmetric Water Solvation: Forces and Densities	96

LIST OF TABLES

2.1	Component and total interfacial potential values (in Volts) of monolayer-water and water-air systems, including results reported for nonpolarizable (CHARMM27), polarizable Drude oscillator, and polarizable CHEQ force field. Results obtained using the CHEQ force field with TIP3P charge substitution are also shown.	29
2.2	Parameters from altering dipole moment variation and influence on ΔV . Potentials in Volts, dipole moments in Debye. Drude scaling from 2.05-2.45 (monolayer-water) and 1.95-2.45 (water-air) as in Harder et al[47]	33
3.1	Hydrogen bond distances and interaction energies between methyl guanidinium and lipid head group analog molecules dimethyl phosphate (DMP) and tetramethyl ammonium (TMA), water, and chloride calculated using the CHARMM CHEQ force field (FF). Quantum mechanical (QM) interaction energies were calculated at the MP2/aug-cc-pvtz level of theory using counterpoise correction. All QM calculations were carried out using the Gaussian 03 package[41]. The H-Bond type indicates the specific atoms involved to differentiate between methyl guanidinium hydrogens belonging to NH_3 , NH , and CH_3 groups. The range in values given for the mguan/TMA FF interaction energy represent the variation in the interactions found given distance separations (measured between the central carbon of mguanH ⁺ and the central nitrogen of TMA) from 5.7 to 22.7 Å between the two like-charged species while the QM interaction is for an analogous structure with a separation of 6.1 Å. The three values given for the interaction energies between mguanH ⁺ and both water and chloride represent three unique and stable geometries around methyl guanidinium.	40

B.1 Non-bonded (Lennard-Jones) parameters, geometric separation, and interaction energy between lipid head group analogs DMP and TMA. R_{P-N} denotes the geometric separation between the two molecules measured as the distance between the phosphorus of DMP and the nitrogen of TMA. The first generation CHEQ force field parameters and interaction energy are labeled as FQ. 90

LIST OF FIGURES

2.1	Coordinate snapshot of the monolayer-water system, generated using Visual Molecular Dynamics[56], with the z-axis normal to the surface of the monolayers. Oxygens are shown in red, hydrogens in white, carbons in light blue, nitrogens in dark blue, and phosphorus in yellow.	11
2.2	Heavy atom number density profiles for selected components (water oxygens, aliphatic lipid tail group carbons, lipid ester oxygens, lipid head group nitrogen and phosphorus) as a function of distance along the monolayer normal.	13
2.3	Free volume profile as a function of distance along the monolayer normal.	15
2.4	Total and component electron density profiles. Components were grouped for comparison with the fitting models of Kucerka et al[70]	16
2.5	Distribution of the angle between the \overrightarrow{PN} dipole vector and the monolayer normal.	17
2.6	Distribution of the angles between $sn-1$ and $sn-2$ carbonyl vectors and the monolayer normal.	19
2.7	Magnitude of the deuterium order parameters for $sn-1$ and $sn-2$ tail groups as a function of position along the hydrocarbon chain. The experimental order parameters for the $sn-2$ tail group are shown for comparison[34]. The stereoscopically different carbons at carbon number 2 are shown with the 2S value denoted as an x.	21
2.8	Profiles of the parallel component of the dielectric permittivity as a function of distance along the monolayer normal. Profiles are given for water (top), DPPC, and the total system (bottom). The lipid tail region is shown in greater detail due to scale (inset) with an average value of 1.3, shown as a dotted line, calculated from $z = 30$ to 40. .	23

2.9	Average molecular dipole moment profile of water as a function of distance along the monolayer normal, from the center of the water layer (bulk phase) through the lipid monolayer and into the vacuum region (gas phase). Dashed line denotes the constant dipole moment of the TIP3P water model while the dotted line denotes the experimental dipole moment of water in the gas phase.	24
2.10	Interfacial potential profiles of the total system and of selected components as a function of distance along the monolayer normal. The potential in the vacuum region is referenced to a value of 0 V.	28
2.11	Comparison of the quadrupole (top) and dipole (bottom) contributions to the interfacial potential of water as a function of distance along the interface normal for both the monolayer-water and water-air systems.	31
2.12	Orientation of water at the monolayer-water and water-air interfaces. The average orientation of water (top) and the average orientation scaled by the z -dependent density relative to bulk density of water (bottom). Dotted horizontal line denoting $\langle \cos \theta \rangle = 0$ is included as a visual guide.	35
3.1	Decomposition of the potential of mean force for the Salt, No Salt, and Water Excluded systems. (a, d, g) The PMFs calculated via umbrella sampling with WHAM analysis as well as through integration of forces. The integrated force profiles have been offset by -5 \AA for clarity. (b, e, h) Decomposition of the total PMF into solvent (red, dashed curves) and lipid contributions (solid, black curves). (c, f, i) Decomposition of the solvent contributions into constituent water (solid, blue curves), chloride ion (red, dashed curves), and potassium ion (black, dotted curves) contributions. Dotted lines at 0 were added to clarify positive and negative PMF contributions.	46
3.2	Number of coordinating lipid phosphate (black) and water (red) molecules surrounding methyl guanidinium (within 5 \AA of the mguanH^+ center of mass) at the center of the lipid membrane as a function of simulation time (top) and as a distribution over all data (bottom) for the Salt system. The number of coordinating water molecules (top, red profile) has been offset by 4 for clarity with the dashed red line indicating zero.	48

3.3	Comparison of the water contributions to the total PMF profiles of the Salt, No Salt, and Water Excluded systems. Number density profiles for select lipid and salt atoms, taken from the Salt system in which methyl guanidinium is in the bulk ($z = -35 \text{ \AA}$), are shown to give a sense of the lipid environment. Vertical dotted lines were added to distance values of -30 , -27.5 , and -25 \AA to guide the reader during the discussion in the main text.	52
3.4	Example of the density weighting of force from water molecules on methyl guanidinium for the Salt system. a), d), and g) Magnitude and direction of the z -component of the force of water molecules (within 10 \AA) acting on methyl guanidinium for mguan ^{H+} -lipid center of mass separations of -35 , -27.5 , and 0 \AA , respectively. Positive force values, directed in the positive z -direction, serve to stabilize methyl guanidinium in the membrane while negative force values, directed in the negative z -direction, are destabilizing. White space indicates areas in which no water molecules were sampled. b), e), and h) Density of water molecules within 10 \AA of methyl guanidinium with each position relative to the total number of water molecules sampled within the 10 \AA cutoff. c), f) and i) Force of water molecules weighted by the relative water densities. The lack of sampling for the window in the bulk (panels a, b, and c) past approximately -7 \AA is due to the fact that this position corresponds to the edge of the central simulation cell.	55
3.5	Difference in the water densities between the No Salt and Salt systems for mguan ⁺ -lipid center of mass separations a) -35 , b) 30 , c) -27.5 , d) -25 , and e) 0 \AA . Positive values indicate that there is an increased density of water in the No Salt system at that position around methyl guanidinium relative to the Salt system while negative values indicate a decreased density in the No Salt system relative to the Salt system. Black circles have added to b) to draw attention to areas in the data discussed in the main text.	58
3.6	Difference in the density weighted forces between the No Salt and Salt systems for mguan-membrane center of mass separations a) -35 , b) 30 , c) -27.5 , d) -25 , and e) 0 \AA	60

3.7	Decomposition of the potential of mean force into “core” lipid and water contributions for the Salt (black, solid curve), No Salt (red, dashed curve), and Water Excluded (blue, dotted curve) systems. Water or lipid molecules are defined as being in the membrane “core” if the water oxygen or lipid phosphorus has a $ z $ -position ≤ 13 Å. Scaled number density profiles for select lipid and salt atoms, taken from the Salt system in which methyl guanidinium is in the bulk ($z = -35$), are included to give a sense of the lipid environment, similar to those in Figure 3.3.	63
3.8	(Top) Heavy atom number density profiles for selected components (water oxygen, lipid head group phosphorus and nitrogen, lipid carbonyl oxygen, and aliphatic lipid tail carbon) of the systems with a water constraint. The membrane-centered methyl guanidinium (with unperturbed lipid) profiles are shown as solid curves while the profiles for the system with methyl guanidinium located in bulk water ($z = -35$ Å) are shown as dotted curves. The black dashed line represents the center of the bilayer ($z = 0$ Å). (Bottom) Distribution of the head group orientation measured as the angle between the \overrightarrow{PN} dipole vector and the bilayer normal (z -axis) for membrane centered (red curve) and bulk (black, dotted curve) mguanH ⁺	65
3.9	Distance profiles of chloride and lipid phosphate atoms closest to methyl guanidinium for four replicate systems in which mguanH ⁺ is at the center of an initially unperturbed bilayer in which the water constraint has been removed at the beginning of the simulation (time = 0 ns). Profiles are measured as the distance from the mguanH ⁺ center of mass to the chloride and phosphorus atoms. Histograms of the number of associating species are shown below the graphs to indicate when a chloride (black) or lipid phosphorus (red) atom is within 5 Å of the mguanH ⁺ center of mass. Chloride distance profiles and histograms have been offset by 30 Å for clarity. Replicate (2) shows two chloride atoms (the second of which is shown in brown) which are able to move toward the center of the bilayer and associate with mguanH ⁺ at different times during the simulation.	68
A.1	Experimentally determined surface potential shifts for various phosphacholine lipid monolayer systems at the argon-water interface, as reported by Smaby and Brockman [Smaby, J. M.; Brockman, H. L. <i>Biophys. J.</i> 1990 , <i>58</i> , 195 - 204.] The lipidic system number designation corresponds to the row in which the lipid is presented in Table 1 of Smaby and Brockman with the experimentally comparable DPPC system explicitly labeled.	88

B.1	Area per lipid as a function of simulation time for different parameter set modifications as well as the unmodified first generation (FQ) force field. The profiles are offset by 5 Å ² for clarity with the horizontal dashed lines corresponding to the experimental area per lipid value of 63 Å ² [69].	91
B.2	Dihedral profiles based on model compounds propylmethylphosphate (PMP) and an esterified glycerol analog ((M)EGLY) and fit to ab initio data used in the most recent parameterization of the CHARMM nonpolarizable lipid force field[66].	92
B.3	Distance between the centers of mass of an unrestrained methyl guanidinium and the lipid membrane as a function of simulation time. The first 2.5 ns of simulation are not shown due to methyl guanidinium crossing the periodic boundary conditions and appearing in the bulk solution on either side of the membrane.	94
B.4	Heavy atom number density profiles for select species (water oxygen, lipid head group phosphorus and nitrogen, carbonyl oxygens, and aliphatic tail carbons) in the Salt (solid curves) and No Salt (dotted curves) systems at mguanH ⁺ -lipid center of mass separations of -35 Å (top) and 0 Å (bottom).	95
B.5	Force (in the <i>z</i> -direction) of the chloride ion on methyl guanidinium for the No Salt system as a function of the <i>z</i> -position of the chloride ion. Results are shown for several PMF windows in which the mguanH ⁺ -lipid center of mass difference is -35, -25, -20, -15, -5, and 0 Å. The vertical dashed line signifies the constrained position of mguanH ⁺ in the membrane system while the horizontal dashed line represents a force value of 0.	97
B.6	Force in the <i>z</i> -direction from individual local water molecules (all atoms within 10 Å of the center of mass of mguanH ⁺) acting on methyl guanidinium for the Salt system. Forces are calculated for mguanH ⁺ -lipid center of mass separations of a) -35, b) -30, c) -27.5, d) -25, and e) 0 Å.	98
B.7	Force in the <i>z</i> -direction from individual local water molecules (all atoms within 10 Å of the center of mass of mguanH ⁺) acting on methyl guanidinium for the No Salt system. Forces are calculated for mguanH ⁺ -lipid center of mass separations of a) -35, b) -30, c) -27.5, d) -25, and e) 0 Å.	99

- B.8 Density of water molecules surrounding methyl guanidinium (all atoms within 10 Å of the center of mass of mguanH⁺) calculated for the Salt system. Densities are calculated for mguanH⁺-lipid center of mass separations of a) -35, b) -30, c) -27.5, d) -25, and e) 0 Å. . . . 100
- B.9 Density of water molecules surrounding methyl guanidinium (all atoms within 10 Å of the center of mass of mguanH⁺) calculated for the No Salt system. Densities are calculated for mguanH⁺-lipid center of mass separations of a) -35, b) -30, c) -27.5, d) -25, and e) 0 Å. . . . 101

Chapter 1

INTRODUCTION

1.1 Background

Membranes and membrane-bound proteins are a vital part of biological systems. Cellular lipid bilayer membranes, a complex milieu of biomacromolecular components, are fundamentally composed of a wide variety of amphiphilic molecules consisting of polar and hydrophobic regions. Cellular membranes have many important physiological roles apart from simply being a permeability barrier between the “inside” and “outside” of cells. Bilayer membranes are involved with cell-signaling mechanisms, supply complex environments to support a wide variety of proteins, and are capable of mechanical deformation in order to accommodate a variety of chemical functionalities within the special region between the cytosol and extra-cellular surroundings[114, 33]. Recent studies have explored structural properties of membranes as well as electrostatic properties such as the dielectric variation within a bilayer[151], the interfacial potential[163], and the interactions of polar or charged amino acid side chains with hydrocarbon tails[89]. Experimental studies have also probed these properties in recent years. For example, structural properties of bilayers have been determined by x-ray and neutron scattering[71, 69] and nuclear magnetic resonance (NMR) spectroscopy[121], while the water penetration into the bilayer interior has been investigated via electron spin spectroscopy[97, 37] and x-ray scattering techniques[98]. However, even current state-of-the-art experimental measurements are not always able to provide the type of detailed atomic level resolution that would provide significant insights into the mechanisms of membrane systems. To this end, computational methods such as molecular dynamics and Monte Carlo simulations

have been employed to study properties and processes in such systems at the atomic level[131, 5, 11, 4, 89, 33, 1, 154, 168, 39, 91, 110, 10, 145].

Molecular dynamics simulations require information about the atomic interactions within and between molecular species. Quantum mechanical calculations would give the most accurate results; unfortunately, such computations are very time-consuming for all but the smallest systems. Because of this limitation, classical “force fields” have been developed which consist of potential energy functions chosen to model inter-species and intra-species interactions. In addition to models in which all atoms are modeled explicitly (i.e. all-atom models), there has been significant effort towards “coarse-grained” models[52, 137] in which entire small molecules or functional groups are represented as a single unit. Development and applications of such models continues today [94, 95, 102, 150, 36, 83]. Implicit solvent and lipid models[57, 153, 152, 76], which represent solvent or lipid as a continuum, are also a viable alternative to all-atom models for simulating large biomolecular systems. However, all-atom simulations remain the standard to which such coarse-grained and implicit models are compared; thus, the need for more accurate atomistic models is clear.

Despite the importance of lipidic systems (i.e., lipid bilayers, monolayers, vesicles, etc.) to a variety of physiological functions, polarizable force fields for molecular simulations of such systems are still in the testing and development stage. Among the numerous approaches currently being pursued, the charge equilibration (CHEQ) approach has been applied to molecular simulations of phosphatidylcholine (PC) based lipid bilayers[28, 26], as well as to the exploration of ion permeation energetics in the simple gramicidin A channel[119]. The CHARMM Drude oscillator model and the AMBER point-polarizable polarizable DOPC force field are the only other polarizable models to have been extensively applied for molecular simulations of lipid bilayer systems[47, 33, 3, 157]. A recent study using Drude oscillator models of the dipalmitoylphosphatidylcholine (DPPC) monolayer explored the surface dipole potential of the water-lipid monolayer system[47]. The authors demonstrated the improvement in the prediction of the relative interfacial potential, $\Delta V = V_{\text{monolayer-water}} - V_{\text{water-air}}$,

over fixed-charge nonpolarizable force field representation. The authors suggest that, compared to the bilayer dipole potential, the monolayer potential is a less ambiguous measurement for comparing force field predictions to experiment. We note that measurements of the bilayer dipole potential, values of which can be found in the literature for a wide spectrum of lipids using a variety of techniques including ion conductance[16, 23, 43], cryo-EM[163], and AFM[169], are based on a number of approximations and are not a direct measure of the individual contributions to interfacial electrostatic properties arising from the presence of a lipid assembly. Ion conductance measurements, for instance, measure the permeability of a membrane to two structurally similar, oppositely charged hydrophobic ions tetraphenylborate (TPB^-) and tetraphenylarsonium (TPA^+) or tetraphenylphosphonium (TPP^+). The conductance measurements operate on the assumption that these ions, having the same interaction energies with hydrating water molecules, will have identical free energies of transfer from water to any other medium and that a value for the membrane dipole potential can be calculated by extension. The validity of this assumption had been challenged using quantum mechanical calculations which found variations in the hydration energies of TPB^- , TPA^+ , and TPP^+ [134]. Though quantum mechanical calculations with various treatments of solvent effects do show differences between the hydration properties of both ions, it is difficult to assess the magnitude of the difference with purely quantum methods which may or may not account for solvation effects. Schurhammer and coworkers have also explored the variation in hydration free energies for the $\text{TPB}^-/\text{TPA}^+$ system using molecular dynamics simulations and free energy perturbation calculations[138]. The authors find that TPB^- is more favorably hydrated than TPA^+ , and that the difference in hydration free energy between the two are strongly dependent on the specific charge distribution; the range of differences in hydration energies is from 4.3 kcal/mol to 25 kcal/mol. Moreover, recent studies investigating the effects of charge asymmetry on hydration free energies of model asymmetric polar molecules by Mobley et al[99] demonstrate significant differences in

hydration free energies of oppositely polarized molecules, with these differences approaching the order of 10 kcal/mol. The notion of asymmetric hydration of small spherical ions as well as larger hydrophobic ions has been pursued extensively in the literature, though there still appears to be no consensus on the decisive relevance of the tetraphenylarsonium tetraphenylborate (TATB) assumption to the absolute bilayer dipole potential[140, 139, 85, 130, 55, 86].

Recent years have also witnessed great interest in the understanding of the molecular origins of the presence of charged and polar amino acid residues in ostensibly hydrophobic lipid bilayer environments [33, 77, 161, 78, 136, 45, 40, 103, 170, 53, 154, 89, 88]. The motivation for such a microscopic understanding stems from the broad range of biophysical processes predicated on the interactions between such protein residues and hydrophobic lipid chains. These processes range from voltage gating in select ion channels[61, 60, 59], permeation of cationic residue enriched cell-penetrating peptides for transporting cargo across the cellular membrane [49, 93, 50, 58, 158, 42, 75], and the action of anti-microbial peptides upon interaction with native cellular membranes. Understanding of these protein-lipid interactions has sought recourse in hydrophobicity scales quantifying relative partitioning propensities of different amino acid side chains from aqueous to bilayer-like environments[92]. Elaborating upon ideas of partitioning of functional chemical groups between hydrophilic and hydrophobic environments, recent work has broadened the palette of hydrophobicity scales attempting to address the relative free energetics of partitioning; this has been possible due to novel experiments on well-characterized integral-membrane protein systems [103] as well as elucidation of structural aspects of the machinery implicated in the synthesis and insertion of membrane proteins upon synthesis in the ribosome[51]. More recently, there appears to be a convergence of molecular modeling based predictions of relative free energetics of different amino acid side chains as part of a macromolecular assembly and experiment[40]. Further factors possibly contributing to interactions of charge and polar species in lipid bilayers include bilayer thickness, non-additivity of interactions

between non-bilayer components[90, 160], specificity of protein sequence to specific bilayer composition[15, 13, 14, 172], interactions of a particular amino side chain in the bilayer with lipid head groups and water, and lipid deformation (coupled with the ease of deformability of the lipid) [53, 167, 93].

In conjunction with recent experimental advances in studying the relative stability of charged amino acid residues in bilayer environments (within several contexts including cell-penetrating peptides, presence of charged voltage-gating and sensing domains in potassium channels, and other biochemical transformations), there has been a steady push for developing novel molecular modeling methods for treating the heterogeneous environments presented by lipid bilayers of various compositions. In particular, non-additive force fields are being pursued for modeling lipid bilayers. Though non-additive force fields have been pursued for over two decades now, only recently have there been substantial, published studies documenting the application of such models to the study of biophysical problems of general interest[44, 122, 30, 63, 123, 62, 6, 74, 73, 72, 81, 171, 47, 120, 116, 117, 9, 84, 27, 174, 120, 164, 28]. Recently, we, along with others, have published results of the first applications of polarizable, non-additive force fields for treating lipid bilayers in a fully atomistic molecular simulation. We have been developing a class of non-additive, polarizable force fields based on the charge equilibration (CHEQ), or fluctuating charge (FQ), formalism. One of the first attempts to apply CHEQ based force fields to lipid bilayers was by Shimizu and coworkers[141]; in their study, the authors explored the consequence of the extent of charge transfer in extended systems defining the nature of charge transfer effects and possible hyperpolarization in such models. The authors demonstrated the need for some approach to control the super-linear polarizability in applying charge equilibration models in a manner that does not constrain charge transfer in a systematic and physically meaningful way. Recently, Vacha et al [157] applied a fully polarizable force field (lipid, water, and ions) to the study of monovalent ion interactions with phosphatidylcholine membranes and associated effects at the membrane-water interface. Furthermore, Harder et al[47] examined the difference in the interfacial dipole potential between the pure liquid-vapor

interface of water and that of a DPPC monolayer. The authors presented the case for polarization helping to accurately predict the potential difference between these two systems compared to existing non-polarizable force fields. Over the last several years, our group has been involved in a substantial effort to develop non-additive electrostatic models for lipid bilayers to be used in conjunction with molecular dynamics simulations. We have presented a systematic parameterization of a first-generation charge equilibration force field based on the DPPC lipid[28, 26]. In this study, we continue further application of our models to explore the free energetics of an analogue of arginine, methyl guanidinium, in a model DPPC bilayer. This complements earlier studies using both polarizable and non-polarizable force fields in conjunction with molecular dynamics simulations to study this canonical system.

1.2 Charge Equilibration Model

The present simulations explicitly treat non-additive electrostatic effects using fully polarizable, charge equilibration (CHEQ) force fields for the entire lipid-solvent system. In the following, we discuss the details of this formalism. Although applied here as a classical potential[124], the CHEQ formalism derives rigorously from the density functional theory of atoms in molecules[113] based on Sanderson’s idea of electronegativity equalization[133, 132]. Polarization is affected via the migration of charge density (condensed to a partial charge in the classical sense) among atomic species within a given molecule. The electronic density adjusts within the molecule so as to equalize the electrochemical potential (or equivalently, the electronegativity) at each point in the molecule. The direction and ease of flow are determined by physical properties of individual atoms as will be discussed. The reader is referred to the literature for more details[126, 129, 105, 106, 107, 115, 124, 113, 127, 34, 21].

The electrostatic energy of a system of M molecules containing N atoms per molecule is:

$$E_{\text{electrostatic}} = \sum_{k=1}^M \sum_{i=1}^N \chi_{ik} Q_{ik} + \frac{1}{2} \sum_{l=1}^M \sum_{\alpha=1}^N \sum_{\beta=1}^N \eta_{\alpha l, \beta l} Q_{\alpha l} Q_{\beta l} +$$

$$\frac{1}{2} \sum_{i=1}^{MN} \sum_{j=1}^{MN} \frac{Q_i Q_j}{r_{ij}} + \sum_{j=1}^{Groups} \lambda \left(\sum_{i=1}^N Q_{ji} - Q_j^{total} \right) \quad (1.1)$$

where χ denotes the atomic electronegativities and η denotes the atomic hardnesses. The former quantity gives rise to a directionality of electron flow, while the latter represents a resistance, or hardness, to electron flow to or from the atom. The second term in Equation 1.1 represents the local charge transfer interaction generally restricted to within a molecule (no intermolecular charge transfer) or some appropriate charge normalization unit. The third term is a standard Coulomb interaction between sites not involved in dihedral, angle, and bonded interactions with each other (the primed notation indicates a summation only over such sites). The last term is a Lagrange multiplier based constraint on total charge on a given normalization unit; this constraint helps to restrict charge equilibration (and hence charge redistribution) over chemically relevant and distinct units[164]. We note that although the electronegativity and hardness follow exactly from the definitions of the electron affinity and ionization potential, they are considered here as empirical parameters to be determined as described below. Homogeneous hardness values (for each atom type) are parameterized as discussed in Patel and Brooks[115]. Heterogeneous elements (interaction elements between different atom types) are derived from the individual atom type values based on the combining rule[107]:

$$\eta_{ij} = \frac{\frac{1}{2}(\eta_i + \eta_j)}{\sqrt{1 + \frac{1}{4}(\eta_i + \eta_j)^2 R_{ij}^2}} \quad (1.2)$$

where R_{ij} is the separation between atoms (or more generally sites) i and j . This local screened Coulomb potential has the correct limiting behavior as $1/r$ for separations greater than about 2.5 Å. This interaction is computed for 1-2, 1-3, and 1-4 sites (sites included in bonds, angles, and dihedrals). Sites in a molecule separated by 5 or more sites interact via a Coulomb interaction; in the case of interacting molecules, the interaction between sites on different molecules is again of the Coulomb form.

The charge equilibration model is indeed a polarizable model as the molecular

polarizability, α , can be derived as follows:

$$\alpha_{\gamma\beta} = \bar{R}_\beta^T \bar{\eta}^{-1} \bar{R}_\gamma \quad (1.3)$$

where $\bar{\eta}$ denotes the molecular hardness matrix, and \bar{R}_β^T and \bar{R}_γ are the β and γ Cartesian components of the atomic position vector, respectively. A more detailed derivation can be found elsewhere[164]. The hardness matrix can be augmented to enforce charge constraints within a molecule[164] for explicit calculations of the polarizability. In addition, the CHEQ model, being an all-atom representation with partial charges assigned to all atomic species, contains all higher-order electrostatic multipole moments, in contrast to point dipole polarizable models[63, 125, 135] and Drude oscillator models[162, 46, 81]. As such, the CHEQ model incorporates higher-order electrostatic interactions explicitly.

The charge degrees of freedom are propagated via an extended Lagrangian formulation that imposes a molecular charge neutrality constraint, thus strictly enforcing electronegativity equalization at each dynamics step. The system Lagrangian is

$$L = \sum_{i=1}^M \sum_{\alpha=1}^{N_i} \frac{1}{2} m_{i\alpha} \dot{r}_{i\alpha}^2 + \sum_{i=1}^M \sum_{\alpha=1}^{N_i} \frac{1}{2} m_{Q,i\alpha} \dot{Q}_{i\alpha}^2 - E(Q, r) - \sum_{i=1}^M \lambda_i \sum_{\alpha=1}^{N_i} Q_{i\alpha} \quad (1.4)$$

where the first two terms represent the nuclear and charge kinetic energies, respectively, while the third term is the total potential energy, and the fourth term is the molecular charge neutrality constraint with λ_i the Lagrange multiplier for each molecule, i . The fictitious charge dynamics, analogous to the fictitious wavefunction dynamics in Car-Parrinello (CP) type methods[18], are determined with a fictitious charge “mass” (adiabaticity parameter in CP dynamics). The units for this mass are $\frac{\text{energy} \cdot \text{time}^2}{\text{charge}^2}$. The charges are propagated based on forces arising from the difference between the average electronegativity of the molecule and the instantaneous electronegativity at an atomic site.

We comment here that the polarizable TIP4P-FQ water model[129] is used to model solvent-solvent and solvent-solute interactions. The TIP4P-FQ water model is a 4-site model, based on the original TIP4P water model of Jorgensen et al[64]. The

charges reside on the hydrogen atoms and a virtual site situated along the perpendicular bisector of the HOH angle 0.15 Å from the oxygen atom. The model has been characterized in previous studies, and the reader is referred to the relevant literature for further details[[129](#), [128](#)].

Chapter 2

MOLECULAR DYNAMICS SIMULATION OF HYDRATED DPPC MONOLAYERS USING CHARGE EQUILIBRATION FORCE FIELDS

Reproduced with permission from Journal of Computational Chemistry, Volume 33(2), 141-152. Copyright 2012, John Wiley and Sons.

2.1 Simulation Protocol

Simulations were carried out utilizing CHEQ formalism in the constant volume and temperature (NVT) ensemble under 3D periodic boundary conditions using the CHARMM package[17]. The DPPC monolayer-water system contained two leaflets of 36 DPPC molecules and a central layer of 2895 TIP4P-FQ water molecules for a total of 20940 atoms. Recent studies have suggested relatively little finite size effects for simulations of 36 or more lipids per leaflet[35, 20]. A representative snapshot of the system is shown in Figure 2.1. A system size of $48.075 \text{ \AA} \times 48.075 \text{ \AA} \times 150.00 \text{ \AA}$ is based on a surface area per lipid of 64.2 \AA^2 from data fit to experimental measurements[70]. The extended z box dimension results in a separation of the two DPPC monolayers by a vacuum region approximately 60 \AA wide. Dynamics were propagated using a Leapfrog Verlet integrator[2] with a time step of 0.5 fs. The temperature of the system was held at 323 K using the Nosé-Hoover method[2, 108] with a thermal piston mass of $3000 \text{ kcal/mol}\cdot\text{ps}^2$; thus, our simulations are performed above the experimental gel-phase transition temperature for pure DPPC membranes (314 K)[148]. Long-range electrostatic interactions were accounted for by Particle mesh Ewald (PME) summation[25, 38] with a $48 \text{ \AA} \times 48 \text{ \AA} \times 100 \text{ \AA}$ Fast Fourier transform (FFT) grid, 4th order interpolation, and screening parameter $\kappa = 0.320$. Several replicate simulations of varying lengths were run for a total simulation time of $\approx 140 \text{ ns}$. Constant surface

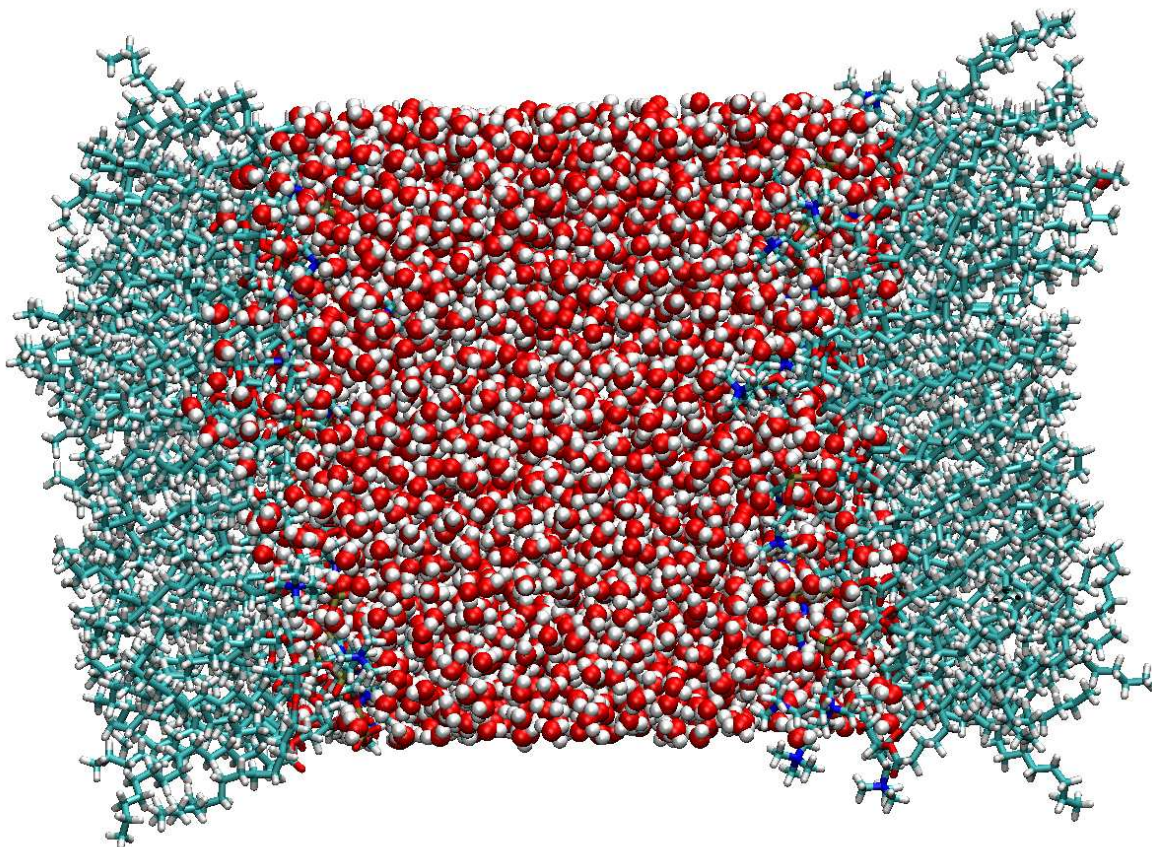


Figure 2.1: Coordinate snapshot of the monolayer-water system, generated using Visual Molecular Dynamics[56], with the z-axis normal to the surface of the monolayers. Oxygens are shown in red, hydrogens in white, carbons in light blue, nitrogens in dark blue, and phosphorus in yellow.

area ensembles have been shown to be equivalent to other ensembles provided that well equilibrated systems are used as starting configurations[35]. We believe that there are no artificial effects due to the chosen ensemble based on the equilibrated states we achieve after long-time simulations.

2.2 Results and Discussion

2.2.1 Atomic and Electron Density Profiles

To characterize the equilibrium structure of the monolayer system we have calculated the number density profiles for various species as a function of distance from

the center of the water layer along the monolayer normal (z -axis). Figure 2.2 shows the number densities for the oxygen atoms of water and several components of the lipid (head group nitrogen and phosphorus atoms, ester carbonyl oxygens atoms, and tail group carbons). The monolayer system shows a stable structure comparable with previous studies performed using the CHEQ model on DPPC and DMPC bilayers[26, 28] as well as with phosphatidylcholine lipid studies utilizing other models[112, 82, 104]. A feature of interest is the extent of water penetration into the monolayer. As water begins to encounter the polar head groups of the lipid, the density decreases in magnitude compared to that of the bulk and remains fairly constant throughout the lipid head groups. For nonpolarizable models the ester carbonyl region is often seen as a barrier past which very little water, if any, will permeate. The treatment of polarizability via the CHEQ force field allows for water to penetrate further into the low dielectric environment of the lipid. This result has been discussed previously in relation to potential mean force calculations of water permeation across a lipid bilayer[26, 28]. The CHEQ alkanes force field, which had been extended for use with the hydrocarbon tail groups of lipids, results in free energies of hydration that are too favorable when compared to experimental energies. A recent study found that altering the specific Lennard-Jones interactions between the alkane carbon and water oxygen atoms reduced the hydration free energies of alkanes to values in better agreement with experiment[27]. Ongoing efforts in our lab investigate the effects of the revised alkanes force field on hydrated lipid membrane systems with respect to water permeation energetics[9]. For the current study, we used the original CHEQ lipid force field. Based on our previous study of DMPC bilayers using revised CHEQ models, we do not anticipate significant differences in the monolayer structure. However, we would expect a reduced permeation of water into the lipid tail region.

We also note that water density exhibits a plateau region in the neighborhood of the phosphate and ester groups. To investigate this feature we calculated the free volume profile as a function of distance along the monolayer normal. The free volume profile serves to quantify the space available to water molecules as they encounter the

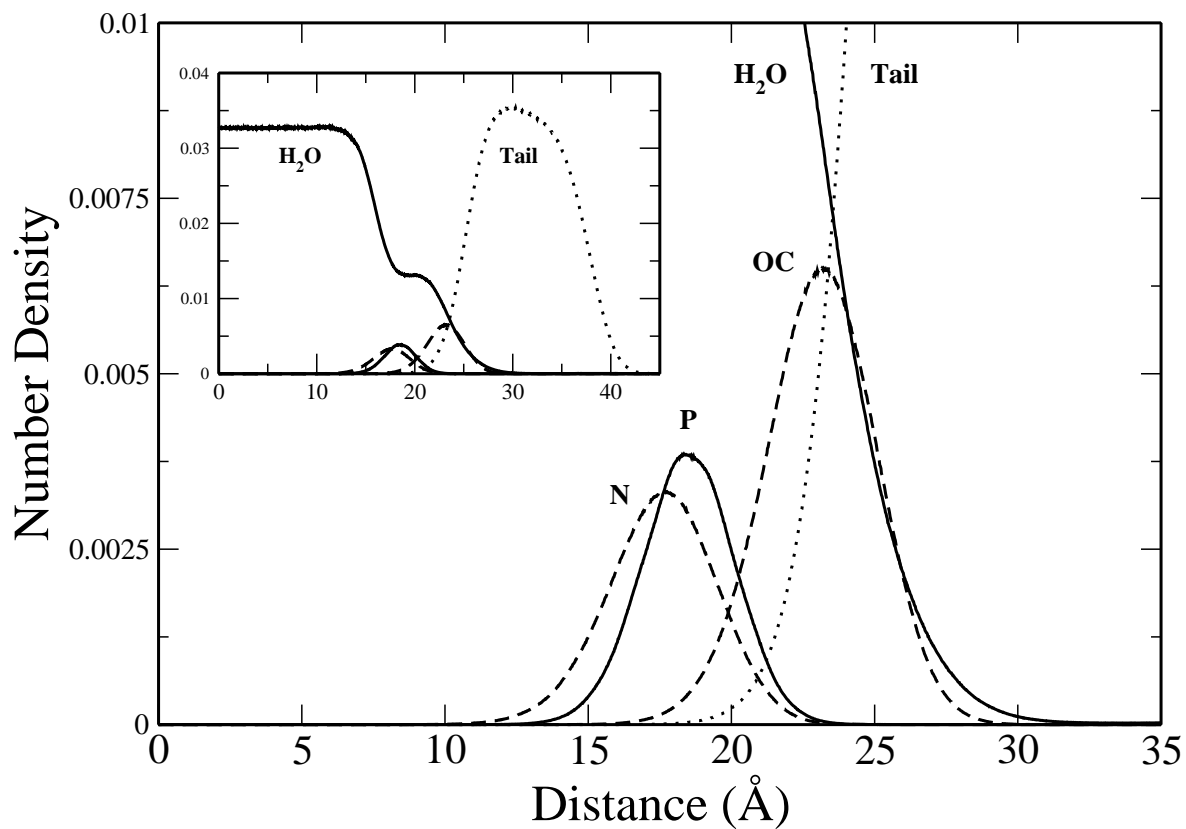


Figure 2.2: Heavy atom number density profiles for selected components (water oxygens, aliphatic lipid tail group carbons, lipid ester oxygens, lipid head group nitrogen and phosphorus) as a function of distance along the monolayer normal.

atoms of the lipid monolayer. This was calculated, as described by Marrink et al[96], by mapping the simulation system onto a 3D grid. All grid points falling within the van der Waals radii of lipid atoms are considered occupied volume while the remaining grid points are considered free volume. The fraction of free volume in the system is simply the ratio of unoccupied grid points to the total number of grid points and can be expressed as a function of distance by dividing the system into intervals (Δz) along the z -axis. Due to the high computational cost of the analysis, only the last 5 ns of each replicate simulation trajectory were considered at a grid spacing of 400 x 400 x 1200, resulting in an interval size of approximately 0.125 Å along the z -axis. The results of the analysis are shown in Figure 2.3, and show a region of fairly constant free volume in the area of the water density plateau. The stability of water molecules in this region is also predicted by independent potential of mean force calculations that show a plateau in the region of these polar lipid groups (data not shown).

Electron density profiles were calculated by summation of the component densities, scaling each constituent atom type by the appropriate number of electrons, and are shown in Figure 2.4. These profiles are *similar* to results previously obtained for DPPC bilayers[26] in both shape and magnitude to profiles fit to experimental data[70], though some differences are evident. Most notably, the CHEQ model overestimates the monolayer phosphate component with respect to the experimental bilayer profile while the carbonyl/glycerol (CG) component is underestimated. Thus, the peak density around 19 Å is slightly higher than that of the experimentally fit data. We emphasize that the comparison with the bilayer properties provided here is simply for reference; we do not suggest that monolayer and bilayer structural properties are necessarily identical under these conditions. Throughout the remainder of the discussion, we will draw attention to similarities and differences between our results on monolayers and past experimental and simulation results on monolayers (if available) or bilayers. This is done in the spirit of previous studies of monolayer systems[32, 100, 101, 87].

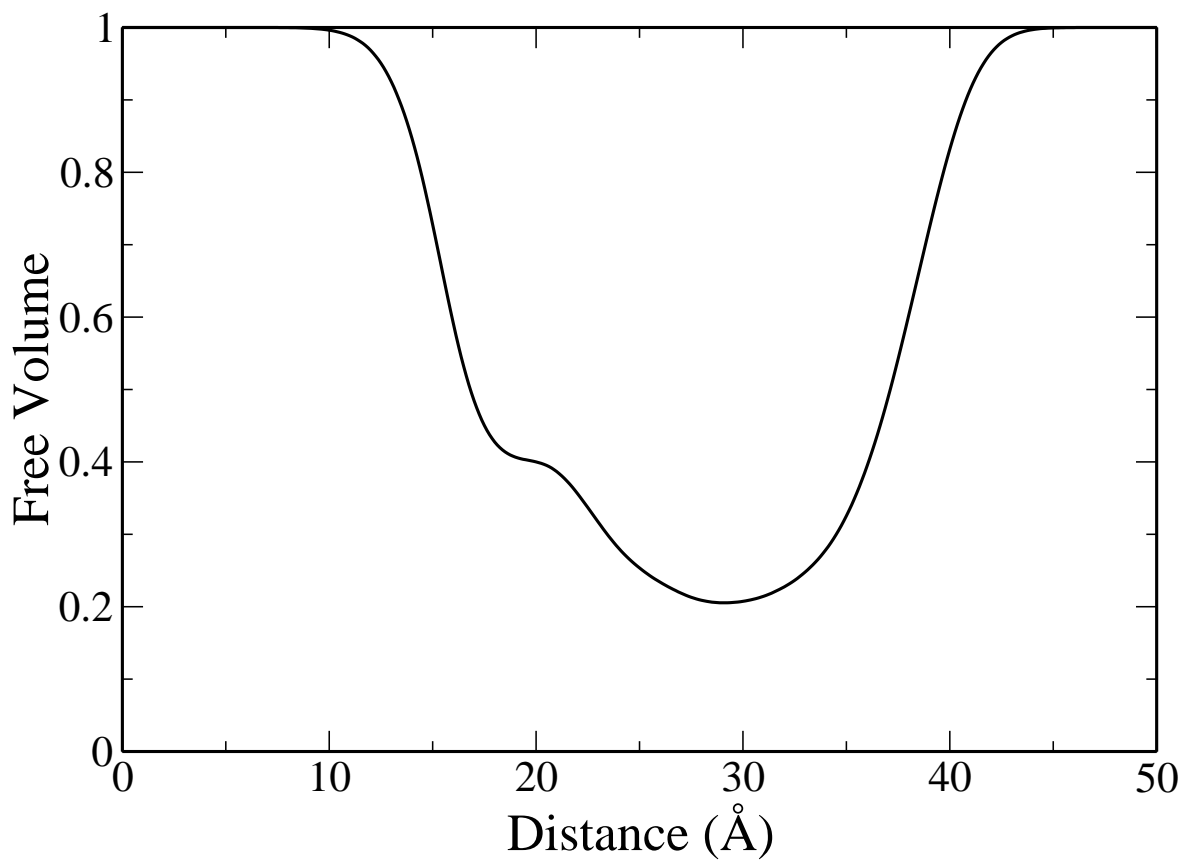


Figure 2.3: Free volume profile as a function of distance along the monolayer normal.

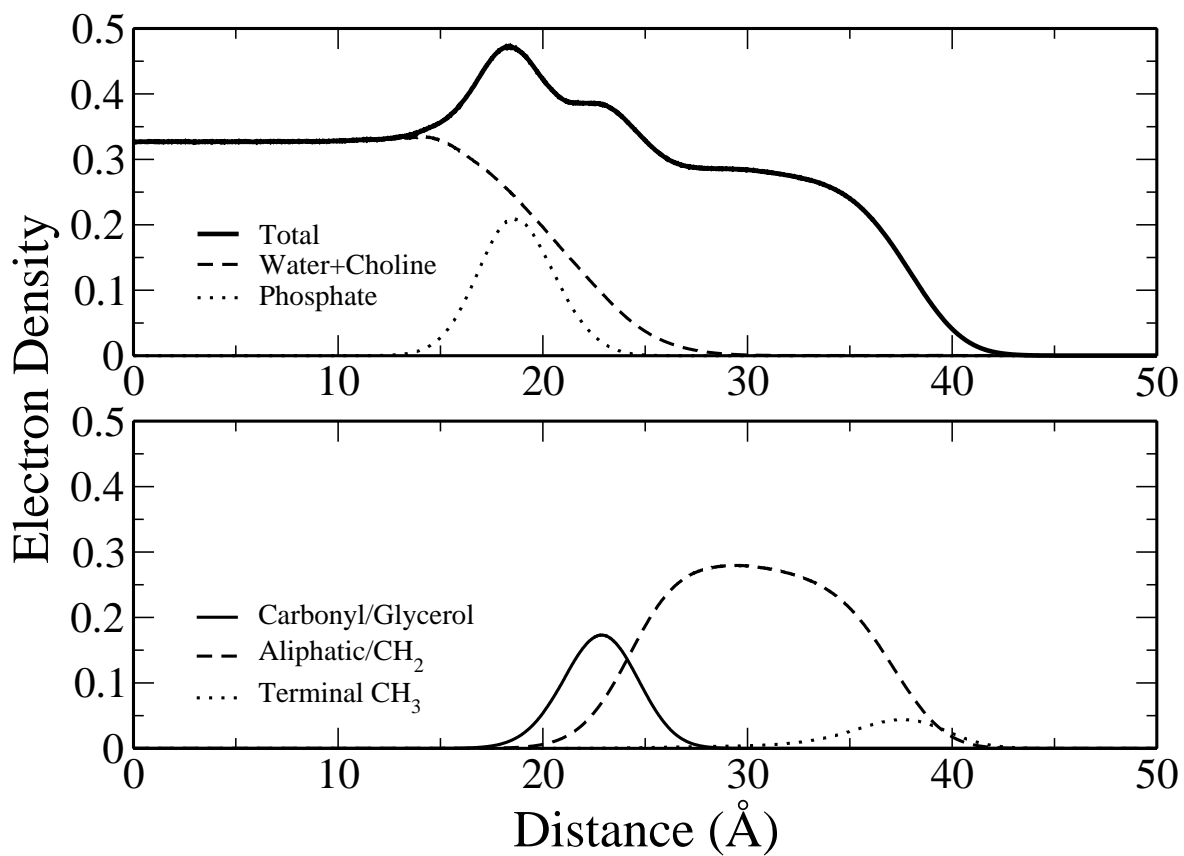


Figure 2.4: Total and component electron density profiles. Components were grouped for comparison with the fitting models of Kucerka et al[70]

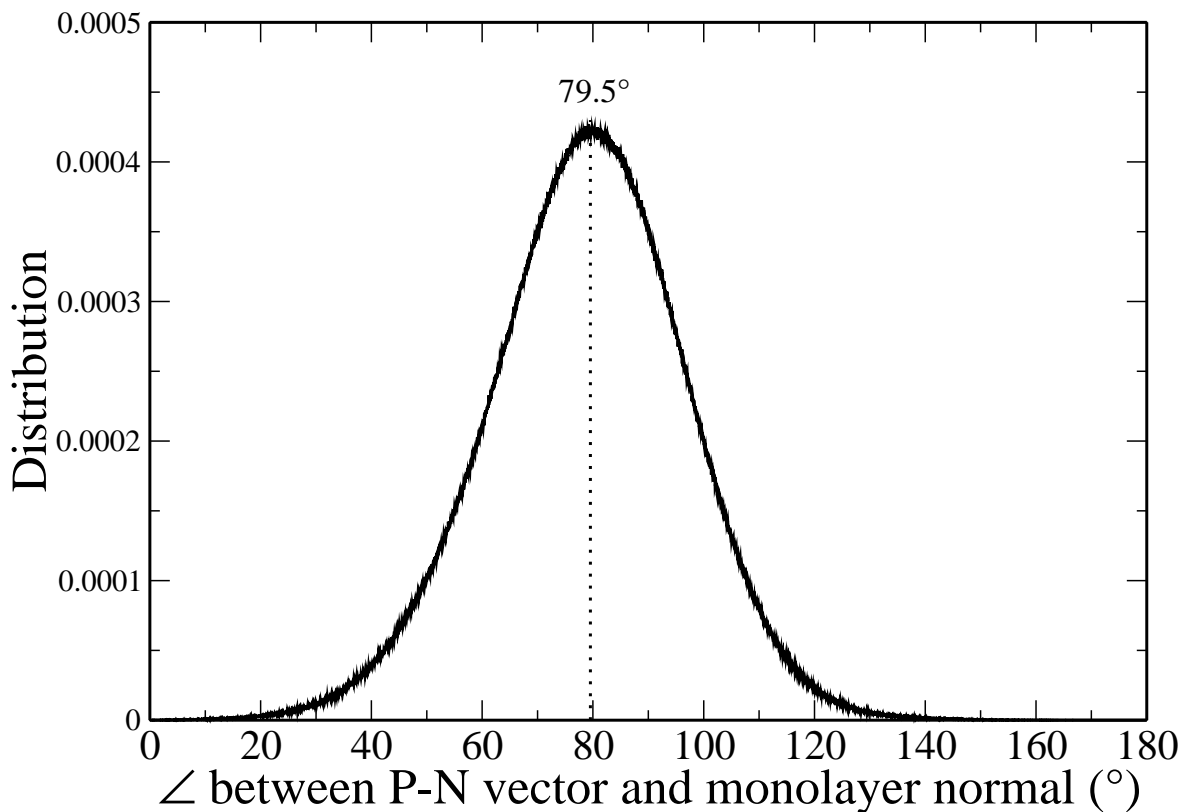


Figure 2.5: Distribution of the angle between the \overrightarrow{PN} dipole vector and the monolayer normal.

2.2.2 Lipid Orientation and Ordering

The orientation of the lipid monolayer head groups can be characterized by calculating the angle between the dipole vector connecting the phosphorus and nitrogen atoms, \overrightarrow{PN} , and the monolayer normal. Due to the geometry of the monolayer system, care must be taken in defining the orientation of \overrightarrow{PN} with respect to the appropriate reference axis. For lipids of the left leaflet (see Figure 2.1 for reference), where $z < 0$, the angle of interest is between the \overrightarrow{PN} and the positive z -axis. For right leaflet lipids, where $z > 0$, the angle is between \overrightarrow{PN} and the negative z -axis. The distribution is shown in Figure 2.5.

The CHEQ model predicts the average head group to be oriented about 79.5° with respect to the monolayer normal, nearly parallel to the plane of the monolayer

surface. This is comparable with previous results for the head group orientation of DPPC bilayers in which angles of 80-90° with respect to the bilayer normal are observed[26, 112, 156, 111], as well as with studies of DPPC monolayers at the water-air interface[32, 100, 101, 87]. Recent arguments indicate that the orientation of the \overrightarrow{PN} dipole has direct implications regarding hydration of the water-lipid interface such that a straightening of the head group orientation (angles decreasing from 90° towards 0° with respect to the membrane normal) allows more water to penetrate into the membrane-water interface[145].

We conduct a similar analysis, with analogous geometric considerations, for the orientation of the carbonyl group of the lipid by calculating the angle between the vector formed by the C=O bonds and the monolayer normal, with results shown in Figure 2.6. The *sn*-1 carbonyl groups assume an average orientation of 64.2° relative to the monolayer normal while the *sn*-2 carbonyl groups orient around an angle of 76.5° relative to the monolayer normal. The CHEQ model’s prediction for the *sn*-1 carbonyl are comparable to an FT-IR study regarding the orientation of carbonyl groups in DPPC multilayers, which reported average orientation angles of $62 \pm 2^\circ$ and $66 \pm 2^\circ$ for the *sn*-1 and *sn*-2 carbonyls, respectively[54]. Though the current model predicts a slightly higher angle for the *sn*-2 chain, the model follows the trend in relative values in *sn*-1 and *sn*-2 carbonyl groups observed for multilayers. We reiterate that this is no suggestion that these properties for monolayers and multilayers should be similar, but just an observation of the current analysis.

The structural order of the lipid tail groups can be evaluated by calculation of the deuterium order parameter, S_{CD} as a function of carbon position along the aliphatic tail. S_{CD} is directly related to the S_{zz} component of the NMR quadrupolar splitting tensor and provides a measure of the order/disorder of alkyl chains in simulated lipid systems[145]. We calculate S_{CD} as

$$S_{CD} = \langle P_2(\cos \theta) \rangle \quad (2.1)$$

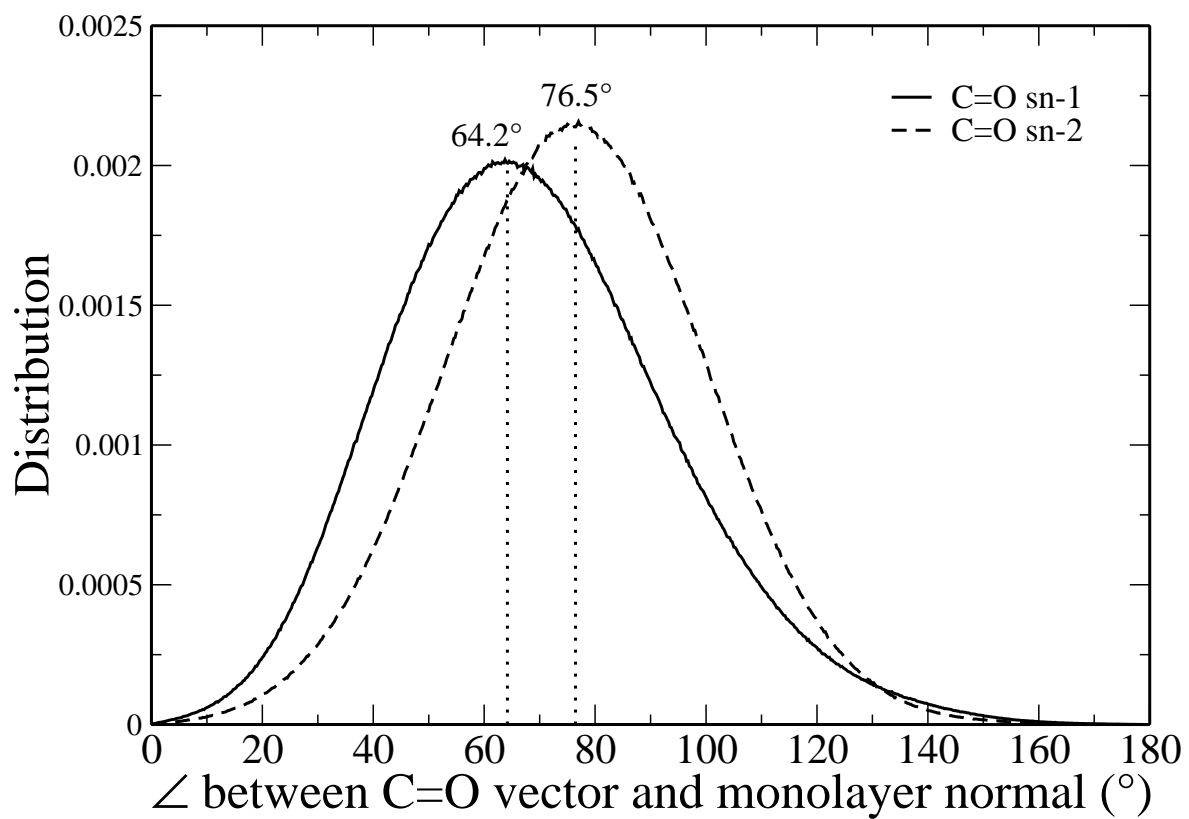


Figure 2.6: Distribution of the angles between *sn*-1 and *sn*-2 carbonyl vectors and the monolayer normal.

where θ is the angle between a C-H bond vector and the monolayer normal and

$$P_2(\cos \theta) = \frac{1}{2}(3 \cos^2 \theta - 1) \quad (2.2)$$

is the second Legendre polynomial. The calculation of the deuterium order parameters yields values between the extremes of -0.5 (\overrightarrow{CH} aligned with the water-monolayer interface) and 1 (\overrightarrow{CH} aligned with the z axis). Results for the calculation of the order parameters for both the $sn-1$ and $sn-2$ chains are shown in Figure 2.7 as well as the experimentally determined order parameters for the $sn-2$ chain of a DPPC bilayer[34]. The C2 carbon has stereoscopically different hydrogens (2R and 2S) between which the CHEQ model is unable to distinguish. Although the CHEQ model does well in predicting the experimental trend of decreasing order further along the hydrocarbon chain[34, 121, 155, 109], it overestimates the order of the carbon chain approaching the ester region (C2-C4) and tends to underestimate the order along the chain (C5-C25). These results are comparable to those found for DPPC bilayers using CHEQ force field[26].

2.2.3 Dielectric Permittivity and Water Dipole Moment Variation

We consider the z -dependent dielectric permittivity profiles for components parallel to the monolayer surface using the approach developed by Stern and Feller[151]. We compute the dielectric profiles for conductive (tin-foil) boundaries using equations 71 and 26 in Reference [151]:

$$\epsilon_{||} = (4\pi h_{||} + 1); \quad (2.3)$$

$$h_{||}(z) = \frac{1}{2k_B T} \langle \mathbf{P}_{||}(z) \cdot \mathbf{M}_{||} \rangle + \langle a_{||}(z) \rangle \quad (2.4)$$

where $\mathbf{P}_{||}(z)$ is the local polarization density, $\mathbf{M}_{||}$ is the total dipole moment parallel to the monolayer surface (xy -plane), and $a_{||}(z)$ represents an explicit polarization contribution. With the CHEQ model $a_{||}(z)$ is self-consistently included in the first term of Equation 2.4. $\mathbf{P}_{||}(z)$ is calculated using a bond-charge approach similar to that of Stern and Feller[151] in which the charge on an atom is determined from a set of bond-charge increments. A more complete derivation can be found in Reference [28].

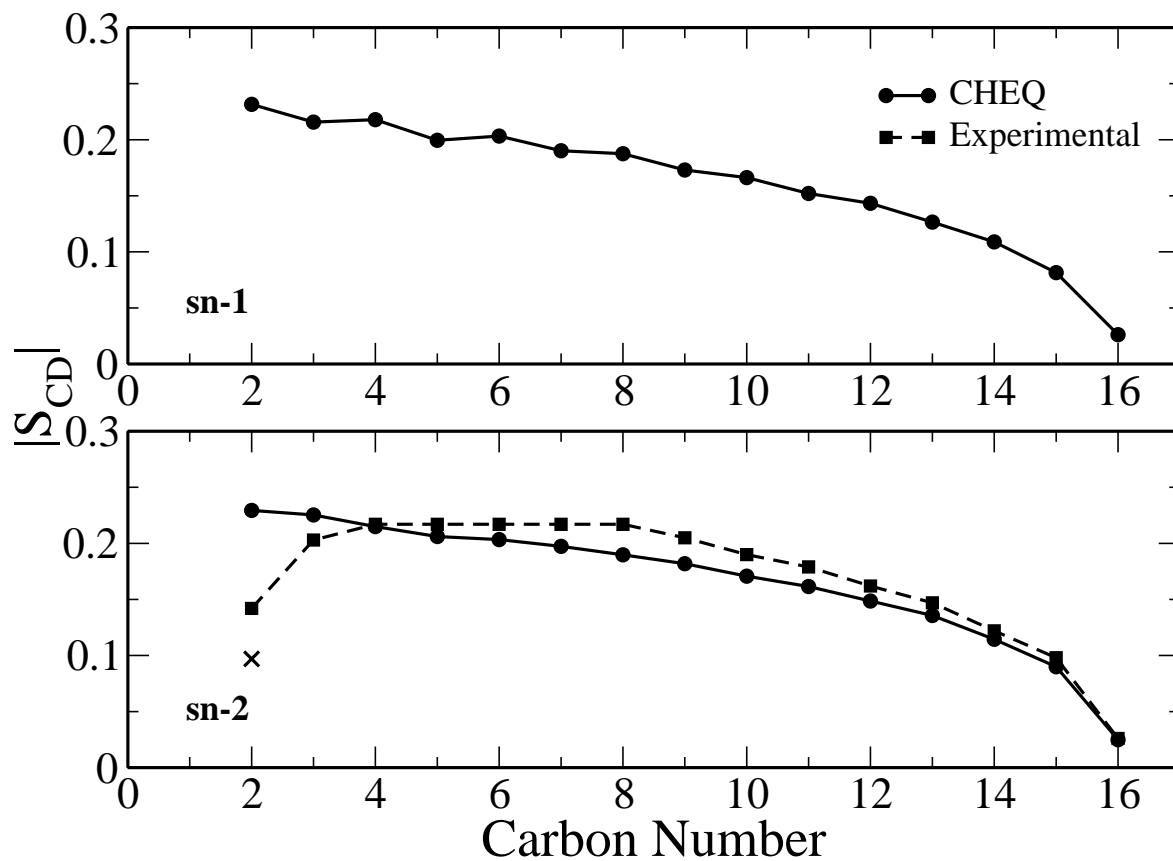


Figure 2.7: Magnitude of the deuterium order parameters for *sn-1* and *sn-2* tail groups as a function of position along the hydrocarbon chain. The experimental order parameters for the *sn-2* tail group are shown for comparison[34]. The stereoscopically different carbons at carbon number 2 are shown with the 2S value denoted as an x.

Figure 2.8 shows the z -dependent parallel component of the dielectric constant as a function of distance from the center of the water layer along the monolayer normal. The dielectric constant of bulk TIP4P-FQ water (near the center of the water layer) is 71.9 ± 1.2 , very close to the experimental dielectric constant for pure water at ~ 1 atm and 320 K (70.93)[80]. Upon entering the monolayer, the dielectric of water decreases monotonically until reaching a shoulder near the polar head groups of the lipid, similar to what is observed for the number density (Figure 2.2) and free volume (Figure 2.3) profiles, and further attenuates towards its gas-phase value upon entering the ester and aliphatic tail region. The head group region of the monolayer exhibits large dielectric values (up to around 1050) whereas in the hydrocarbon tail region the average value is about 1.3. The large dielectric found in the head groups has been attributed to the large dipole magnitudes (19 - 25 Debye) in this region[151]. These results are comparable with studies performed on DPPC and DMPC bilayers using the CHEQ formalism[26, 28]. We note that the exact values for these properties are not directly experimentally accessible, and as such, predicted values are expected to demonstrate a significant spread in values.

A characteristic of polarizable force fields is that they allow for charges to respond to variations in the local electrostatic environment. It follows that the average molecular dipole moment of water varies from the bulk phase into the lipid monolayer. Figure 2.9 shows the molecular dipole moment distributions found by averaging the dipole moment of water found in slabs 0.05 \AA along the monolayer normal. In the center of the water layer the dipole moment reaches a value of 2.55 D, within the range of 2.5 to 3.0 D given by empirical and ab initio estimates of dipole moment of water in the condensed-phase[7, 144, 68, 149]. The bulk value is slightly lower than the frequently-cited value for TIP4P-FQ of 2.62 D, which is expected since the current simulations are performed at 323 K as opposed to 298 K for the literature work[19, 22, 143, 144, 166]. Water’s dipole moment monotonically decreases as it moves through the lipid and, upon entering the aliphatic tail region, the dipole moment approaches the gas-phase value of 1.85 D[80]. Unlike the Drude oscillator based SWM4-NDP, the TIP4P-FQ

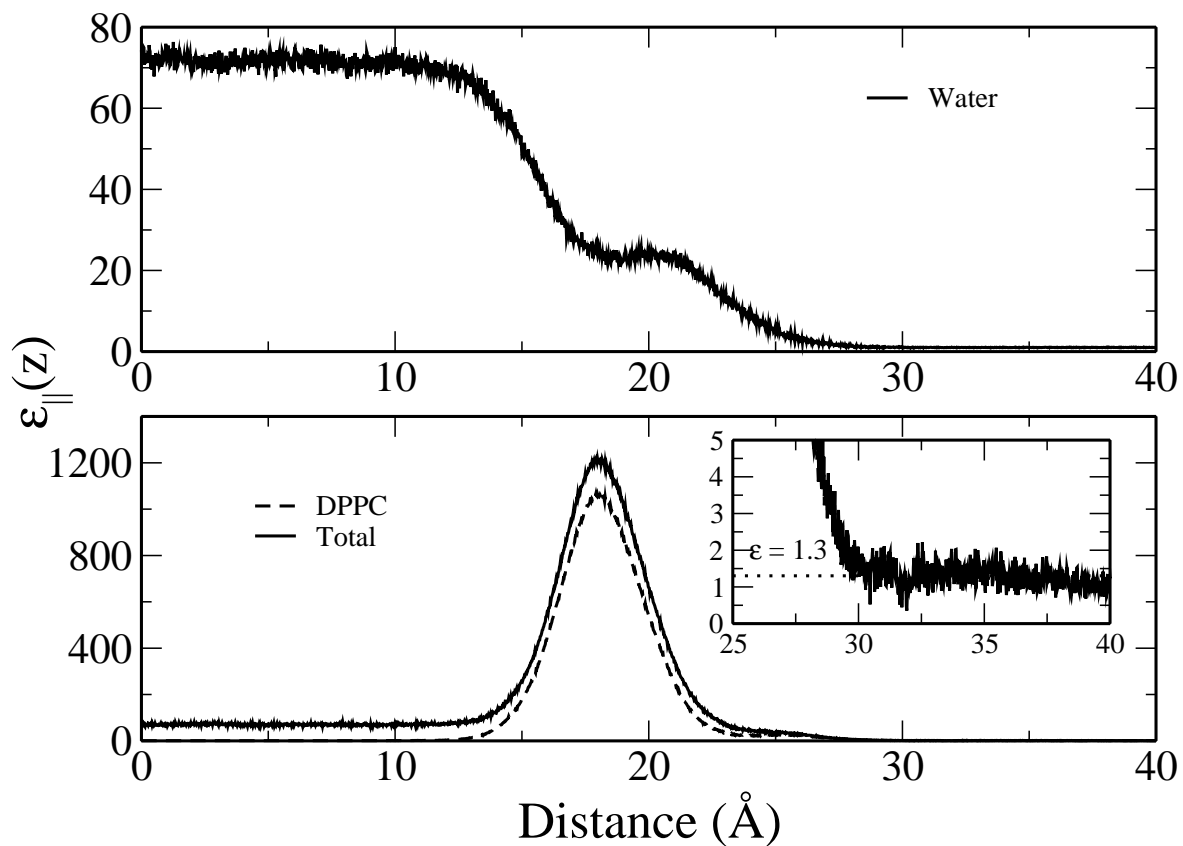


Figure 2.8: Profiles of the parallel component of the dielectric permittivity as a function of distance along the monolayer normal. Profiles are given for water (top), DPPC, and the total system (bottom). The lipid tail region is shown in greater detail due to scale (inset) with an average value of 1.3, shown as a dotted line, calculated from $z = 30$ to 40.

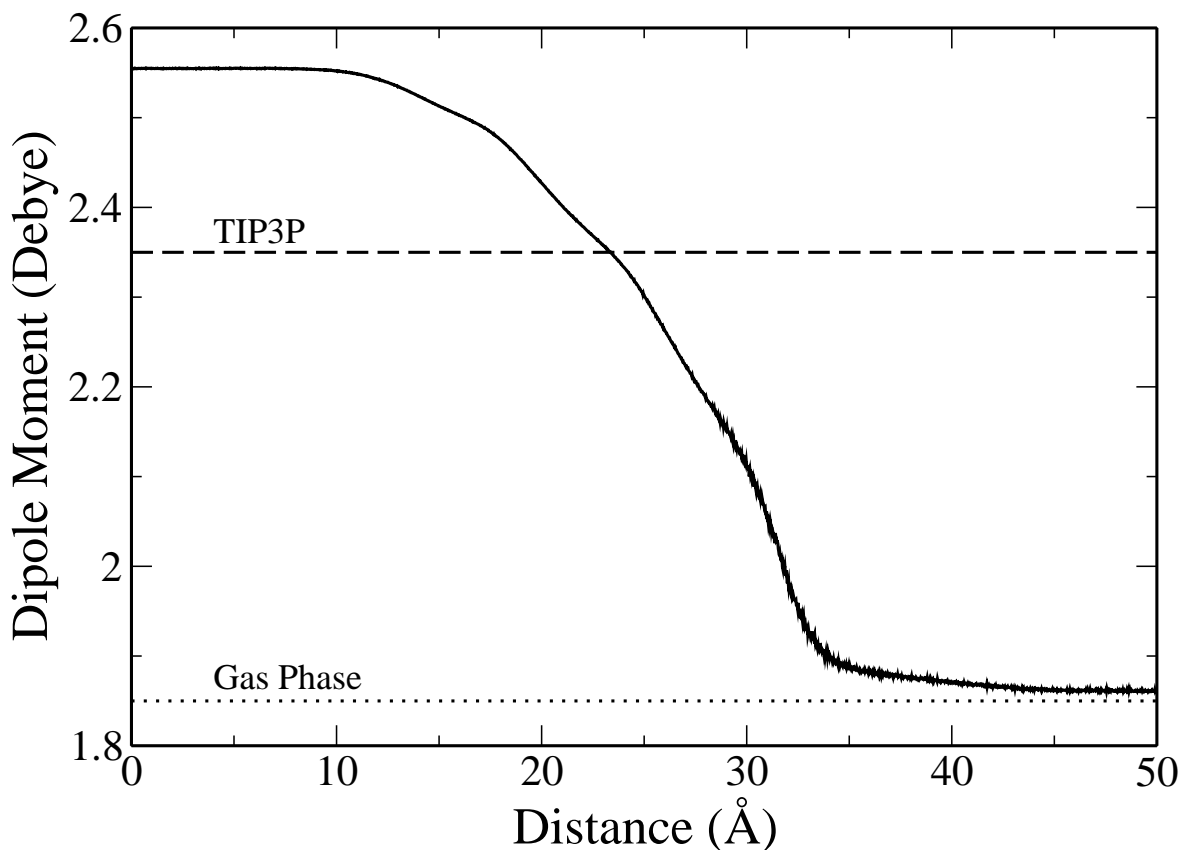


Figure 2.9: Average molecular dipole moment profile of water as a function of distance along the monolayer normal, from the center of the water layer (bulk phase) through the lipid monolayer and into the vacuum region (gas phase). Dashed line denotes the constant dipole moment of the TIP3P water model while the dotted line denotes the experimental dipole moment of water in the gas phase.

water model accommodates a larger variability in dipole moment. A study by Harder et al[47] using Drude polarizable models predicts that the average molecular dipole moment for water is reduced about 0.55 D within the lipid monolayer relative to bulk water. This is slightly lower than the difference of 0.7 D for TIP4P-FQ water (bulk water dipole moment of 2.55 D).

2.2.4 Surface Tension and Pressure

The total surface tension of the lipid monolayer-water system is related to the anisotropy of the pressure tensor within an interfacial region by the relationship:

$$\gamma_t = L_z \left\langle P_{zz} - \frac{P_{xx} + P_{yy}}{2} \right\rangle \quad (2.5)$$

where L_z is the length of the simulation cell, P_{zz} is the component of the pressure tensor normal to the monolayer surface, and P_{xx} and P_{yy} are the components tangential to the surface. Accounting for the two interfaces in the present simulation, we can define surface tension for a single monolayer at the interface as

$$\gamma_m = \frac{1}{2} \gamma_t. \quad (2.6)$$

The pressure tensor was monitored continuously for multiple replicate monolayer systems until surface tensions were considered to be sufficiently stable. The resulting average for the surface tension of the DPPC monolayer systems is 42.35 ± 1.16 dyne/cm, consistent with the experimental value of 40.9 dyne/cm[147] and with the value of 43.9 ± 0.8 obtained using state-of-art nonpolarizable force field simulations[65]. To calculate the surface pressure of the monolayer system we follow a method analogous to that of Mohammad-Aghaie et al[100]:

$$\Pi = \gamma_w - \gamma_m \quad (2.7)$$

where γ_w is the surface tension of pure TIP4P-FQ water at 323 K. The value for γ_w was calculated as the average from three replicate molecular dynamics simulations of systems of 1024 TIP4P-FQ water molecules at the water-air interface simulated using CHARMM package[17] for a total of 9 ns. We obtain an average surface tension of 65.27 ± 0.57 dyne/cm, underestimating the experimental value for the surface tension of pure water at 323 K of 67.94 dyne/cm[80]. From the values reported for γ_m and γ_w , we find a surface pressure of 22.92 ± 1.29 dyne/cm. This value is slightly lower than those reported from captive bubble experiments performed by Crane et al[24] in which expansion isobars for phospholipid monolayers at varying temperatures and

area per lipid values are reported (see Figure 3A in Reference [24]) and yield a surface pressure range of 25-30 dyne/cm for a DPPC monolayer at 323 K with an area per lipid of 64.2 \AA^2 ; the measurements by Crane and co-workers are considered to be among the more reliable in terms of minimization of experimental artifacts such as leakage, pH, impurities, compression rate, and ionic strength[100, 35, 8]. There appears to be a wide dispersion of experimental surface pressure values based on protocol and conditions[35]. This makes an absolute comparison to experiment difficult, but we see that our predicted values are of comparable order of magnitude with available experimental data.

2.2.5 Monolayer Dipole Potential

Within the interior of a lipid membrane exists a positive potential which has ramifications on the penetration and permeability of ionic hydrophobes into and through the membrane. This potential is referred to as the membrane dipole potential and may also have implications regarding the association of proteins with a membrane surface as well as the penetration, structure, and function of transmembrane proteins. To determine the nature of the membrane dipole potential we compare the surface potential of the monolayer-water interface ($V_{\text{monolayer-water}}$) with that of a water-air interface ($V_{\text{water-air}}$). The surface potential of a system can be calculated through double integration of charge density as a function of distance from the center of the water layer along the monolayer normal[48]:

$$V(z) = -\frac{1}{\epsilon_0} \int_{-\infty}^z \int_{-\infty}^{z'} \rho(z'') dz'' dz'. \quad (2.8)$$

Here, ϵ_0 is the permittivity of vacuum and $\rho(z)$ is the charge density achieved by segmenting the system into slices of width dz and summing the charges within each slice. This effectively solves the Poisson Equation assuming in-plane isotropy at a particular depth into the monolayer. For both of the interfacial systems the vacuum regions are referenced to a potential of 0 V and integration in Equation 2.8 is taken from the vacuum region (∞) to a point at the center of the bulk water layer. To characterize the

total membrane surface potential the charge densities of individual molecular species were twice integrated to yield constituent contributions to the electrostatic potential. Independently the surface potentials of these systems do not provide experimentally meaningful quantities but comparing the difference between the two,

$$\Delta V = V_{\text{monolayer-water}} - V_{\text{water-air}}, \quad (2.9)$$

yields the shift in the surface potential upon addition of a lipid monolayer onto the water-air interface. The monolayer dipole potential calculated in this way is an explicit property of the system and should provide insight into the electrostatic properties of lipid membranes. The results of this analysis for the total and constituent contributions to the surface potential of the monolayer system are shown in Figure 2.10. To calculate the surface potential of the water-air interface three replicate interface systems of 1024 waters using the TIP4P-FQ potential were simulated, starting from pre-equilibrated structures, in the NVT ensemble with a cell size of 24 Å x 24 Å x 100 Å at 323 K implemented through the CHARMM package[17] for a total simulation time of 14 ns. Surface potential calculations performed on the replicate water-air interface systems yield an average $V_{\text{water-air}} = 0.54 \pm 0.01$ V.

The values of the total and component potentials shown in Figure 2.10, as well as those for the water-air interface, are given in Table 2.1. For comparison, Table 2.1 also includes surface potential values reported by Harder et al. (utilizing a fully polarizable Drude oscillator model[47]) as well as their results using the nonpolarizable CHARMM27 force field and the TIP3P water model. To investigate the effects of the variation of the water model on the potential calculation, the partial charges of the TIP4P-FQ water model used with the CHEQ force field were substituted with the those of the nonpolarizable TIP3P water model in both the monolayer-water and water-air systems. The results of this analysis are also included in Table 2.1.

Experimentally determined surface potential changes for PC lipids at the argon-water interface range from 0.30 to 0.45 V[146]. A graphical representation of the experimental range is presented in Appendix A. In Figure 2.10 it is shown that, using the

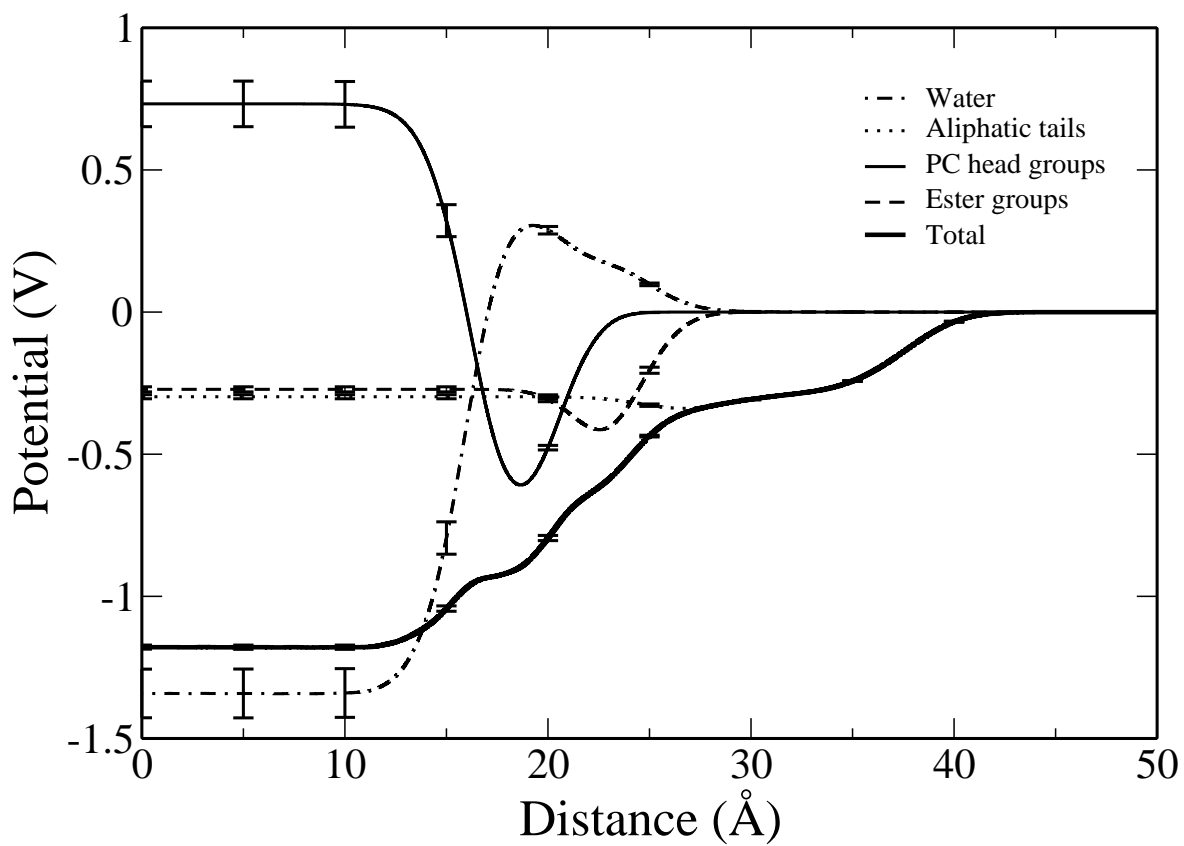


Figure 2.10: Interfacial potential profiles of the total system and of selected components as a function of distance along the monolayer normal. The potential in the vacuum region is referenced to a value of 0 V.

	Drude[47]	CHARMM27[47]	CHEQ	CHEQ/TIP3P
V_{water}	4.2	2.6	1.34	1.10
$V_{\text{PC/head}}$	-2.9	-2.4	-0.73	-0.73
V_{ester}	-0.1	0.7	0.27	0.27
$V_{\text{aliphatic/tail}}$	-0.3	0.4	0.30	0.30
$V_{\text{monolayer-water}}$	0.9	1.3	1.18	0.94
$V_{\text{water-air}}$	0.55	0.5	0.54	0.59
ΔV	0.35	0.8	0.64	0.35
$\Delta V_{\text{Expt.}}$		0.30 - 0.45		

Table 2.1: Component and total interfacial potential values (in Volts) of monolayer-water and water-air systems, including results reported for nonpolarizable (CHARMM27), polarizable Drude oscillator, and polarizable CHEQ force field. Results obtained using the CHEQ force field with TIP3P charge substitution are also shown.

CHEQ model, the resulting monolayer dipole is 0.64 ± 0.02 V, offering an improvement to the value of 0.8 V reported for the nonpolarizable CHARMM27 force field[47] though still overestimating this property relative to experiment. It is encouraging that the addition of explicit electronic polarization within a partial atomic charge formalism moves the prediction of monolayer potential closer to experiment relative to the fixed-charge force field. When the partial charges of TIP4P-FQ water are substituted with those of TIP3P, the membrane potential decreases to a value of 0.35 ± 0.02 V, matching the value reported for the Drude oscillator model and in close agreement with the experimental range. The change in the value of the dipole potential difference resulting from the artificial modification of water model charges at most suggests that the nature of the charge distributions and polarizability of the water model may be a first-order perturbation to consider when refining the combination of lipid and solvent force fields for molecular simulations of these types of biological systems (as will be discussed below).

We define the dipolar contribution to the potential as

$$V^{\text{water,dipole}} = -\frac{1}{\epsilon_0} \int_{-\infty}^z \mu_z(z) dz \quad (2.10)$$

where the dipole moment density $\mu_z(z)$ is defined as

$$\mu_z(z) = \frac{1}{V} \left\langle \sum_m \delta(z - z_m) \left(\sum_i q_{im} z_{im} \right) \right\rangle \quad (2.11)$$

and in which the indices m and i refer to a molecule and an atomic site within that molecule, respectively. The coordinate z_{im} is taken to be an arbitrary, molecule-specific center, chosen to be the oxygen atom in the case of water. Similarly, the quadrupolar contribution to the potential is defined as

$$V^{\text{water,quadrupole}} = -\frac{1}{\epsilon_0} [Q_{zz}(z) - Q_{zz}^0], \quad (2.12)$$

where the reference value Q_{zz}^0 is taken to be 0 and the quadrupole moment density ($Q_{zz}(z)$) can be expressed as

$$Q_{zz}(z) = \frac{1}{V} \left\langle \sum_m \delta(z - z_m) \left(\frac{1}{2} \sum_i q_{im} z_{im}^2 \right) \right\rangle. \quad (2.13)$$

Figure 2.11 presents the decomposed water potentials and shows that the quadrupolar contribution changes little upon addition of the lipid onto water-air interface and does not contribute substantially to the overall potential shift. This is a direct consequence of the density dependence of the quadrupole potential[159]. The contribution from the water molecular quadrupole moment will essentially vanish when considering the monolayer dipole potential difference which is measured experimentally. Thus, the nature of the quadrupole moment of the force field model is not as critical in assessing the monolayer dipole potential difference. This makes the monolayer dipole potential difference a more robust metric of the quality of the force field in the context of measuring the interfacial electrostatics in such systems. However, for pure bilayer systems, the contribution from the quadrupole term cannot be ignored, and may give rise to the spread in force field based values of the dipole potential. The dipolar contribution, however, changes sign and magnitude upon spreading of the lipid, leading to a net positive contribution of ≈ 0.8 V to the surface potential shift.

We conclude this section by commenting on the possible implications of the differences in the nature of the polarizable water model used in conjunction with the

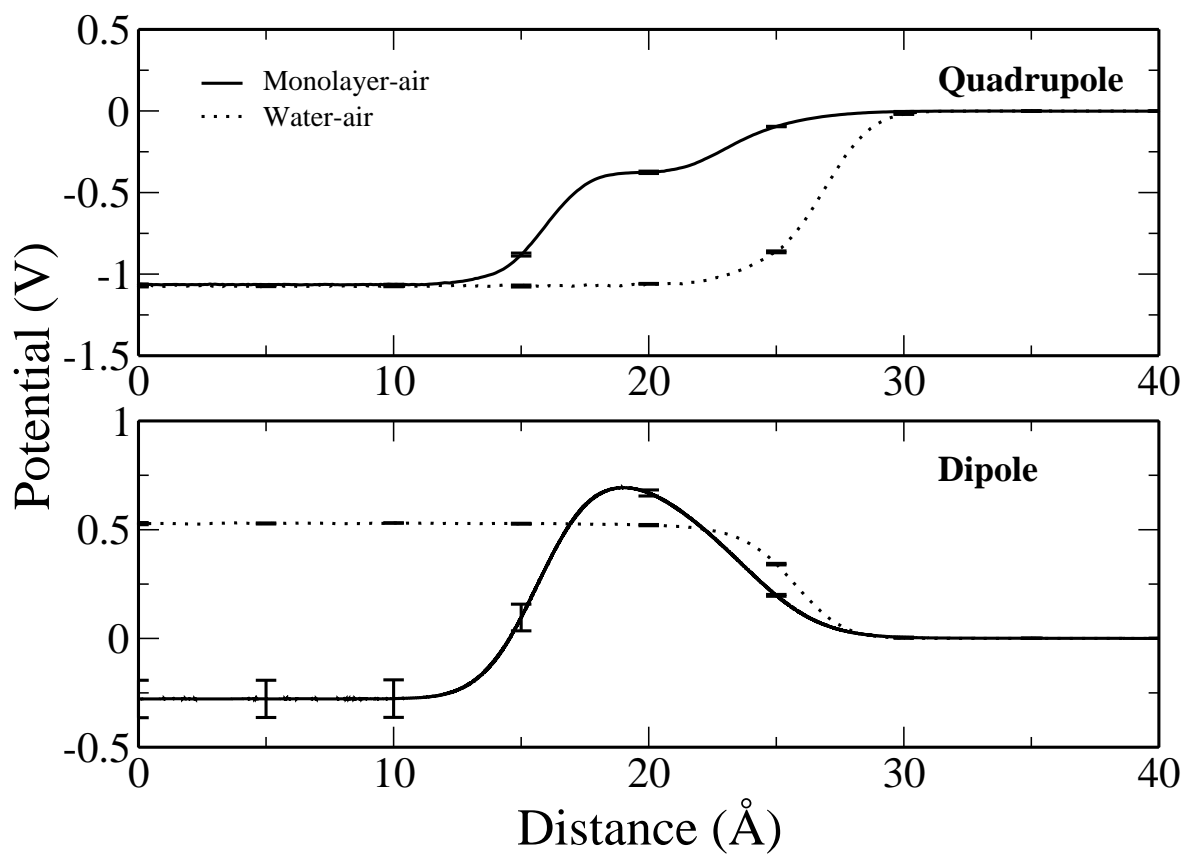


Figure 2.11: Comparison of the quadrupole (top) and dipole (bottom) contributions to the interfacial potential of water as a function of distance along the interface normal for both the monolayer-water and water-air systems.

polarizable lipid membrane model. Harder et al[47] use the Drude water model, and comparing the water density and water dipole moment profiles of the Drude model versus the TIP4P-FQ water model used in this study, we observe some differences. Furthermore, the average orientation of the two water models is different, and since the water contribution to the surface dipole potential is directly related to average water orientation, one can inquire about the effects of this difference on the overall monolayer potential and the resulting difference in the ΔV values computed as in this study. We address these questions, qualitatively, next. The Drude water model has a lower polarizability than the TIP4P-FQ model used in this study (0.978 \AA^3 versus 1.12 \AA^3)[72, 129]. Furthermore, in the Drude bilayer system, the magnitude of variation of the average water molecular dipole moment along the monolayer normal is less than for the TIP4P-FQ. In order to consider the effects of the influence of the dipole moment variation on the dipole potential the average dipole moment of water is fit to an error function of the form:

$$f(z) = a - b \cdot \operatorname{erf}\left(\frac{z - c}{d}\right) \quad (2.14)$$

where the variation in dipole moment is from $a + b$ (bulk water) to $a - b$ (low density), c is the inflection point, and d represents the characteristic width of the transition. Based on our data, these parameters are: $a_{\text{monolayer-water}} = 2.21$; $b_{\text{monolayer-water}} = 0.35$; $c_{\text{monolayer-water}} = 26.679$; $d_{\text{monolayer-water}} = 9.27369$ for the lipid membrane systems and $a_{\text{water-air}} = 2.21$; $b_{\text{water-air}} = 0.35$; $c_{\text{water-air}} = 29.0967$; $d_{\text{water-air}} = 4.589$ for the water-air interfacial systems. The magnitude of the dipole moment variation from bulk water to low density water is the same in both systems and only the position and rate of change differs. We can modulate the magnitude of the dipole moment variation in each system by an empirical adjustment of the a and b parameters (assuming constant c and d):

$$f'(z) = a' - b' \cdot \operatorname{erf}\left(\frac{c - z}{d}\right). \quad (2.15)$$

Thus, we can effectively consider the impact of changing the dipole magnitude on the

Set	a ⁷	b ⁷	μ_{bulk}	μ_{gas}	ΔV
1	2.06	0.20	2.26	1.86	0.70
2	2.11	0.25	2.36	1.86	0.74
3	2.16	0.30	2.46	1.86	0.77
4 (CHEQ)	2.21	0.35	2.56	1.86	0.81
5	2.26	0.40	2.66	1.86	0.84
6	2.31	0.45	2.76	1.86	0.88
7	2.36	0.50	2.86	1.86	0.93
8 (Drude)	2.25/2.20	0.2/0.25	2.45/2.45	2.05/1.95	0.76
9 (Drude (nomin))	2.25/2.20	0.2/0.25	2.45/2.45	2.05/1.95	1.44

Table 2.2: Parameters from altering dipole moment variation and influence on ΔV . Potentials in Volts, dipole moments in Debye. Drude scaling from 2.05-2.45 (monolayer-water) and 1.95-2.45 (water-air) as in Harder et al[47]

dipole potential by the application of a scaling function

$$g(z) = \frac{f'(z)}{f(z)} \quad (2.16)$$

to the dipole density (defined in Equation 2.11). The scaled dipole moment density, $\mu'_z(z) = g(z) \cdot \mu_z(z)$, can then be integrated as in Equation 2.10 to give the respective water dipole contribution. In Table 2.2, we consider several variations (1.86 - 2.26 D to 1.86 - 2.86 D) and their influence on the water dipolar contribution to the potential difference. The magnitude of the dipole moment variation has limited influence on the dipole potential. That is, changing the CHEQ variation from 1.86 - 2.56 D to 1.86 - 2.26 D would only reduce ΔV by 0.105 V; increasing the variation to 1.86 - 2.86 increases ΔV by 0.12 V. In order to make a more direct comparison to results based on fully polarizable Drude models[47], we also consider dipole variation from 2.05 - 2.45 D at the monolayer-water interface and 1.95 - 2.45 D at the water-air interface. From this, we see a 0.051 V reduction in ΔV , in closer agreement with the experimental range.

The water contribution to the dipole potential is not only affected by the magnitude of water dipole moment, but it is also influenced by the preferential orientation

of water at the interface. We measure the orientation of water as $\langle \cos \theta \rangle$, where θ is the angle formed between the permanent dipole vector of water and the z -axis; results are shown in Figure 2.12 (top). Values of $\langle \cos \theta \rangle = \pm 1$ indicate the average water dipole is perfectly aligned with the $\pm z$ -axis (normal to the interface), whereas $\langle \cos \theta \rangle = 0$ denotes orientations that do not contribute to the dipole potential (isotropic orientations and alignment parallel to the interface). Approaching the monolayer from bulk water, water molecules preferentially align in the positive z direction. Beyond $z < 19$ Å (approximately the peak position of the lipid head group phosphorus density) the orientation of water is reversed with a strong alignment in the negative z direction. Although water density is strongly aligned in the negative z -direction throughout 20 Å $< z < 40$ Å, there are fewer water molecules in this portion than in the region approaching the head groups from bulk water. We can consider how water orientation contributes to the surface potential by scaling the orientation by the density of water, $\rho(z)/\rho_{\text{bulk}}$. Scaled orientation profiles (Figure 2.12 (bottom)) demonstrate reduced magnitudes in the peak and minimum in the monolayer-water profile. The minimum in the monolayer-water profile is a feature not seen in the similar study using Drude polarizable models. We can remove the influence of this minimum from this profile by an effective scaling (we use a sharply decreasing error function from 1 to 0 to keep the peak in the orientation profile, while scaling the minimum to zero). When we remove the effect of the orientational minimum from the dipole density profile, the resulting water dipole contribution is 0.933 V at the lipid-air interface (considering the Drude dipole scaling), ≈ 0.7 V higher than the original. We comment that the water contribution to the dipole potential is a complex combination of water atomic partial charge variation across the interface and water orientation. In our simplistic analysis, the water orientation appears to be the significant contributor to the dipole potential, with the details of the charge distribution contributing second order effects. Of course, the response of the lipid electrostatics has not been considered in this analysis, and this must be considered for a proper accounting of all simultaneous effects.

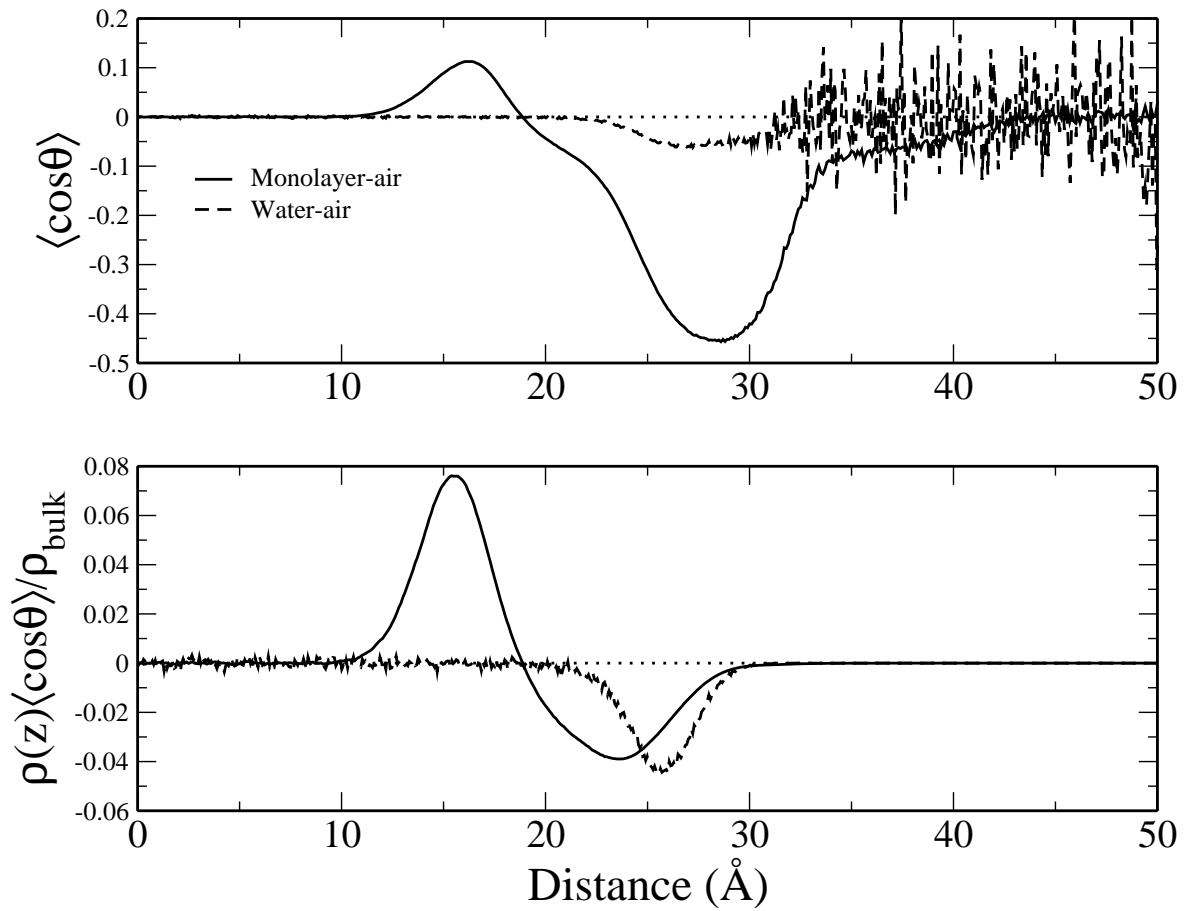


Figure 2.12: Orientation of water at the monolayer-water and water-air interfaces. The average orientation of water (top) and the average orientation scaled by the z -dependent density relative to bulk density of water (bottom). Dotted horizontal line denoting $\langle \cos \theta \rangle = 0$ is included as a visual guide.

Chapter 3

FREE ENERGETICS AND THE ROLE OF WATER IN THE PERMEATION OF METHYL GUANIDINIUM ACROSS THE BILAYER-WATER INTERFACE

Reproduced with permission from Journal of Physical Chemistry, submitted for publication. Unpublished work copyright 2012, American Chemical Society.

In the following chapter, we explore the free energetics of charged species, in this case methyl guanidinium, permeating across a model lipid bilayer. We consider a model DPPC bilayer as the oft-used proxy for a physiological membrane. We consider pure water and 1 M KCl systems, the salt concentration being higher than physiological conditions in order to sufficiently sample configurations of the ions in the vicinity of the membrane-water interface. We further explore the nature of water and its ability to mediate deformations of the lipid bilayer in stabilizing a charged species at the center of this model bilayer. There has been much literature on the permeation of polar and charged solutes into lipid membranes with accompanying hydration shell of water molecules[88, 89]. We address the idea that this accompanying water also mediates the interactions between the lipid head groups and permeating solute. We attempt to study this effect by performing molecular simulations where water is expelled from the core of the bilayer. We then proceed to remove this constraint in order to observe any deformations that accompany the permeation of water into the bilayer. Section 3.1.1 addresses the validation of the methyl guanidinium force field through the calculation of hydration enthalpies and comparison to previous literature data. Section 3.1.2 discusses results of the potential of mean force (PMF) for methyl guanidinium permeation. Section 3.2 presents extended discussion of the results of hydration free energy calculations, the potential of mean force, decomposition of the potential of mean

force into contributions from system components, an explanation of the differences of the PMF’s computed in salt solution versus pure aqueous environments, and finally discussion of the role of water in potentially mediating membrane deformation.

3.1 Simulation Setup

The membrane system consists of 72 DPPC lipid molecules, arranged in a bilayer (36 molecules per leaflet), solvated with an approximately 1 M potassium chloride solution composed of 3203 TIP4P-FQ water molecules[129], 57 K^+ and 58 Cl^- ions, and containing a single positively charged methyl guanidinium ($mguanH^+$) molecule. We performed molecular dynamics simulations using the CHEQ formalism in the constant particle, normal pressure, lateral surface area, and temperature ($NP_A T$) ensemble at a pressure of 1 atm, a temperature of 323 K, and an area per lipid of 63.0 \AA^2 , above the temperature of the liquid-gel phase transition[12] and within the experimental range for the area per lipid[69]. The pressure was maintained using the Langevin piston method[2] with a piston mass of 2025 amu in the z -direction, normal to the bilayer. The temperature of the simulation was controlled using the Nosé-Hoover method[2, 108] with a thermal piston mass of $3000 \text{ kcal/mol} \cdot \text{ps}^2$. Long-range electrostatics were accounted for by Particle mesh Ewald (PME) summation[25, 38] with a $48 \times 48 \times 80 \text{ \AA}^3$ Fast Fourier transform (FFT) grid, fourth order B-spline interpolation, and screening parameter $\kappa = 0.32$. Dynamics were propagated using the Leapfrog Verlet integrator[2] with a 0.5 fs time step.

The CHEQ lipid force field has been developed and validated for simulations of hydrated bilayer and monolayer systems in the $NP_A T$ and NVT ensembles[28, 26, 84]. In the current simulations we use an intermediate, revised version of the CHEQ lipid force field in which 1.) the Lennard-Jones (LJ) non-bond parameters between head group atoms were varied to facilitate surface tensionless MD simulations in constant NPT simulations, and 2.) selected dihedral parameters were adjusted to better match *ab initio* torsion profiles. The details of the lipid force field modification are given in Appendix B, with area per lipid and torsion fitting results presented in Figures B.1

and B.2, respectively. The CHEQ polarizable force field model for methyl guanidinium was constructed by adapting the CHARMM CHEQ force field for proteins[115, 120], extending the electrostatic parameters, hardnesses and electronegativities from the protein force field for an arginine side chain.

The methyl guanidinium was partitioned into two charge normalization units to control polarizability scaling. The first unit encompasses the methyl (-CH₃) and secondary amine (-NH) groups while the second unit includes the central carbon and two primary amine groups (-C(NH₂)₂). This partitioning allows for consistency with the existing CHARMM CHEQ protein force field and permits use of the existing non-bond (LJ and electrostatic) parameters for arginine from the polarizable force field. The approach has been applied previously by our group in the treatment of proteins, lipids, and carbohydrates[164, 29, 28, 26, 119, 174, 173]. The isotropic, gas-phase molecular polarizability for this molecule was determined to be 6.4 Å³ compared to the value of 7.0 Å³ from MP2/aug-cc-pVTZ calculations. A reduction in the force field molecular polarizability is consistent with the decrease in the intrinsic molecular polarizability observed, in theory, when going from gas to condensed-phase. However, the exact magnitude of this reduction is currently unknown and poses a challenge for force field development. We consider only the protonated methyl guanidinium model compound for our studies. Recent studies[170, 79, 77] have explored the shift in stability of the protonated and unprotonated species, as manifested in pKa shifts, along the bilayer normal. For thin membranes, it has been suggested that the protonated state is plausible, and sustained by a combination of lipid membrane deformation and long-lived polar (water and lipid) pores across the bilayer stabilizing the charge. Acknowledging these studies, we focus here on the free energetics of partitioning of the charged species.

The non-bond (Lennard-Jones) interactions between methyl guanidinium and lipid head group analogues dimethyl phosphate (DMP) and tetramethyl ammonium (TMA), as well as with solvent species (water and chloride), were validated through

the comparison of gas-phase small molecule geometries and interaction energies calculated using the CHEQ force field with those calculated using high level quantum mechanics. All QM dimer structures were optimized at the MP2/aug-cc-pVTZ level with the exception of the mguanH⁺/DMP dimer, which was optimized using the 6-31++g(2d,p) basis set. Interaction energies were calculated at the MP2/aug-cc-pVTZ level using the previously optimized structures. Hydrogen bond distances and interaction energies are shown in Table 3.1 and, although overestimated, the hydrogen bond distances exhibit suitable agreement between the force field and MP2/aug-cc-pVTZ optimized structures. Interaction energies are consistently underestimated but are in fair agreement with QM values. In the absence of laborious reparameterization of the methyl guanidinium interactions with all system species, we consider it sufficient that for the purposes of the present work, the trend of relative interaction strengths based on QM and force field calculations are equivalent, with the strongest interactions occurring between mguanH⁺ and DMP.

3.1.1 Methyl Guanidinium Hydration Free Energy via Thermodynamic Integration

To further describe the quality of the present methyl guanidinium interactions with solvent, as well as to compare with existing literature data from earlier computational and experimental studies, hydration free energies of methyl guanidinium in dilute aqueous and hexane solutions were calculated using a cubic box of 988 TIP4P-FQ water molecules (or 216 hexane molecules) and one mguanH⁺ molecule via thermodynamic integration (TI). Following the two step decoupling procedure described by Warren et al for single ion hydration[165], the mguanH⁺ is first electrostatically decoupled from the solvent followed by a decoupling of the non-bonded Lennard-Jones (LJ) interactions.

$$\Delta G_{\lambda_1+\lambda_2}^{TI} = \Delta G_{\lambda_1}^{TI} + \Delta G_{\lambda_2}^{TI} = \int_0^1 d\lambda_1 \left\langle \frac{dH(\lambda_1)}{d\lambda_1} \right\rangle_{\lambda_2=0} + \int_0^1 d\lambda_2 \left\langle \frac{dH(\lambda_2)}{d\lambda_2} \right\rangle_{\lambda_1=1} \quad (3.1)$$

Molecule	H-Bond Type	R_{H-X}^{FF} (Å)	R_{H-X}^{QM} (Å)	E_{int}^{FF} (kcal/mol)	E_{int}^{QM} (kcal/mol)
DMP	H ₂ NH-O	1.69	1.57	-113.73	-120.33
	H ₂ NH-O	1.69	1.60		
TMA	-	-	-	58.67-14.46	51.94
Water	H ₂ NH-O	2.18	2.02	-12.82	-16.57
	H ₂ NH-O	2.18	2.00		
	NH-O	2.31	2.00	-12.00	-16.42
	H ₂ NH-O	2.10	2.02		
	H ₂ NH-O	2.02	1.83	-11.80	-13.39
	H ₂ CH-O	2.83	2.76		
	H ₂ CH-O	2.83	3.00		
Chloride	H ₂ NH-Cl	2.30	1.96	-93.62	-114.55
	H ₂ NH-Cl	2.31	2.01		
	NH-Cl	2.36	1.92	-92.19	-112.32
	H ₂ NH-Cl	2.26	2.05		
	H ₂ NH-Cl	2.18	1.70	-91.63	-115.63
	H ₂ CH-Cl	2.92	3.07		
	H ₂ CH-Cl	2.92	2.74		

Table 3.1: Hydrogen bond distances and interaction energies between methyl guanidinium and lipid head group analog molecules dimethyl phosphate (DMP) and tetramethyl ammonium (TMA), water, and chloride calculated using the CHARMM CHEQ force field (FF). Quantum mechanical (QM) interaction energies were calculated at the MP2/aug-cc-pvtz level of theory using counterpoise correction. All QM calculations were carried out using the Gaussian 03 package[41]. The H-Bond type indicates the specific atoms involved to differentiate between methyl guanidinium hydrogens belonging to NH₃, NH, and CH₃ groups. The range in values given for the mguan/TMA FF interaction energy represent the variation in the interactions found given distance separations (measured between the central carbon of mguanH⁺ and the central nitrogen of TMA) from 5.7 to 22.7 Å between the two like-charged species while the QM interaction is for an analogous structure with a separation of 6.1 Å. The three values given for the interaction energies between mguanH⁺ and both water and chloride represent three unique and stable geometries around methyl guanidinium.

where $H(\lambda)$ is the Hamiltonian for the system while λ_1 and λ_2 are path coordinates for the electrostatic and LJ decoupling, respectively. This scheme allows for a complete decoupling of solute-solvent interactions while avoiding any errors arising from an exposed charge in the absence of any LJ-repulsion. Double wide sampling (forward and reverse) is employed for both decoupling schemes to reduce sampling bias. Each lambda window was sampled for a total of 225 ps of molecular dynamics, with the first 25 ps taken as equilibration and the last 200 ps considered for averaging. Simulations were performed in the NPT ensemble with a pressure of 1 atm and temperature of 323 K. To account for non-bonded LJ interactions beyond the finite cutoff distance, a long range correction is estimated, as described previously by Zhong et al[174], using an analytic repulsion-dispersion correction suggested by Shirts[142]:

$$E_{LRC}(r_{ij}) = \sum_i \sum_j 16 \pi \rho \epsilon_{ij} \int_{r=r_{on}}^{\infty} \left[\left(\frac{\sigma_{ij}}{r_{ij}} \right)^{12} - \left(\frac{\sigma_{ij}}{r_{ij}} \right)^6 \right] (1 - S(r_{ij})) r_{ij}^2 dr \quad (3.2)$$

where i and j run over the solute and solvent atoms, respectively, ρ is the number density of the solvent molecules, ϵ_{ij} is the LJ well-depth, σ_{ij} solute-solvent effective LJ diameter, r_{on} is the separation at which the switching function activates, and r_{off} is the separation distance at which the LJ cutoff potential is zero (the switching function is zero). The switching function, $S(r_{ij})$, is defined in CHARMM as

$$S(r_{ij}) = \begin{cases} 1 & r_{ij} \leq r_{on} \\ \frac{(r_{off}^2 - r_{ij}^2)^2 (r_{off}^2 + 2r_{ij}^2 - 3r_{on}^2)}{(r_{off}^2 - r_{on}^2)^3} & r_{on} < r_{ij} \leq r_{off} \\ 0 & r_{ij} > r_{off} \end{cases} \quad (3.3)$$

We also add an *a posteriori* correction to account for contributions from the interfacial potentials of the air-water and air-hexane interfaces. The interfacial potential of a system can be calculated through double integration of charge density as a function of distance from the center of the solvent layer along the interface normal as was shown in Equation 2.8[48].

3.1.2 Potential of Mean Force

To calculate the equilibrium potential of mean force (PMF) for methyl guanidinium traversing the lipid membrane, umbrella sampling windows were constructed along a reaction coordinate representing the z -component of the difference between the centers of mass of mguanH⁺ and the lipid bilayer. Windows were constructed at 1 Å intervals in bulk solution ($-35 \text{ Å} \leq z \leq -33 \text{ Å}$) and 0.5 Å intervals at the water-lipid interface and in the interior of the membrane ($-32.5 \text{ Å} \leq z \leq 0 \text{ Å}$) for a total of 69 independent simulation windows. Each window was sampled between approximately 5.0 and 7.5 ns. The Weighted Histogram Analysis Method (WHAM)[67] was used for post-simulation unbiasing. The center of mass restraint was imposed using the CHARMM miscellaneous mean field potential (MMFP) utility[31] and was continuously monitored to ensure sufficient overlap between adjacent windows. In order to maintain the system geometry an additional planar restraint was enforced on the center of mass of the bilayer to prevent drift of the lipid in the z -direction.

To independently confirm the PMF computed via umbrella sampling and WHAM unbiasing of probability distributions as well as establish a method to allow decomposition of the overall PMF into contributions from various system components (such as water, lipid, ions, etc.), we use a somewhat *ad hoc* force-based approach as follows. The force decomposition method and caveats related to the use of a lipid reference and cutoff versus PME electrostatics has been discussed in detail by Li et al[77], and we refer the reader to that reference and the associated Supporting Information for relevant details. We compute the PMF defined as:

$$\Delta W = - \int_{\zeta=0}^{\zeta=-35} \langle F_z(\zeta) \rangle d\zeta \quad (3.4)$$

where ζ is the z -component of the center of mass distance between mguanH⁺ and the lipid bilayer, $\langle F_z \rangle$ is the average force in the z -direction (normal or the bilayer) experienced by the mguanH⁺ when it is at position ζ . The PMF represents the reversible work associated in changing the relative center of mass distance from a value of -35 Å

(methyl guanidinium in bulk solution) to 0 Å (methyl guanidinium in bilayer center). Since we are using data from the harmonically-restrained MD simulations (which allow a narrow Gaussian distribution of positions centered at the unique positions selected along the reaction coordinate) the average force along the reaction coordinate, $\langle F_z \rangle$, is not exactly associated with a unique value of the reaction coordinate, but averaged over this narrow Gaussian distribution of positions; in this sense, we consider this an *ad hoc* approach. Based on the current results (and those published previously[9]), we see that both approaches lead to self-consistent results. Finally, we consider the total force acting on the methyl guanidinium as well as the decomposition of the total force into constituent contributions:

$$\begin{aligned}
\Delta W &= \Delta W_{\text{Lipid}} + \Delta W_{\text{MguanH}^+} + \Delta W_{\text{Solvent}} \\
&= - \int_{\zeta=0}^{\zeta=-35} \langle F_{z,\text{Lipid}}(\zeta) \rangle d\zeta - \int_{\zeta=0}^{\zeta=-35} \langle F_{z,\text{MguanH}^+}(\zeta) \rangle d\zeta \\
&\quad - \int_{\zeta=0}^{\zeta=-35} \langle F_{z,\text{Solvent}}(\zeta) \rangle d\zeta
\end{aligned} \tag{3.5}$$

where the solvent contribution can be further decomposed into water and inorganic ion (potassium and chloride ion) contributions:

$$\begin{aligned}
\Delta W_{\text{Solvent}} &= \Delta W_{\text{Water}} + \Delta W_{\text{Potassium}} + \Delta W_{\text{Chloride}} \\
&= - \int_{\zeta=0}^{\zeta=-35} \langle F_{z,\text{Water}}(\zeta) \rangle d\zeta - \int_{\zeta=0}^{\zeta=-35} \langle F_{z,\text{Potassium}}(\zeta) \rangle d\zeta \\
&\quad - \int_{\zeta=0}^{\zeta=-35} \langle F_{z,\text{Chloride}}(\zeta) \rangle d\zeta
\end{aligned} \tag{3.6}$$

To investigate the effect of the inorganic ion concentration on the PMF, we construct a KCl-free mguanH⁺-lipid system in pure water. This No Salt system is similar to the 1 M KCl Salt system described previously except that all of the inorganic ions have been removed (except one Cl⁻ to maintain charge neutrality). A series of

umbrella sampling windows were constructed analogous to those of the Salt system (69 total) and MD simulations were run for approximately 10 ns.

To study the importance of continuous solvation on the ability of mguanH^+ to penetrate the bilayer and its ramifications on the PMF for permeation we construct a Water Excluded system, analogous to the 1 M KCl Salt system, with an added restraint to prevent water from entering the center of the membrane. The planar restraint was added using the MMFP utility which imposes a penalty function to prevent water from penetrating the lipid further than $\pm 12 \text{ \AA}$ from the membrane center in the z -direction. This effectively dehydrates the lipid below the carbonyl groups and prevents mguanH^+ from bringing any solvating waters into the membrane. Umbrella sampling windows were constructed similar to the previous systems but with additional windows spaced at 0.25 \AA intervals added in the lipid interior ($-4.75 \text{ \AA} \leq z \leq 0 \text{ \AA}$). Higher harmonic force constants were required due to the difficulty of generating adjacent windows at distances further than 0.25 \AA while approaching the center of the membrane. Each window of the Water Excluded system (79 total) was run for approximately 10 ns.

3.2 Results and Discussion

3.2.1 Hydration Free Energies

Correction factors for the long-range LJ interactions (past the finite cutoff) for the mguanH^+ /water and mguanH^+ /hexane systems were calculated to be -0.90 and -5.52 kcal/mol , respectively. The interfacial potential of TIP4P-FQ water (at 323 K) was previously found to be -12.45 kcal/mol [84] while that of hexane (at 298 K) was found to be -4.12 kcal/mol [118]. We assume that the interfacial potential of hexane will not change significantly within the temperature range of 298 to 323 K . Taking into account the correction factors results in a hydration free energy for mguanH^+ in pure TIP4P-FQ (air to water) to be $-58.1 \pm 0.09 \text{ kcal/mol}$ and that of mguanH^+ in pure hexane (air to hexane) to be $-30.0 \pm 0.05 \text{ kcal/mol}$ which results in a partitioning free energy (water to hexane) of $28.1 \pm 0.07 \text{ kcal/mol}$. These values compare fairly well with those of Vorobyov et al using Drude polarizable force fields in

which the authors find the hydration free energies for mguanH^+ in water and in hexane to be -61.72 ± 0.09 kcal/mol and -27.54 ± 0.16 kcal/mol, respectively, and an overall partitioning free energy (water to hexane) of 34.69 ± 0.19 [161]. The lower value we find for the hydration free energy of mguanH^+ in TIP4P-FQ water may be related to the underestimated interaction energy found using the CHEQ force field versus quantum mechanical calculations.

3.2.2 Salt PMF

Figure 3.1a shows the total PMF based on umbrella sampling (red, solid curve) and integrated force (black, dashed curve) for mguanH^+ traversing the lipid bilayer; the dashed curve is shifted by -5 kcal/mol for clarity. The PMF shows a minimum of -4.6 kcal/mol (relative to bulk water) in the region of the lipid head groups. The stability of methyl guanidinium near the lipid head groups has also been observed in simulations of an unrestrained mguanH^+ which crosses the bilayer-water interface and preferentially resides in the head group region (see Appendix B and Figure B.3 therein). The barrier reaches a peak of around 28 kcal/mol (relative to the global minimum in the head group region) at the center of the membrane. This barrier is about 5-10 kcal/mol higher than, but reasonably consistent with, previous results using polarizable, non-polarizable and coarse-grained force fields to simulate the transfer of guanidinium, methyl guanidinium, propyl guanidinium, and an exposed arginine attached to a polyleucine alpha-helix across a lipid membrane[136, 33, 77, 161, 78].

The decomposition of the integrated force PMF (Figure 3.1b) shows that the stabilizing contribution of the lipid (solid, black curve) is offset by the slightly more destabilizing contribution from the solvent (red, dashed curve). After further decomposition (Figure 3.1c) of the solvent, the destabilizing contribution arises solely from chloride (red, dashed curve). The water (solid, blue curve) and potassium (dotted, black curve) contributions are stabilizing but not sufficiently adequate to balance the large (about 560 kcal/mol) chloride contribution. The slopes of the profiles are indicative of the sign (direction) of the z -component forces acting on mguanH^+ at varying

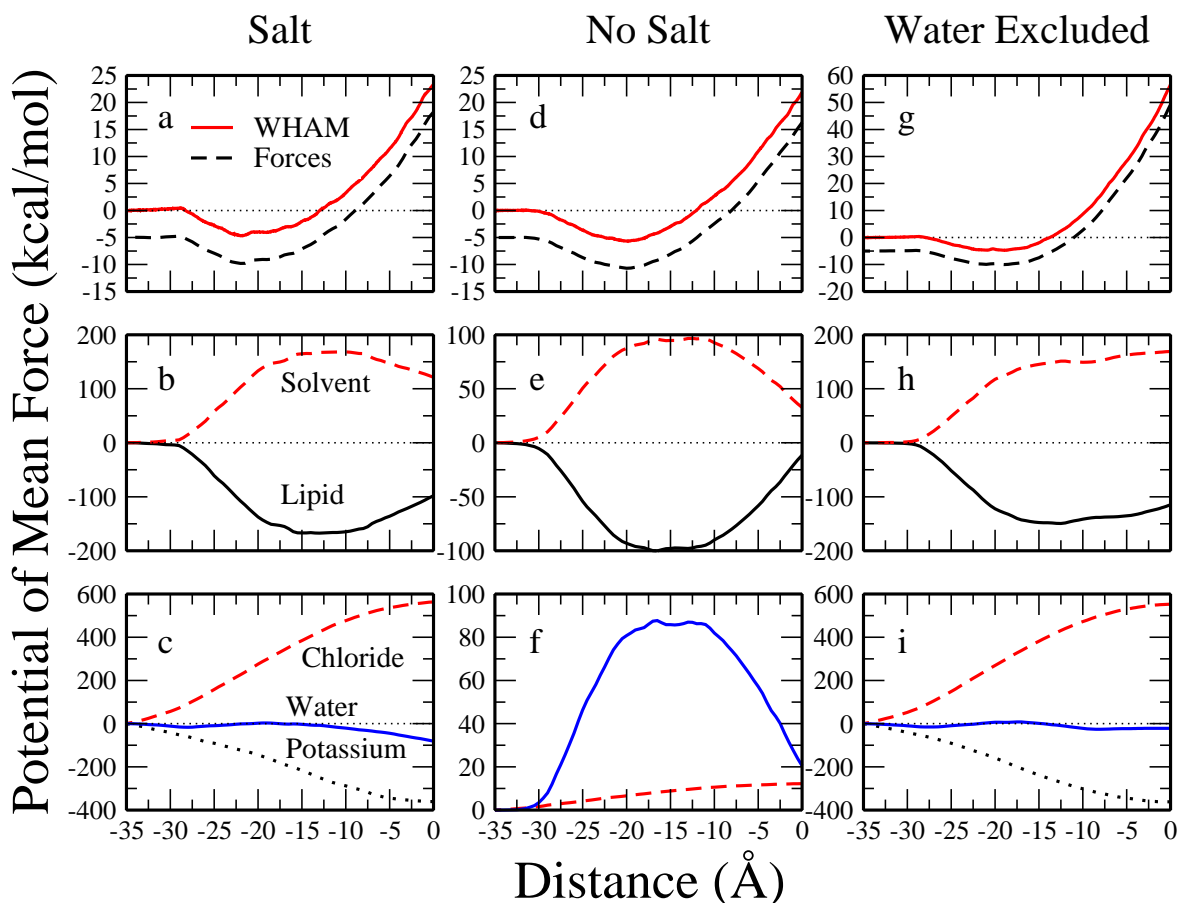


Figure 3.1: Decomposition of the potential of mean force for the Salt, No Salt, and Water Excluded systems. (a, d, g) The PMFs calculated via umbrella sampling with WHAM analysis as well as through integration of forces. The integrated force profiles have been offset by -5 \AA for clarity. (b, e, h) Decomposition of the total PMF into solvent (red, dashed curves) and lipid contributions (solid, black curves). (c, f, i) Decomposition of the solvent contributions into constituent water (solid, blue curves), chloride ion (red, dashed curves), and potassium ion (black, dotted curves) contributions. Dotted lines at 0 were added to clarify positive and negative PMF contributions.

distances from the center of the bilayer. The total lipid contribution is increasingly stabilizing as the mguanH^+ travels into the membrane head group region from the bulk, reaching a plateau from about -15 to -10 Å (in the area of the lipid carbonyls), and becomes less stabilizing as mguanH^+ approaches the membrane center; a large destabilization (positive slope leading to negative z-direction forces) arises from the large electrostatic forces of the head groups and carbonyl moieties of distant lipids attracting the positively-charged cation. Similar but opposite behavior is seen with the solvent contribution which is increasingly destabilizing moving from the bulk and into the membrane interface, plateauing in the carbonyl region, and becoming less destabilizing towards the center of the bilayer due to the increased stabilization from water solvating mguanH^+ at the center of the membrane. The ion contributions show fairly linear behavior from the bulk and into the lipid, reaching a plateau towards the center of the membrane where the force of the ions on mguanH^+ will be minimal. We observe over the course of the simulation that, for the window in which the mguanH^+ is in the center of the bilayer ($z = 0$), there is at least one lipid phosphate group strongly associating with the mguanH^+ 94 % of the time as well as several water molecules (1 to 7 on average, and up to 12 in rare instances) surrounding it. We define a lipid or water molecule as strongly associating if the lipid phosphate or water oxygen atoms are within 5 Å of the mguanH^+ center of mass. Coordination profiles and histograms are presented in Figure 3.2. The profile showing the number of coordinating waters as a function of time (top, red profile) has been offset by 4 for clarity with a dashed red line added to indicate zero. Our results are in qualitative agreement with the solvation profiles observed for mguanH^+ in the work of Li et al[77]. We will consider the nature of the water contributions in the various systems (as shown in Figure 3.3) further below.

3.2.3 No Salt PMF

The large and sole destabilizing contribution of the chloride anions to the total PMF leads us to explore the effects of ion concentration on the free energetics of

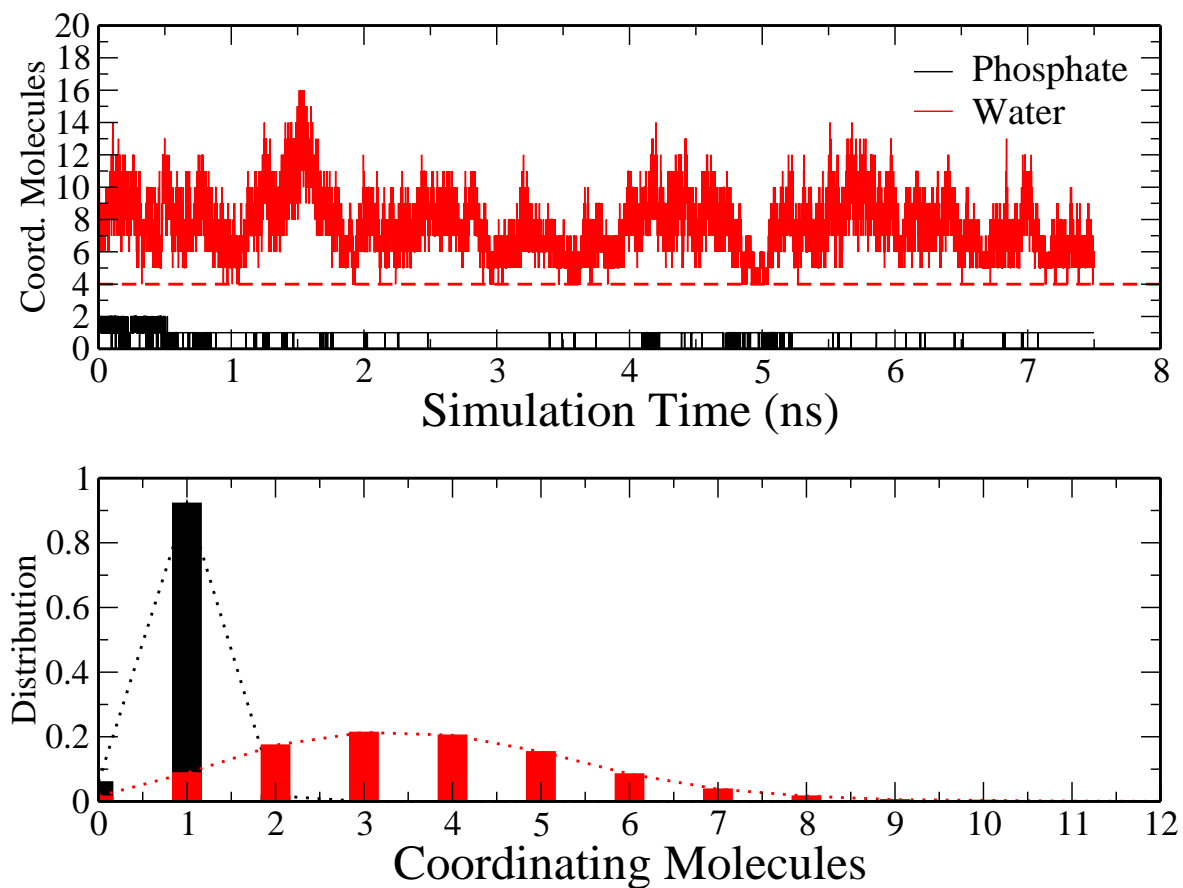


Figure 3.2: Number of coordinating lipid phosphate (black) and water (red) molecules surrounding methyl guanidinium (within 5 Å of the mguanH⁺ center of mass) at the center of the lipid membrane as a function of simulation time (top) and as a distribution over all data (bottom) for the Salt system. The number of coordinating water molecules (top, red profile) has been offset by 4 for clarity with the dashed red line indicating zero.

mguanH⁺ permeation into the bilayer; we thus consider the extreme case of zero salt concentration. Figure 3.1d shows the total PMF profiles (WHAM-based and integrated forces) for the No Salt system, which is similar in shape and magnitude with the PMF of the Salt system; the black dashed line is the result of the force-based PMF, shifted by -5 kcal/mol for clarity. A global minimum of -5.7 kcal/mol is seen in the head group region of the lipid, similar to the -4.6 kcal/mol minimum found in the Salt system. This slight (1.1 kcal/mol) difference may be caused by the accessibility of additional mguanH⁺ bonding sights in the lipid that had previously been occupied by potassium ions. Taking into account the slightly deeper minimum we see a barrier peak of about 28 kcal/mol at the center of the membrane, consistent with the Salt system. In order to demonstrate that absence of ions will have no affect on the overall lipid structure, we compare heavy atom number density profiles between the Salt and No Salt systems, with details and results shown in Appendix B, Figure B.4.

The similarities between Salt and No Salt systems are intriguing due to the very large contributions that the ions have in the total Salt PMF. To further explore this we decompose the PMF into constituent contributions, as done for the Salt system, via Eqs. 3.5 and 3.6 with results shown in Fig 3.1e and f. As in the Salt system, the favorable lipid contribution (solid, black curve) is offset by an unfavorable solvent contribution (red, dashed line). While the overall shape and sign of the contribution profiles resemble that of the Salt system we note that the magnitude of the lipid and solvent interactions are much lower at the center of the bilayer in the system without salt. Further decomposition of the solvent contributions (Figure 3.1f) shows that the single chloride ion (red, dashed line) destabilizes the system by 12.5 kcal/mol. That the forces from the single chloride are indeed destabilizing (i.e, in the negative z -direction) while the methyl guanidinium is asymmetrically positioned in the negative side of the bilayer is demonstrated in Figure B.5 of Appendix B. Water (solid, blue line), having been stabilizing for the Salt system (-81 kcal/mol), now exhibits a destabilizing contribution of about 20.5 kcal/mol at the center of the bilayer. The slopes of the lipid and solvent profiles are similar with those of the Salt system with the lipid contribution

increasingly stabilizing from the bulk to the head group region, reaching a plateau from around -17.5 to -12.5 Å (slightly closer to the bulk region than in the Salt system), and becoming less stabilizing towards the center of the membrane. The solvent contribution is increasingly destabilizing until reaching a plateau and becoming less destabilizing approaching the membrane center. The water contribution, which comprises the majority of the solvent contribution, is increasingly destabilizing moving from the bulk toward the lipid and upon entering the membrane, reaching a plateau (similar to that of the solvent and lipid contributions) before becoming less destabilizing towards the center of the membrane. This behavior is starkly different from the water contribution in the system with salt; we address possible origins of this difference in Section 3.2.5.

3.2.4 Water Excluded PMF

We have seen that mguanH^+ is able to deform the membrane while remaining solvated by several water molecules which serves to stabilize the cation in the center of the membrane. We investigate the effects of removing this stabilizing water by excluding water from the center of the membrane and effectively dehydrating mguanH^+ and the lipid head groups that form the lipid deformation. The resulting umbrella sampling and force based PMFs for the Water Excluded system is shown in Figure 3.1g, the shape of which shows a much steeper rise, starting at around $z = -15$ Å (near the lipid carbonyl groups), than the PMF profiles for the Salt and No Salt systems. The PMF reaches a peak value of about 66 kcal/mol (relative to the global minimum of -4.7 kcal/mol in the head group region) at the center of the bilayer, more than twice as high than those found for the Salt and No Salt systems in which water is allowed to permeate the membrane and continuously solvate mguanH^+ and any lipid head groups accompanying the cation into the bilayer.

Decomposition of the PMF into solvent and lipid contributions shows that, as in the Salt and No Salt systems, that the solvent contribution is strongly destabilizing while the lipid contribution is stabilizing but not strong enough to offset the solvent. Decomposition of the solvent contributions shows similarities with the Salt system, in

that the chloride contribution is the only destabilizing species while the lipid, water, and potassium all stabilize the mguanH^+ in the center of the bilayer.

3.2.5 Water Contribution to Total PMFs

After decomposing the PMFs of the three systems above we find that the water contribution profiles for the 1 M systems (Salt and Water Excluded) are quite similar with one another (at least until the region where the planar water constraint takes effect), while that of the No Salt system is markedly different in magnitude and somewhat in shape. In particular, the water contribution for the Salt system shows that the water is initially stabilizing as the mguanH^+ enters the bilayer, a behavior which is not observed for the system devoid of salt. This is apparent in the direct comparison of the three water contribution profiles shown in Figure 3.3. Number density profiles for select lipid atoms (taken from a Salt system window where methyl guanidinium was in the bulk) are shown to help illustrate the various regions of the membrane. We show in Appendix B (Figure B.4) that the average lipid component distributions are similar for the Salt and No Salt systems. It appears that the local solvation of the methyl guanidinium as it enters the bilayer in the presence of salt may be similar to the solvation near the center of the bilayer, thus providing a stabilizing effect. To corroborate this conjecture, we next consider the detailed hydration forces acting on the cation as it passes through the bilayer, with particular attention to the nature (direction and magnitude) of forces from water at different locations around the cation at various positions along the bilayer normal, as well as the density weighted average force to account for variations in the amount of water in close proximity to the cation. Finally, we consider differences in the average forces in the Salt and No Salt systems.

3.2.5.1 Asymmetric Water Solvation

To investigate the difference in the water contributions to the total PMF of the Salt and No Salt systems we analyze the forces that individual water molecules exert on methyl guanidinium at various positions in the membrane. For purposes of

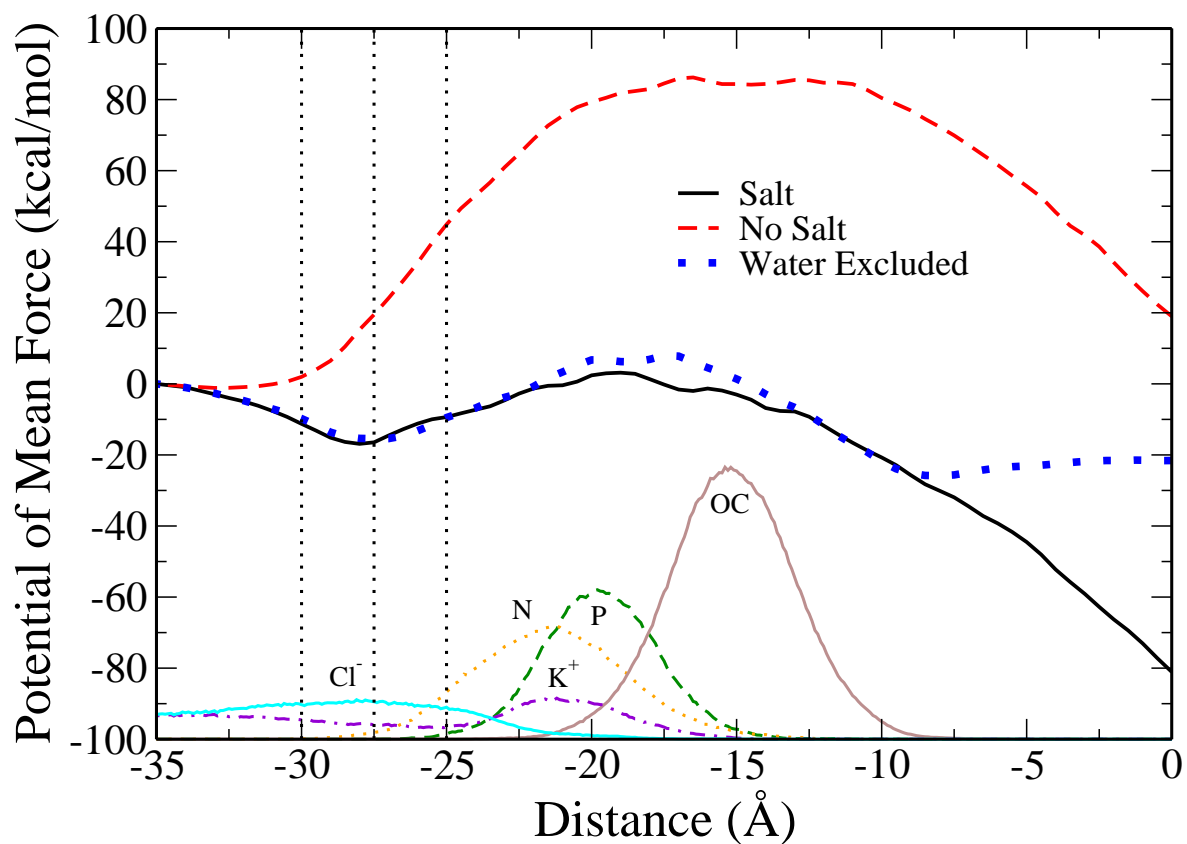


Figure 3.3: Comparison of the water contributions to the total PMF profiles of the Salt, No Salt, and Water Excluded systems. Number density profiles for select lipid and salt atoms, taken from the Salt system in which methyl guanidinium is in the bulk ($z = -35$ Å), are shown to give a sense of the lipid environment. Vertical dotted lines were added to distance values of -30, -27.5, and -25 Å to guide the reader during the discussion in the main text.

making the analysis less complicated, we consider the effects of local water arising from proximal solvation shells. As the mguanH^+ passes through the various chemical environments, from bulk solution, through the lipid head groups, and into the center of the membrane, the forces from solvating waters acting on it vary. In the bulk solution the solvation is isotropic (symmetric) and results in zero overall net force from water acting on the mguanH^+ . Once the mguanH^+ begins interacting with the lipid and penetrates the bilayer, solvation becomes increasingly asymmetric with differential magnitudes of force experienced on either side (solution side or bilayer-center side) of the mguanH^+ . To study the effects of asymmetric solvation, we consider water molecules local to mguanH^+ (waters with all atoms less than 10 Å from the center of mass of methyl guanidinium) and calculate the z -component of the force from these water molecules on methyl guanidinium at several positions of mguanH^+ as it crosses the bilayer. This calculation allows us to determine the average z -direction force on methyl guanidinium as a function of the position of the water molecule relative to the center of mass of methyl guanidinium. The reference coordinate system we choose to represent the relative position is a spherical polar coordinate system. We first define a vector $\vec{r}_{\text{cation,water}}$ between the center of mass of the methyl guanidinium and the water molecule under consideration. The angle between the z -axis of the overall system and this vector is taken to be θ , and the angle between the x -axis and the projection of $\vec{r}_{\text{cation,water}}$ onto the x - y plane is taken to be ϕ . We can thus consider the z -direction force on methyl guanidinium arising from a water molecule at a relative position defined by $|\vec{r}_{\text{cation,water}}|, \theta, \phi$ as $F_z(|\vec{r}_{\text{cation,water}}|, \theta, \phi)$. For visualization of the position-dependent force on methyl guanidinium from hydration waters, we choose to plot in ensuing figures F_z as a function of the angle θ by essentially averaging over the x - y plane angle ϕ . We use two more mappings related to the angle θ . First, the z -position of the water molecule relative to the methyl guanidinium center of mass is simply $z = |\vec{r}_{\text{cation,water}}| \cos(\theta)$. Thus, plotting with $|\vec{r}_{\text{cation,water}}| \cos(\theta)$ as one axis of the figure gives information on the z -position of the water molecule. Second, the distance in the x - y plane from the center of mass of methyl guanidinium to the water

molecule is simply $|\vec{r}_{cation,water}| \sin(\theta)$; thus, we choose this distance as the second axis in our ensuing figures.

Forces were calculated using CHARMM with PME (the same grid size used for full bilayer simulations). Coordinate files were extracted from trajectories and all lipid, salt, and water (with any atoms outside of 10 angstroms from methyl guanidinium center of mass) were deleted. The force from individual water molecules was calculated by looping through the remaining waters and calculating the position of the water and the total force on the cation. We correct for the force of methyl guanidinium on itself by deleting all waters and calculating the force on the cation in isolation.

Extracting the forces exerted by water molecules surrounding methyl guanidinium allows us to map the variation between contributions from first and higher solvation shell waters as well as show at which positions water will have a stabilizing or destabilizing effect. We analyze the final 3 ns of data from several umbrella sampling windows for both the Salt and No Salt systems. To account for any variation in water density between windows we weight the forces by the density of water (relative to the total number of water molecules sampled surrounding mguanH⁺). An example of the position-dependent (“raw”) force, relative density, and density weighted forces for the Salt system at three positions (bulk solution (-35 Å), beginning of the head group region (-27.5 Å), and the center of the membrane (0.0 Å)) is shown in Figure 3.4.

3.2.5.2 Position Dependent Forces

Panels a, d, and g of Figure 3.4 show the average force per water molecules at positions around a centered methyl guanidinium when the cation is in the umbrella sampling windows at -35, -27.5, and 0.0 Å relative separation, respectively. Shown are results for the Salt system, with analogous profiles for the No Salt systems (shown in Appendix B). The lack of data for window -35.0 Å at z -position values less than approximately -7 Å corresponds to the edge of the central simulation cell. Positive forces (lighter color) bias the cation towards the bilayer center (positive z -direction);

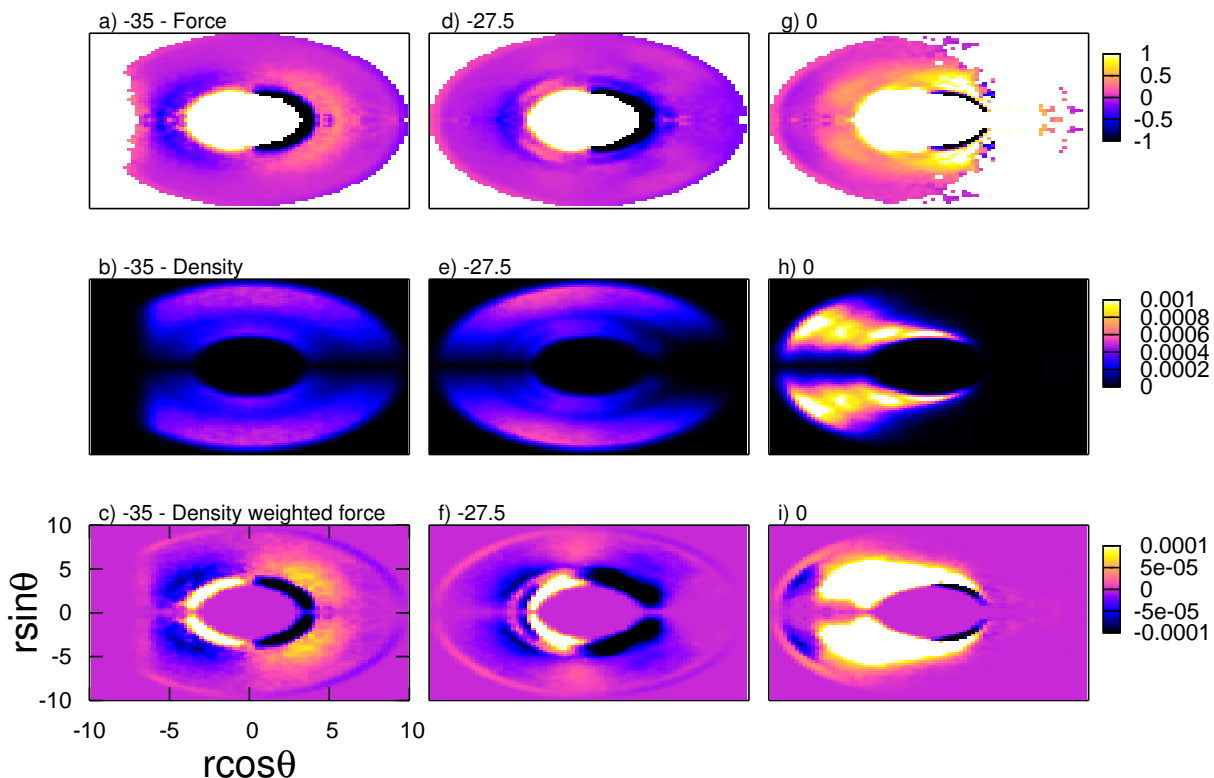


Figure 3.4: Example of the density weighting of force from water molecules on methyl guanidinium for the Salt system. a), d), and g) Magnitude and direction of the z -component of the force of water molecules (within 10 \AA) acting on methyl guanidinium for mguanH⁺-lipid center of mass separations of -35 , -27.5 , and 0 \AA , respectively. Positive force values, directed in the positive z -direction, serve to stabilize methyl guanidinium in the membrane while negative force values, directed in the negative z -direction, are destabilizing. White space indicates areas in which no water molecules were sampled. b), e), and h) Density of water molecules within 10 \AA of methyl guanidinium with each position relative to the total number of water molecules sampled within the 10 \AA cutoff. c), f) and i) Force of water molecules weighted by the relative water densities. The lack of sampling for the window in the bulk (panels a, b, and c) past approximately -7 \AA is due to the fact that this position corresponds to the edge of the central simulation cell.

negative forces (darker color) bias the cation towards the bulk solution (negative z -direction). We note some general characteristics. In the locations closest to the cation (regardless of the ϕ angle in the x - y plane), water contributes a repulsive z -direction force. Thus, a first-solvation layer water molecule toward the bulk solution side of the cation center of mass will push the cation towards the center (as evidenced by the light color) and a first-solvation layer water molecule toward the bilayer center side will push the cation towards the bulk (dark color). Water molecules in second and higher solvation shells generally tend to attract the cation, thus contributing in a manner opposite to the first solvation layer molecules. In the bulk window, -35 \AA , contributions from water within 10 \AA are present from all positions; only at the bilayer center does the nature of water forces become asymmetric as quite evident in panel g of Figure 3.4. Panels a, d, and g only show forces at positions where water is found. This explains the lack of force data in panel g. Panels b, e, and h show the local water density, with lighter color signifying higher density than darker color. In the bulk window, the density is symmetric along the z -direction. The symmetry is lowered at -27.5 \AA , and a highly asymmetric water density distribution is found at the bilayer center where the the highest density is towards the head group and carbonyl group region. In panels c, f, and i, the total density-weighted force maps are shown. These panels recapitulate the stabilizing behavior of water in the various regions as shown for the Salt system curve in Figure 3.3. In bulk, the symmetry of water density and forces around methyl guanidinium leads to net zero total force. At the -27.5 \AA position, just past the position of the minimum in the water potential of mean force contribution in Figure 3.3, the contributions to the overall density weighted force are asymmetric, thus leading to a destabilizing force from water in this region (the slope of the PMF is positive, leading to a negative z -direction force). At the bilayer center, the strong asymmetry in water density, coupled with the stabilizing forces from water at almost all positions around the cation, leads to a net overall force in the positive z -direction, which in this case stabilizes the cation at the bilayer center. Thus, the overall effect of water conferring stability to the methyl guanidinium in the bilayer in the Salt system

arises from a combination of water density distribution and the character (sign and strength) of the force from water at various positions around the methyl guanidinium.

3.2.5.3 Density and Density-Weighted Force Differences between Salt and No Salt Systems

With our motivation being to elucidate the underlying cause for the differences in the water contributions profiles of the Salt and No Salt systems we directly compare the water densities and density weighted forces between the two systems by taking the difference between the No Salt system values and those of the Salt system; that is we compute density and density-weighted force differences as $\rho_{\text{NoSalt}} - \rho_{\text{Salt}}$ (in the case of density for instance). We compute this difference for several windows corresponding to features in the PMF water contribution profiles in Figure 3.3. The difference in water densities between the No Salt and Salt systems is shown in Figure 3.5 where positive values correspond to a higher local water density in the No Salt system relative to the Salt system; negative values correspond to the opposite. In the bulk, density differences are small. At a position of -30.0 \AA , an asymmetry emerges, with the Salt system showing more water density on the bilayer-center side of the methyl guanidinium center of mass; this region would contribute stabilizing forces on the cation and the position of -30.0 \AA corresponds to the biggest difference in the water contribution behavior; that is, the slopes of the water contributions to the PMF are opposite.

We note that based on analysis of the orientation of mguanH^+ , the molecule is oriented with the long molecular axis parallel to the z -direction, in order to maintain contact between the cationic groups and the lipids functionalities. In Appendix B, we show the position-dependent forces (Figures B.6 and B.7) and densities (Figures B.8 and B.9) for the Salt and No Salt systems for the reader's reference.

Based on the biggest difference in the water contributions to the PMF occurring at -30 \AA (Figure 3.3, the slopes are of opposite sign) we consider differences at this position. Figure 3.6 shows the density-weighted force difference (No Salt - Salt). At -30 \AA , there is a preponderance of regions of negative values around the cation, suggesting

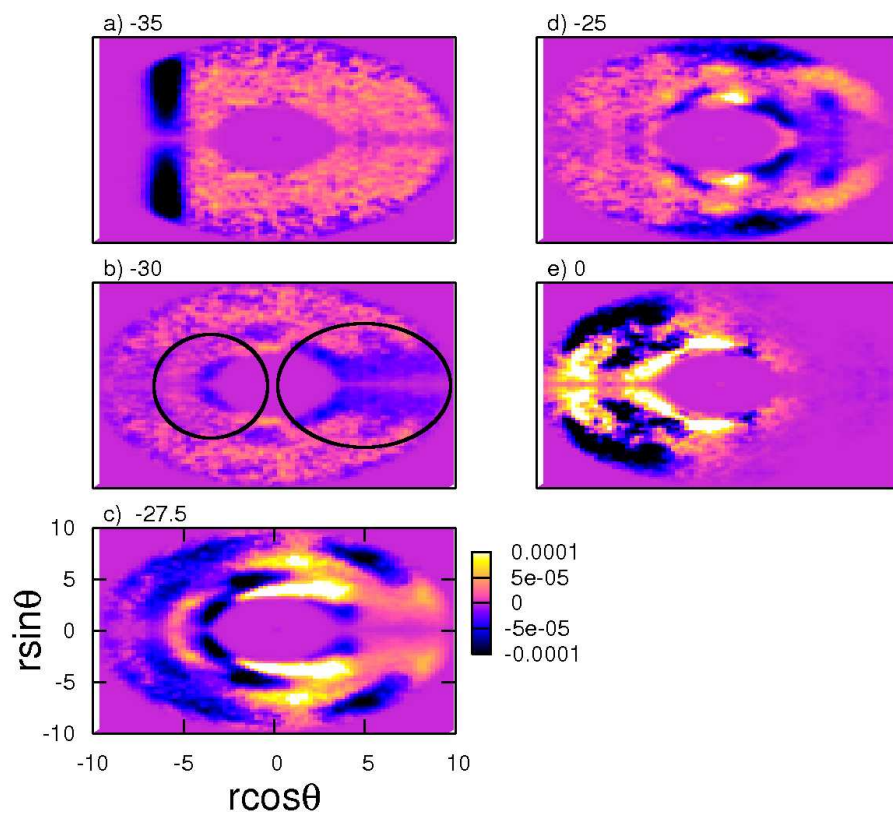


Figure 3.5: Difference in the water densities between the No Salt and Salt systems for mguan⁺-lipid center of mass separations a) -35, b) 30, c) -27.5, d) -25, and e) 0 Å. Positive values indicate that there is an increased density of water in the No Salt system at that position around methyl guanidinium relative to the Salt system while negative values indicate a decreased density in the No Salt system relative to the Salt system. Black circles have added to b) to draw attention to areas in the data discussed in the main text.

that the Salt system is contributing more stabilizing forces (the z -direction forces at most positions around the cation are more stabilizing in the Salt case than in the No Salt system as signified by the large proportion of dark colored regions). This result corresponds to the negative slope in the Salt system’s water contribution to the PMF in this region (shown in Figure 3.3). The origin of this singular difference in the behavior of water in the Salt and No Salt systems is based on the interplay of water density differences and position-dependent forces around the cation in this region. Figures B.6b and B.7b show that the nature of the position dependent z -direction forces for the Salt and No Salt system are similar (general characteristics have been discussed above). The densities, Figures B.8b and B.9b, exhibit differences in the regions corresponding to both stabilizing and destabilizing forces in both systems. Comparing Figures B.8b and B.9b shows that in the No Salt system, water density is lower in the positions where water contributes forces that tend to push the cation away from the bulk solution (simply put, at the “ends” of the cation). This is mirrored in the density difference, Figure 3.5b. In Figure 3.5b, the Salt system has higher density for z -positions between -3 to -4 Å from the center of mass of the cation; also, there is higher water density in the Salt system for values of $|\vec{r}_{cation,water}| \cos(\theta)$ from 3 to 10 Å and $|\vec{r}_{cation,water}| \sin(\theta)$ values of ± 5 Å. From Figures B.6b and B.7b, water molecules in these regions exert stabilizing forces (towards the bilayer center) except for the small region between $|\vec{r}_{cation,water}| \cos(\theta)$ values of 3 to 5 Å. Effectively, the reduced density of water in the No Salt system in the locations where water exerts forces to pull the cation towards the center leads to the dramatic differences in the water contributions to the PMF. Moreover, this effect is local (based on water molecules local to the cation).

The higher local water density in the Salt system correlates with the position of the chloride anion density profile. Because the chloride prefers to be hydrated either by water or polar head groups, it is reasonable that chloride anions bring with them water molecules to some extent. The chloride anion density reaches a maximum around -27.5 Å which corresponds to the minimum in the water contribution to the PMF. Thus, as methyl guanidinium enters the bilayer, as long as there is a local stabilizing asymmetry

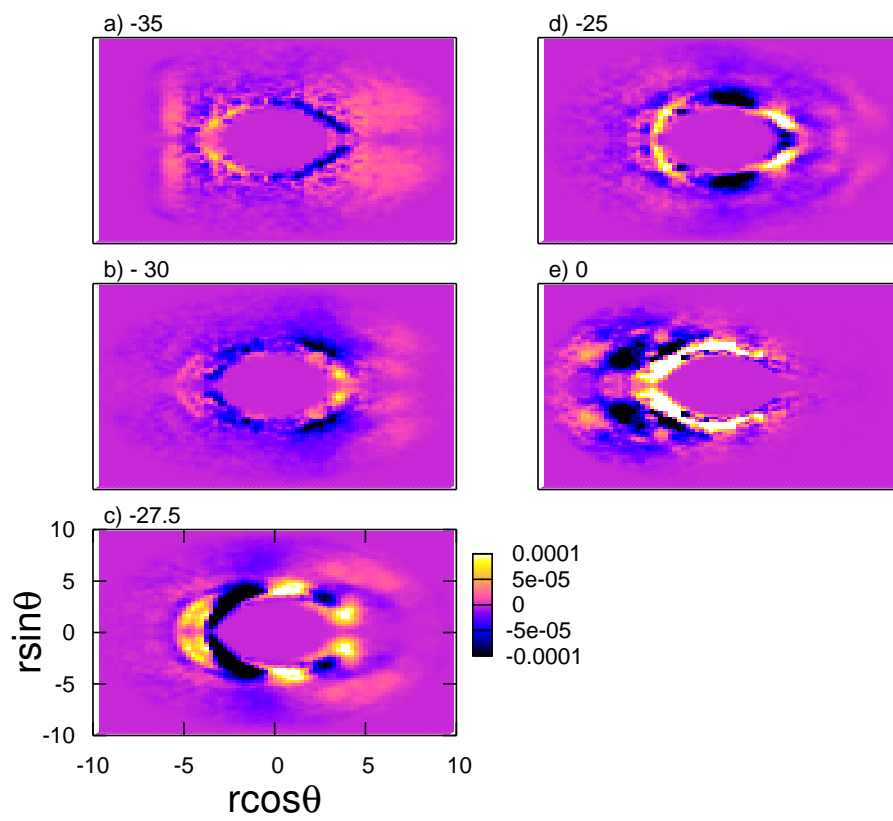


Figure 3.6: Difference in the density weighted forces between the No Salt and Salt systems for mguan-membrane center of mass separations a) -35, b) 30, c) -27.5, d) -25, and e) 0 Å.

in water density, brought about by the asymmetry in the chloride anion density, the water contribution to the PMF is stabilizing. For methyl guanidinium residing at positions between 0 and -27.5 Å, since the chloride anion density is increasing towards the bilayer, thus increasing the stabilizing water density, the water contribution to the PMF is stabilizing. Moving further into the bilayer, the same water molecules now become destabilizing, thus giving rise to the barrier before finally becoming stabilizing at the bilayer center.

Finally, we comment that at a separation of -27.5 Å, we observe more light colored regions around the cation, suggesting that contributions from local water molecules are becoming destabilizing (to an even greater extent than in the No Salt case so as to counter balance the stabilizing water contribution up to this position). Moving further into the bilayer center, the regions where the Salt system is more or less stabilizing than the No Salt system become equal, and the behavior of the water contribution in both the No Salt and Salt systems becomes analogous. At the bilayer center, due to the asymmetry in water distribution, water in both systems contributes stabilizing forces. Panel e of Figure 3.6 shows that in the No Salt system, the water molecules closer to the cation provide greater stabilization than the same water molecules in the Salt system. Moving further towards the interfacial side of the cation, the water molecules in the Salt system stabilize the cation to a greater degree than similarly positioned water molecules in the No Salt system.

3.2.6 Core Lipid and Water Contributions

To address the change in the slopes of the profiles for the lipid and water contributions to the total PMF (Figure 3.1) as the core region of the bilayer is encountered, we explore the energetics towards the center of the bilayer, in the “core” of the membrane. A water or lipid molecule is considered to be in the core if a water oxygen or lipid phosphorus has a magnitude of $|z|$ -position ≤ 13 Å. The results of this analysis for the Salt, No Salt, and Water Excluded systems are shown in Figure 3.7. For the Salt and No Salt systems we find similarly shaped profiles. The core water contribution

is negligible while mguanH^+ is in the bulk and becomes destabilizing as it approaches the carbonyl groups, with waters forced into the membrane center interacting with mguanH^+ presenting an effective “barrier” as these water molecules prefer remain in the polar environment of the carbonyl region. As mguanH^+ moves past the carbonyl groups, dragging a lipid phosphate into the center of the membrane, the solvating water mainly exists in the region of the lipid deformation and yields an increasingly stabilizing contribution. This is a partitioning of the mguanH^+ into the bilayer rather than the waters energetically stable in the carbonyl group region. This effect has been observed by Li et al[77] though to a lesser extent based on Figure 7 of Reference [77] as well as Figure S4A and S4B of the associated Supporting Information. The lipid contribution is slightly stabilizing as the lipid phosphate groups pull mguanH^+ into the membrane but becomes increasingly destabilizing as mguanH^+ moves to the other side of the phosphate groups, pulling them into the membrane, and forming a deformation of the membrane. This is qualitatively similar to what is observed by Li et al[77]. The overall profiles for the the core lipid molecules are strongly destabilizing (about 62 kcal/mol) while core water molecules are strongly stabilizing (about -57 kcal/mol) and largely offset the core lipid contribution.

Our results contrast to the results of Li et al [77] using non-polarizable force fields in that they find the core lipid, while still destabilizing (nearly 50 kcal/mol) is more than offset by the contribution from core water of about -90 kcal/mol. In our case, the contributions are of roughly equal magnitude. This difference may be due to the stronger mguanH^+ -phosphate interactions and an underestimated mguanH^+ -water interaction energy (versus QM calculated values) found using the CHEQ force field compared to the non-polarizable force field used by Li et al[77]. Nevertheless, the qualitative behavior of water in the core region appears to be independent of force field; water in the core region is relatively stabilizing as has been noted in a series of earlier studies. The Water Excluded systems shows a negligible water contribution due to the lack of water molecules solvating mguanH^+ in the center of the membrane.

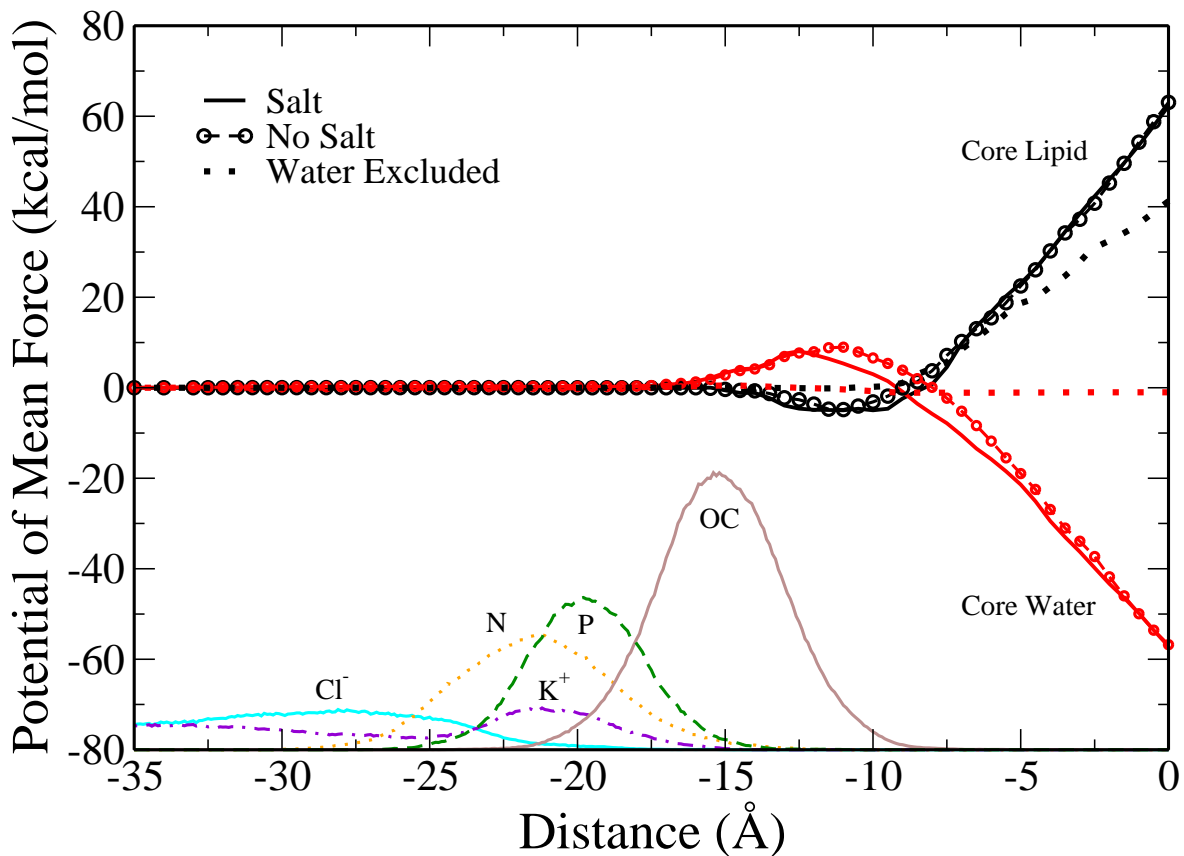


Figure 3.7: Decomposition of the potential of mean force into “core” lipid and water contributions for the Salt (black, solid curve), No Salt (red, dashed curve), and Water Excluded (blue, dotted curve) systems. Water or lipid molecules are defined as being in the membrane “core” if the water oxygen or lipid phosphorus has a $|z|$ -position ≤ 13 Å. Scaled number density profiles for select lipid and salt atoms, taken from the Salt system in which methyl guanidinium is in the bulk ($z = -35$), are included to give a sense of the lipid environment, similar to those in Figure 3.3.

3.2.7 Water Defect Mediated Lipid Deformation

Finally, to investigate the role of water penetration in the lipid deformation process we constructed a system in which the mguanH⁺ was generated and held at the center ($z = 0$) of the lipid bilayer, as opposed to slowly crossing down from bulk solution and through the lipid. A harmonic constraint was used to hold the mguanH⁺ at the center of the bilayer while a planar constraint, analogous to the one used in the Water Excluded umbrella sampling windows, prevents water from entering into the hydrophobic core of the membrane. This prevents the mguanH⁺ from being solvated at any point during the simulation. Four replicate systems were run for around 27 ns each. We find that, over the course of the replicate simulations and in the absence of water penetration into the bilayer, the lipid head groups do not deform to associate with the mguanH⁺. To test if the structure of the bilayer is truly unperturbed while mguanH⁺ is at the center of the membrane, we compare the heavy atom density profiles and head group orientation (\overline{PN} angle) with those of the umbrella sampling window in which the mguanH⁺ is located in bulk water ($z = -35 \text{ \AA}$), with results of this comparison shown in Figure 3.8. The number density profiles and \overline{PN} angle distributions show that the structure of the lipid membrane with mguanH⁺ in the center remains intact and is comparable with that of the Water Excluded umbrella sampling window with mguanH⁺ in the bulk solvent.

After several nanoseconds of dynamics on the Water Excluded, unperturbed systems, coordinate snapshots were extracted and used to create four replicate systems in which the water constraint was subsequently removed. We find that within a nanosecond, water begins to penetrate the membrane to solvate the mguanH⁺. Once water is allowed to flow into the membrane we see both lipid deformation and the penetration of chloride ions into the bilayer. Three of the replicates see a chloride ion (or ions) associating with the mguanH⁺ before the lipid phosphate can move into the center of the bilayer. Lipid phosphate then replaces the chloride in associating with the mguanH⁺ after several nanoseconds. The other replicate shows immediate membrane deformation with the lipid phosphate associating with the mguanH⁺ shortly

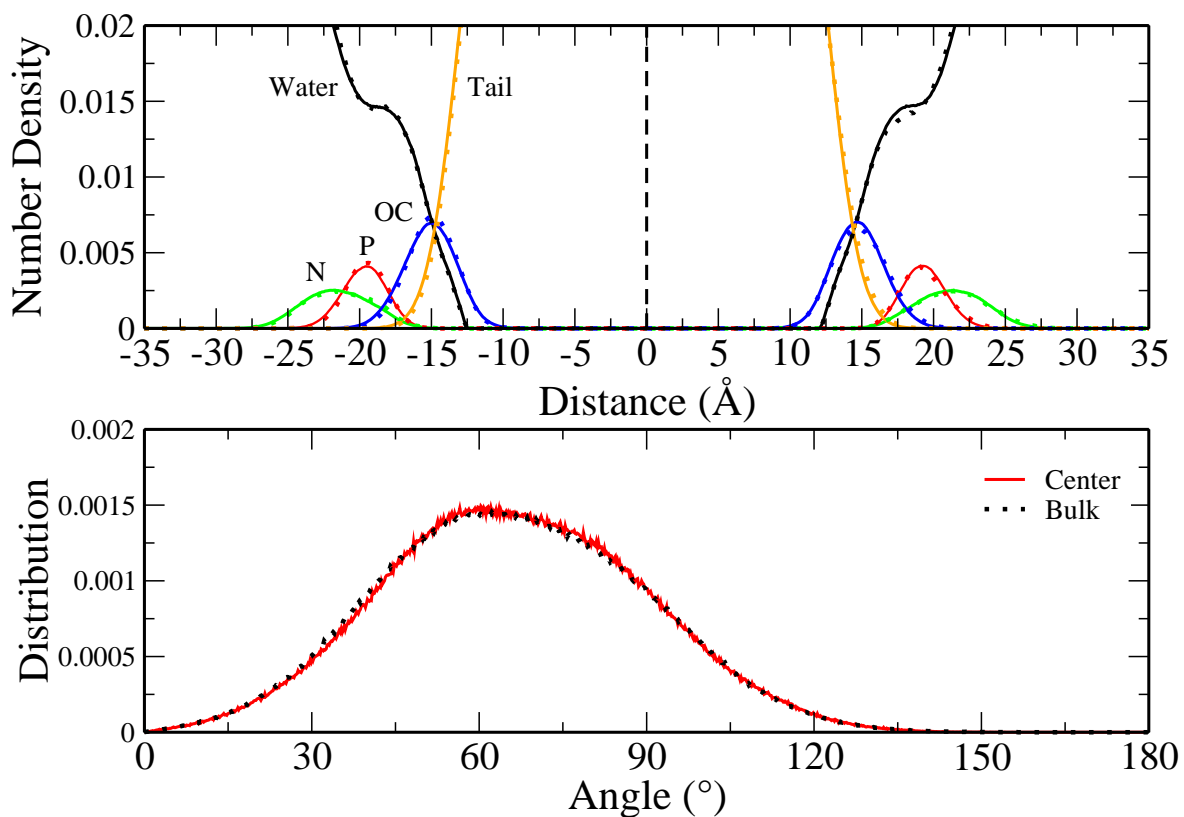


Figure 3.8: (Top) Heavy atom number density profiles for selected components (water oxygen, lipid head group phosphorus and nitrogen, lipid carbonyl oxygen, and aliphatic lipid tail carbon) of the systems with a water constraint. The membrane-centered methyl guanidinium (with unperturbed lipid) profiles are shown as solid curves while the profiles for the system with methyl guanidinium located in bulk water ($z = -35$ Å) are shown as dotted curves. The black dashed line represents the center of the bilayer ($z = 0$ Å). (Bottom) Distribution of the head group orientation measured as the angle between the \overrightarrow{PN} dipole vector and the bilayer normal (z -axis) for membrane centered (red curve) and bulk (black, dotted curve) methyl guanidinium.

after water begins to surround the arginine analog and stays as such throughout the simulation.

To explore this further we measure the distance between the the center of mass of the mguanH⁺ to the associating chloride and lipid phosphorus atoms as a function of time for each of the four replicates, with the results shown in Figure 3.9. Histograms of the number of associating species are shown below the distance profiles to indicate when a chloride (black) or lipid phosphorus (red) atom is within 5 Å of the mguanH⁺ center of mass. Chloride profiles and histograms have been shifted by 30 Å for clarity. We find that, in all of the cases in which chloride penetrates the membrane and associates with the mguanH⁺, the chlorides are originally in bulk solution and quickly move through the lipid. In one case (replicate 2) we see an exchange of chlorides where one penetrates the membrane, interacts closely with mguanH⁺, and then is replaced with a second chloride (brown profile) that moves down into the membrane center (labelled Cl⁻ 1 and Cl⁻ 2 in Figure 3.9). The positions of the phosphate groups indicates that the membrane begins to deform from a starting separation of 20 Å from the center mass of the mguanH⁺ at the beginning of the simulation (consistent with the average position of the unperturbed lipid phosphate head groups in Figure 3.8) and slowly moves towards the center of the membrane where it competes with chloride to interact directly with mguanH⁺. In replicate 3, however, we see the membrane deform quickly and the phosphate groups are able to associate with mguanH⁺ before any chlorides can enter the center of the membrane. In the cases where chloride penetrates into the membrane, it does so quickly, on the order of 1 ns or less. Moreover, the chloride is solvated by varying water molecules as it permeates from the bulk and through the membrane, as opposed to moving with a larger, constant solvation structure. Analyzing a sampling of the water that surrounds the chloride atoms in the first hydration shell (within 3.8 Å) we find that, although the chloride stays continuously hydrated throughout the simulation, the water molecules that comprise the hydration shell vary rapidly and are relatively transient. The results of this exercise demonstrate the importance of water in mediating the deformation of phosphate groups, even when the methyl

guanidinium is already at the center of the bilayer. This seems to suggest that the deformation of the lipid in terms of one or two phosphate groups associating with the charged species in the bilayer center is the inherent state when the arginine resides in the center. That is, the deformation of the lipid head groups is not an artifact of the simulation protocol that involves “pulling” along lipid molecules by their head groups as the methyl guanidinium is slowly (reversibly) transferred into the bilayer via some biasing potential.

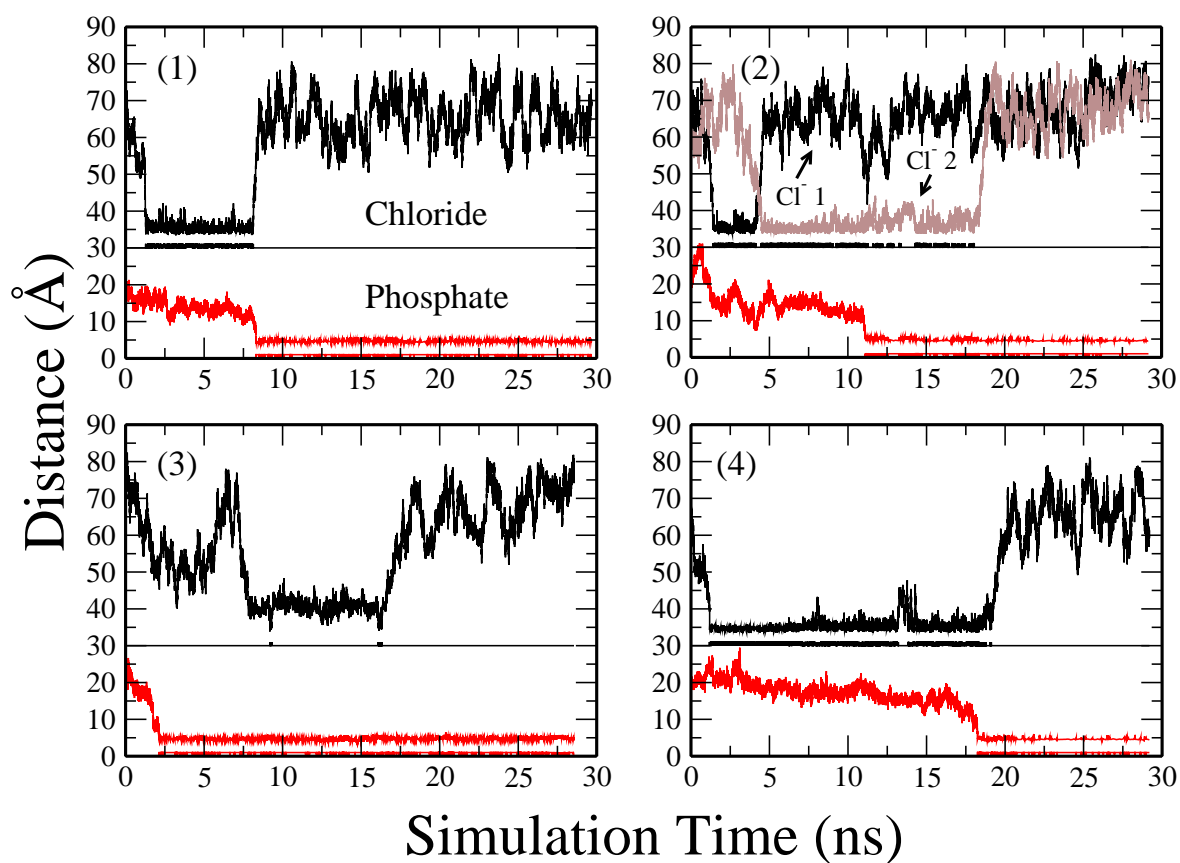


Figure 3.9: Distance profiles of chloride and lipid phosphate atoms closest to methyl guanidinium for four replicate systems in which mguanH^+ is at the center of an initially unperturbed bilayer in which the water constraint has been removed at the beginning of the simulation (time = 0 ns). Profiles are measured as the distance from the mguanH^+ center of mass to the chloride and phosphorus atoms. Histograms of the number of associating species are shown below the graphs to indicate when a chloride (black) or lipid phosphorus (red) atom is within 5 \AA of the mguanH^+ center of mass. Chloride distance profiles and histograms have been offset by 30 \AA for clarity. Replicate (2) shows two chloride atoms (the second of which is shown in brown) which are able to move toward the center of the bilayer and associate with mguanH^+ at different times during the simulation.

Chapter 4

CONCLUSION

We have presented results of the predictions of several properties of a DPPC-water monolayer using novel CHEQ force fields in conjunction with molecular dynamics simulations. The study further explored the application of non-additive electrostatic models for representing the interaction between atomic species in lipidic systems. To date, this is the second study to consider the monolayer-water properties of DPPC using fully polarizable water and lipid force fields. The CHEQ force fields used here explicitly treat electronic polarization in a classical treatment of intermolecular interactions. Structural properties of the lipid monolayer are comparable with experiment and earlier simulation studies of lipid membrane systems of equivalent size. For the polarizable force field, we note enhanced penetration of water molecules into the lipid monolayer, in agreement with the behavior observed for polarizable water in DMPC and DPPC bilayers. We find that the water dipole moment monotonically decreases from a bulk value of 2.55 D (at 323 K) to the gas-phase value in the aliphatic tail region of the monolayer.

The surface pressure, determined as the difference between the monolayer and pure water surface tensions at 323 K, is predicted to be 22.92 ± 1.29 dyne/cm, just slightly below the broad range of experimental values reported for this system. The surface tension for the DPPC-water monolayer is predicted to be 42.35 ± 1.16 dyne/cm. This value agrees with experimental results[147] as well as with DPPC monolayer simulations using state-of-the-art nonpolarizable force fields[65]. The current results of simulations predict a monolayer-water potential difference relative to the pure water-air interface of 0.64 ± 0.02 V, an improved prediction compared to the fixed-charge CHARMM27 force field, and overestimating the experimental range of 0.30 to 0.45 V.

Since the CHEQ model is a charge-based model for polarization, the current results suggest that explicitly-modeled polarization effects can offer improvements in describing interfacial electrostatics in such systems. Further development of CHARMM charge equilibration force field is ongoing and continues to correct the existing deficiencies in the spirit of force field development[114].

Using an intermediate, revised lipid force field we then investigated the thermodynamics of permeation of an amino acid side-chain analogue, methyl guanidinium, through a model lipid bilayer, DPPC. Using both umbrella sampling and reweighting in conjunction with average force decomposition, we obtained the potential of mean force for the reversible transfer of methyl guanidinium through the bilayer. We further decomposed the overall PMF into contributions from various system components including water, lipid, ions, and “core” water and lipids. We explored the effects of high salt concentrations in the bulk solution, particularly with respect to the influence of ions on the water contribution to the total PMF. We also investigated the impact of water permeation into the bilayer on lipid deformability. Finally, we performed our calculations using a charge equilibration force field developed in our laboratory (and recently modified as discussed in Appendix B). This is a further application of a new class of force fields that can allow for differences in charge distributions, in a very gross sense, when particular molecular species encounter widely varying electrochemical environments.

With respect to the overall free energetics of methyl guanidinium permeation through the bilayer, our results are qualitatively in agreement with a range of previous simulation studies. We find a free energy minimum in the head group region, which is corroborated by molecular dynamics simulations of the unrestrained methyl guanidinium (as shown in Figure B.3 of Appendix B). We find the potential of mean force for permeation to be approximately 28 kcal/mol (relative to the minimum in the head groups), within the range of values reported for similar types of simulations using fixed-charge force fields. By decomposing the overall free energy profile into contributions from various components, we find that the lipid in total confers a stabilization of the

charge cation in a range from -12 to -100 kcal/mole depending on the ionic strength of the bulk solution. For systems with 1 M KCl salt concentration in the bulk solution, the chloride anion is the sole species destabilizing methyl guanidinium in the bilayer center, with the potassium, water, and lipids all contributing stabilizing forces. In the absence of bulk electrolyte (except for a single chloride anion included in the simulation to maintain charge neutrality), we find that the overall water contribution becomes destabilizing, in stark contrast to the contributions when 1 M KCl is included in the bulk solution. Upon examining differences in local water density and density-weighted forces acting on the permeating cation, we find that the interplay between these two components leads to differences in the asymmetry of water forces on the cation that manifests in two starkly different behaviors. The presence of chloride anions in one case gives rise to an enhancement of local water density as the methyl guanidinium enters the bilayer. These results reinforce current views on the importance of surface active ions of the Hofmeister series and their interactions with phosphatidylcholine-based lipid bilayers, particularly with the penetration of such ions along with hydration layers into the solution-bilayer interface[157]. This enhanced water density in regions around the methyl guanidinium conferring stabilizing forces, relative to the case where no ions are included in the simulation, leads to the observed opposite slope in the water contribution to the total PMF as the methyl guanidinium enters the bilayer. The nature of water contributions to the free energetics of the permeant are similar to the case where no salt is included in the bath in regions along the reaction coordinate where no chloride ions are present. At the core of the bilayer, both systems display stabilizing water contributions arising from a marked water distribution asymmetry.

Finally, we find that water permeation into the bilayer is required for the deformation of individual lipid molecules and permeation of ions into the membrane. Through a series of simulations in which water is first prevented from entering the bilayer center where methyl guanidinium is restrained, and after equilibration allowed to enter the bilayer, we find that in the absence of any water defects/permeation into the bilayer, the lipid head groups do not follow the methyl guanidinium. Only after

water is allowed to enter the bilayer do we see deformation of individual lipid molecules allowing association with the amino acid analogue at bilayer center. Moreover, using the force field we have, we find that it is possible for chloride anions to enter the bilayer center very quickly after the water is allowed to enter, thus associating with the methyl guanidinium initially. However, due to the relative energetics of the interaction models used in this work, we observe that the anions in time are displaced by the lipid head group phosphates that deform (with the aid of water defects) to associate with the methyl guanidinium. We believe that this suggests that the deformation of the lipid in terms of one or two phosphate groups associating with the charged species in the bilayer center is the inherent state when the arginine resides in the center. Bekker et al[160] have elegantly demonstrated that the cation, in deforming the membrane, effectively creates an interface that precludes it from experiencing the full positive dipole potential expected for an unperturbed bilayer[161]. The deformation maintains an interface between high and low potential environments, implying that entry of a second charged species would be facilitated by the entry of the first. This non-additivity has also been demonstrated by MacCallum et al[90]. Thus, the deformation of the lipid head groups is not an artifact of the simulation protocol that involves “pulling” along lipid molecules by their head groups as the methyl guanidinium is slowly (reversibly) transferred into the bilayer via some biasing potential. This further supports numerous earlier studies pointing to the importance of water defects on a local scale in facilitating structural and dynamic aspects of membrane biophysics[88, 89, 160].

BIBLIOGRAPHY

- [1] M. P. Aliste and D. P. Tieleman. Computer simulation of partitioning of ten pentapeptides ace-wlxll at the cyclohexane/water and phospholipid/water interfaces. *BMC Biochem.*, 6:30, 2005.
- [2] M. P. Allen and D. J. Tildesley. *Computer Simulations of Liquids*. Clarendon, 1987.
- [3] T. W. Allen, O. S. Andersen, and B. Roux. Ion permeation through a narrow channel: Using gramicidin to ascertain all-atom molecular dynamics potential of mean force methodology and biomolecular force fields. *Biophys. J.*, 90:3447–3468, 2006.
- [4] Toby W. Allen, Olaf S. Andersen, and Benoit Roux. Energetics of ion conduction through the gramicidin channel. *PNAS*, 101(1):117–122, 2004.
- [5] Toby W. Allen, Turgut Bastug, Serdar Kuyucak, and Shin-Ho Chung. Gramicidin a channel as a test ground for molecular dynamics force fields. *Biophys. J.*, 84:2159–2168, 2003.
- [6] V. M. Anisimov, G. Lamoureux, I. V. Vorobyov, N. Huang, B. Roux, and A. D. MacKerell Jr. Determination of electrostatic parameters for a polarizable force field based on the classical Drude oscillator. *J. Chem. Theory Comput.*, 1:153–168, 2005.
- [7] Y. S. Badyal, M. L. Saboung, D. L. Price, S. D. Shastri, D. R. Haeffner, and A. K. Soper. Electron distribution in water. *J. Chem. Phys.*, 112:9206, 2000.
- [8] S. Baoukina, L. Monticelli, S. J. Marrink, and D. P. Tieleman. Pressure-area isotherm of a lipid monolayer from molecular dynamics simulations. *Langmuir*, 23:12617–12623, 2007.
- [9] B. A. Bauer, T. R. Lucas, D. Meninger, and S. Patel. Water permeation through DMPC lipid bilayers using polarizable charge equilibration force fields. *Chem. Phys. Lett.*, 508:289–294, 2011.
- [10] M. L. Berkowitz, D. L. Bostick, and S. A. Pandit. Aqueous solutions next to phospholipid membrane surfaces: Insights from simulations. *Chem. Rev.*, 106:1527–1539, 2006.

- [11] Simon Berneche and Benoit Roux. The ionization state and the conformation of glu-71 in the kcsa k⁺ channel. *Biophys. J.*, 82:772–780, 2002.
- [12] R. L. Biltonen and D. Lichtenberg. The use of differential scanning calorimetry as a tool to characterize liposome preparations. *Chem. Phys. Lipid*, 64:129–142, 1993.
- [13] Mikhail Bogdanov, P. N. Heacock, and William Dowhan. A polytopic membrane protein displays a reversible topology dependent on membrane lipid composition. *EMBO J.*, 21:2107–2116, 2002.
- [14] Mikhail Bogdanov, J. Xie, P. N. Heacock, and William Dowhan. To flip or not to flip: Lipid-protein charge interactions are a determinant of the final membrane protein topology. *J. Cell Biol.*, 182:925–935, 2008.
- [15] Mikhail Bogdanov, Jun Xie, and William Dowhan. Lipid-protein interactions drive membrane protein topogenesis in accordance with the positive inside rule. *Journal of Biological Chemistry*, 284(15):9637–9641, 2009.
- [16] H. Brockman. Dipole potential of lipid-membranes. *Chem. Phys. Lipids*, 73:57–79, 1994.
- [17] B. R. Brooks, R. E. Bruccoleri, B. D. Olafson, D. J. States, S. Swaminathan, and M. Karplus. Charmm: A program for macromolecular energy, minimization, and dynamics calculations. *J. Comput. Chem.*, 4:187–217, 1983.
- [18] R. Car and M. Parrinello. Unified approach for molecular dynamics and density functional theory. *Phys. Rev. Lett.*, 55:2471–2474, 1985.
- [19] S. L. Carnie and G. N. Patey. Fluids of polarizable hard-spheres with dipoles and tetrahedral quadrupoles: Integral-equation results with application to liquid water. *Mol. Phys.*, 47(5):1129–1151, 1982.
- [20] F. Castro-Roman, R. W. Benz, S. H. White, and D. J. Tobias. Investigation of finite system-size effects in molecular dynamics simulations of lipid bilayers. *J. Phys. Chem. B*, 110:24157–24164, 2006.
- [21] R. Chelli and P. Procacci. A transferable polarizable electrostatic force field for molecular mechanics based on the chemical potential equilization principle. *J. Chem. Phys.*, 117:9175–9189, 2002.
- [22] Bin Chen, Jianhua Xing, and J. Ilja Siepmann. Development of polarizable water force fields for phase equilibrium calculations. *J. Phys. Chem. B*, 104:2391–2401, 2000.
- [23] R. J. Clarke. The dipole potential of phospholipid membranes and methods for its detection. *Adv. Colloid Interface Sci.*, 89:263–281, 2001.

- [24] J. M. Crane, G. Putz, and S. B. Hall. Persistence of phase coexistence in disaturated phosphatidylcholine monolayers at high surface pressures. *Biophys. J.*, 77:3134–3143, 1999.
- [25] T. Darden, D. York, and L. Pedersen. Particle mesh ewald: An $N \cdot \log(N)$ method for ewald sums in large systems. *J. Chem. Phys.*, 98:10089–10092, 1993.
- [26] J. E. Davis and S. Patel. Charge equilibration force fields for lipid environments: application to fully hydrated dppc bilayers and dmpe-embedded gramicidin a. *J. Phys. Chem. B*, 113:9183–9196, 2009.
- [27] J. E. Davis and S. Patel. Revised charge equilibration parameters for more accurate hydration free energies of alkanes. *Chem. Phys. Lett.*, 484:173–176, 2010.
- [28] J. E. Davis, O. Rahaman, and S. Patel. Molecular dynamics simulations of a DMPC bilayer using nonadditive interaction models. *Biophys. J.*, 96:385–402, 2009.
- [29] J. E. Davis, G. L. Warren, and S. Patel. Revised charge equilibration potential for liquid alkanes. *J. Phys. Chem. B*, 112:8298–8310, 2008.
- [30] B. de Courcy, J-P. Piquemal, C. Garbay, and N. Gresh. Polarizable water molecules in ligand-macromolecule recognition. impact on the relative affinities of competing pyrrolopyrimidine inhibitors for fak kinase. *J. Amer. Chem. Soc.*, 132:3312, 2010.
- [31] D. Deglov and B. Roux. Finite representation of an infinite bulk system: solvent boundary potential for computer simulations. *J. Chem. Phys.*, 100:9050, 1994.
- [32] H. Dominguez, A. M. Smondyrev, and M. L. Berkowitz. Computer simulations of phosphatidylcholine monolayers at air/water and ccl_4 /water interfaces. *J. Phys. Chem. B*, 103:9582–9588, 1999.
- [33] S. Dorairaj and T. W. Allen. On the thermodynamic stability of a charged arginine sidechain in a transmembrane helix. *PNAS*, 104:4943–4948, 2007.
- [34] Jean-Paul Douliez, Alain Leonard, and Erick J. Duforc. Restatement of order parameters in biomembranes: Calculation of c-c bond order parameters from c-d quadrupolar splitting. *Biophys. J.*, 68:1727–1739, 1995.
- [35] S. L. Duncan and R.G. Larson. Comparing experimental and simulated pressure-area isotherms for dppc. *Biophys. J.*, 94:2965–2986, 2008.
- [36] B. Ensing, S. O. Nielsen, P. B. Moore, and M. L. Klein. Energy conservation in adaptive hybrid atomistic/coarse-grain molecular dynamics. *J. Chem. Theory Comput.*, 3:1100–1105, 2007.

- [37] Denis A. Erilov, Rosa Bartucci, Rita Guzzi, Alexander A. Shubin, Alexander G. Maryasov, Derek Marsh, Sergei A. Dzuba, and Luigi Sportelli. Water concentration profiles in membranes measured by eesem of spin-labeled lipids. *J. Phys. Chem. B*, 109:12003–12013, 2005.
- [38] U. Essmann, T. Darden, H. Lee, L. Perera, Max L. Berkowitz, and L Pederson. A smooth particle mesh ewald method. *J. Chem. Phys.*, 103:8577–8593, 1995.
- [39] Scott E. Feller. Molecular dynamics simulations of lipid bilayers. *Curr. Opin. Colloid Interface Sci.*, 5:217–223, 2000.
- [40] Patrick J. Fleming, J. Alfredo Freites, C. Preston Moon, Douglas J. Tobias, and Karen G. Fleming. Outer membrane phospholipase a in phospholipid bilayers: A model system for concerted computational and experimental investigations of amino acid side chain partitioning into lipid bilayers. *Biochimica et Biophysica Acta (BBA) - Biomembranes*, 1818(2):126 – 134, 2012.
- [41] M. J. Frisch, G. W. Trucks, H. B. Schlegel, G. E. Scuseria, M. A. Robb, J. R. Cheeseman, J. A. Montgomery, Jr., T. Vreven, K. N. Kudin, J. C. Burant, J. M. Millam, S. S. Iyengar, J. Tomasi, V. Barone, B. Mennucci, M. Cossi, G. Scalmani, N. Rega, G. A. Petersson, H. Nakatsuji, M. Hada, M. Ehara, K. Toyota, R. Fukuda, J. Hasegawa, M. Ishida, T. Nakajima, Y. Honda, O. Kitao, H. Nakai, M. Klene, X. Li, J. E. Knox, H. P. Hratchian, J. B. Cross, V. Bakken, C. Adamo, J. Jaramillo, R. Gomperts, R. E. Stratmann, O. Yazyev, A. J. Austin, R. Cammi, C. Pomelli, J. W. Ochterski, P. Y. Ayala, K. Morokuma, G. A. Voth, P. Salvador, J. J. Dannenberg, V. G. Zakrzewski, S. Dapprich, A. D. Daniels, M. C. Strain, O. Farkas, D. K. Malick, A. D. Rabuck, K. Raghavachari, J. B. Foresman, J. V. Ortiz, Q. Cui, A. G. Baboul, S. Clifford, J. Cioslowski, B. B. Stefanov, G. Liu, A. Liashenko, P. Piskorz, I. Komaromi, R. L. Martin, D. J. Fox, T. Keith, M. A. Al-Laham, C. Y. Peng, A. Nanayakkara, M. Challacombe, P. M. W. Gill, B. Johnson, W. Chen, M. W. Wong, C. Gonzalez, and J. A. Pople. Gaussian 03, Revision D.02. Gaussian, Inc., Wallingford, CT, 2004.
- [42] S. Futaki. Oligorarginine vectors for intracellular delivery: design and cellular uptake mechanisms. *Biopolymers*, 84:241–249, 2006.
- [43] K. Gawrisch, D. Ruston, J. Zimmerberg, V. A. Parsegian, R. P. Rand, and N. Fuller. Membrane dipole potentials, hydration forces, and the ordering of water at membrane surfaces. *Biophys. J.*, 61:1213–1223, 1992.
- [44] N. Gresh, G. A. Cisneros, T. A. Darden, and J-P. Piquemal. Anisotropic, polarizable molecular mechanics studies of inter- and intramolecular interactions and ligand-macromolecule complexes. a bottom-up strategy. *J. Chem. Theory Comput.*, 3:1960–1986, 2007.

- [45] J. Gumbart and B. Roux. Determination of membrane-insertion free energies by molecular dynamics simulations. *Biophys. J.*, 102:795–801, 2012.
- [46] E. Harder, V. M. Anisimov, I. V. Vorobyov, P. E. M. Lopes, S. Y. Noskov, Jr. A. D. MacKerell, and B. Roux. Atomic level anisotropy in the electrostatic modeling of lone pairs for a polarizable force field based on the classical drude oscillator. *J. Chem. Theory. Comput.*, 2(6):1587–1597, 2006.
- [47] E. Harder, A. D. MacKerell Jr., and B. Roux. Many-body polarization effects and the membrane dipole potential. *J. Am. Chem. Soc.*, 131:2760–2761, 2009.
- [48] E. Harder and B. Roux. On the origin of the electrostatic potential difference at a liquid-vacuum interface. *J. Chem. Phys.*, 129:234706, 2008.
- [49] H. D. Herce and A. E. Garcia. Cell penetrating peptides: how do they do it? *J. Biol. Phys.*, 33:345–356, 2007.
- [50] H. D. Herce, A. E. Garcia, J. Litt, R. S. Kane, P. Martin, N. Enrique, A. Rebolledo, and V. Milesi. Arginine-rich peptides destabilize the plasma membrane, consistent with a pore formation translocation mechanism of cell-penetrating peptides. *Biohys. J.*, 97:1917–1925, 2009.
- [51] T. Hessa, S. H. White, and G. von Heijne. Membrane insertion of a potassium channel voltage sensor. *Science*, 307:1427, 2005.
- [52] C. D. Holcomb, P. Clancy, S. M. Thompson, and J. A. Zollweg. A critical study of simulations of the lennard-jones liquid-vapor interface. *Fluid Phase Equilib.*, 75:185–196, 1992.
- [53] K. Hristova and W. C. Wimley. A look at arginine in membranes. *J. Membr. Biol.*, 239:253–259, 2011.
- [54] Wigand Hübner and Henry H. Mantsch. Orientation of specifically $^{13}\text{C}=\text{o}$ labeled phosphatidylcholine multilayers from polarized attenuated total reflection ft-ir spectroscopy. *Biophys. J.*, 59:1261–1272, 1991.
- [55] G. Hummer, L. R. Pratt, and A. E. Garcia. Free energy of ionic hydration. *J. Phys. Chem.*, 100:1206–1215, 1996.
- [56] W. Humphrey, A. Dalke, and K. Schulten. Vmd - visual molecular dynamics. *J. Molec. Graphics*, 14:33–28, 1996.
- [57] W. Im, M. Feig, and III C. L. Brooks. An implicit embrane generalized born theory for the study of structure, stability , and interactions of membrane proteins. *Biophys. J.*, 85:2900–2918, 2003.
- [58] Peter Jarver and Ulo Langel. Cell-penetrating peptides: A brief introduction. *Biochimica et Biophysica Acta (BBA) - Biomembranes*, 1758(3):260 – 263, 2006.

- [59] M. O. Jensen, V. Jogini, D. W. Borhani, A. E. Leffler, R. O. Dror, and D. E. Shaw. Mechanism of voltage gating in potassium channels. *Science*, 336:229–233, 2012.
- [60] Y. Jiang, A. Lee., J. Chen, M. Cadene, B. T. Chait, and R. MacKinnon. The open pore conformation of potassium channels. *Nature*, 417:523–526, 2002.
- [61] Y. Jiang, A. Lee., J. Chen, V. Ruta, M. Cadene, B. T. Chait, and R. MacKinnon. X-ray structure of a voltage-dependent k⁺ channel. *Nature*, 423:33–41, 2003.
- [62] D. Jiao, P. A. Golubkov, T. A. Darden, and P. Ren. Calculation of protein-ligand binding free energy by using a polarizable potential. *Proc. Nat. Aca. Sci.*, 105(17):6290–6295, 2008.
- [63] D. Jiao, C. King, A. Grossfield, T. A. Darden, and P. Ren. Simulation of ca²⁺ and mg²⁺ solvation using polarizable atomic multipole potential. *J. Phys. Chem. B*, 110(37):18553–18559, 2006.
- [64] W. L. Jorgensen, J. Chandrasekhar, J. D. Madura, R. W. Impey, and M. L. Klein. Comparison of simple potential functions for simulating liquid water. *J. Chem. Phys.*, 79:926–935, 1983.
- [65] J. B. Klauda, R. M. Venable, J. A. Freites, J. W. O’Connor, D. J. Tobias, C. Mondragon-Ramirez, I. Vorobyov, Jr. MacKerell, A. D., and R. W. Pastor. Update of the charmm all-atom additive force field for lipids: Validation on six lipid types. *J. Phys. Chem. B*, 114:7830–7843, 2010.
- [66] J. B. Klauda, R. M. Venable, J. A. Freites, J. W. O’Connor, D. J. Tobias, C. Mondragon-Ramirez, I. Vorobyov, A. D. MacKerell Jr, and R. W. Pastor. Update of the CHARMM all-atom additive force field for lipids: Validation on six lipid types. *J. Phys. Chem. B*, 114:7830–7843, 2010.
- [67] S. Kumar, D. Bouzida, R. H. Swendsen, P. A. Kollman, and J. M. Rosenberg. The weighted histogram analysis method for free-energy calculations on biomolecules. I. The method. *J. Comp. Chem.*, 13:1011–1021, 1992.
- [68] I. F. W. Kuo, C. J. Mundy, B. L. Eggimann, M. J. McGrath, J. I. Siepmann, B. Chen, J. Vieceli, and D. J. Tobias. Structure and dynamics of the aqueous liquid-vapor interface: A comprehensive particle-based simulation study. *J. Phys. Chem. B*, 110:3738–3746, 2006.
- [69] N. Kučerka, J. F. Nagle, J. N. Sachs, S. E. Feller, J. Pencer, A. Jackson, and J. Katsaras. Lipid bilayer structure determined by the simultaneous analysis of neutron and x-ray scattering data. *Biophys. J.*, 95:2356–2367, 2008.
- [70] N. Kučerka, S. Tristram-Nagle, and J. F. Nagle. Closer look at structure of fully hydrated fluid phase dppc bilayers. *Biophys. J.*, 90:L83–L85, 2006.

- [71] Norbert Kučerka, Yufeng Liu, Nanjun Chu, Horia I. Petrache, Stephanie Tristram-Nagle, and John F. Nagle. Structure of fully hydrated fluid phase dmpc and dlpc lipid bilayers using x-ray scattering from oriented multilamellar arrays and from unilamellar vesicles. *Biophys. J.*, 88:2626–2637, 2005.
- [72] G. Lamoureux, E. Harder, I. V. Vorobyov, B. Roux, and A. D. MacKerell Jr. Polarizable model of water for molecular dynamics simulations of biomolecules. *Chem. Phys. Lett.*, 418:245–249, 2006.
- [73] G. Lamoureux, A. D. MacKerell Jr., and B. Roux. A simple polarizable model of water based on classical Drude oscillators. *J. Chem. Phys.*, 119:5185, 2003.
- [74] G. Lamoureux and B. Roux. Modeling induced polarization with classical Drude oscillators: Theory and molecular dynamics simulations algorithm. *J. Chem. Phys.*, 119:3025, 2003.
- [75] G. Lattig-Tunnemann, M. Prinz, D. Hoffmann, J. Behlke, C. Palm-Apergi, I. Morano, H. D. Herce, and M. C. Cardoso. Backbone rigidity and static presentation of guanidinium groups increases cellular uptake of arginine-rich cell-penetrating peptides. *Nature Commun.*, 2:453, 2011.
- [76] T. Lazaridis. Effective energy function for proteins in lipid membranes. *Proteins Struct. Funct. Genet.*, 52:176–192, 2003.
- [77] L. Li, I. Vorobyov, and T. W. Allen. Potential of mean force and pK_a profile calculation for the lipid membrane-exposed arginine side chain. *J. Phys. Chem. B*, 112:9574–9587, 2008.
- [78] L. Li, I. Vorobyov, S. Dorairaj, and T. W. Allen. Charged protein side chain movement in lipid bilayers explored with free energy simulation. *Curr. Top. Membr.*, 60:505–459, 2008.
- [79] Libo B. Li, Igor Vorobyov, and Toby W. Allen. The role of membrane thickness in charged protein-lipid interactions. *Biochimica et Biophysica Acta (BBA) - Biomembranes*, 1818(2):135 – 145, 2012.
- [80] David P. Lide, editor. *CRC Handbook of Chemistry and Physics*. CRC Press, 88 edition, 2007.
- [81] P. E. M. Lopes, G. Lamoureux, B. Roux, and Jr. A. D. MacKerell. Polarizable empirical force field for aromatic compounds based on the classical drude oscillator. *J. Phys. Chem. B*, 111(11):2873–2885, 2007.
- [82] C. F. Lopez, S. O. Nielsen, M. L. Klein, and P. B. Moore. Hydrogen bonding structure and dynamics of water at the dimyristoylphosphatidylcholine lipid bilayer surface from a molecular dynamics simulation. *J. Phys. Chem. B*, 108:6603–6610, 2004.

- [83] C. F. Lopez, S. O. Nielsen, G. Srinivas, W. F. DeGrado, and M. L. Klein. Probing membrane insertion activity of antimicrobial polymers via coarse-grain molecular dynamics. *J. Chem. Theory Comput.*, 2:649–655, 2006.
- [84] T. R. Lucas, B. A. Bauer, J. E. Davis, and S. Patel. Molecular dynamics simulation of hydrated DPPC monolayers using charge equilibration force fields. *J. Comp. Chem.*, 33:141–152, 2012.
- [85] V. Luzhkov and A. Warshel. Microscopic models for quantum mechanical calculations of chemical processes in solutions: Ld/ampac and scaas/amac calculations of solvation energies. *J. Comp. Chem.*, 13:199–213, 1992.
- [86] R. M. Lynden-Bell and J. C. Rasaiah. From hydrophobic to hydrophilic behaviour: A simulation study of solvation entropy and free energy of simple solutes. *J. Chem. Phys.*, 107:1981–1991, 1997.
- [87] G. Ma and H. C. Allen. Dppc langmuir monolayer at the air-water interface: probing the tail and head groups by vibrational sum frequency generation spectroscopy. *Langmuir*, 22:5341–5349, 2006.
- [88] J. L. MacCallum, W. F. D. Bennett, and D. P. Tieleman. Partitioning of amino acid side chains into lipid bilayers: Results from computer simulations and comparison to experiment. *J. Gen. Physiol.*, 129:371–377, 2007.
- [89] J. L. MacCallum, W. F. D. Bennett, and D. P. Tieleman. Distribution of amino acids in a lipid bilayer from computer simulations. *Biophys. J.*, 94:3393–3404, 2008.
- [90] J. L. MacCallum, W. F. D. Bennett, and D. P. Tieleman. Transfer of arginine into lipid bilayers is nonadditive. *Biophys. J.*, 101:110–117, 2011.
- [91] J. L. MacCallum and D. P. Tieleman. Computer simulation of the distribution of hexane in a lipid bilayer: spatially resolved free energy, entropy, and enthalpy profiles. *J. Am. Chem. Soc.*, 128:125–130, 2006.
- [92] Justin L. MacCallum and D. Peter Tieleman. Hydrophobicity scales: a thermodynamic looking glass into lipid protein interactions. *Trends in Biochemical Sciences*, 36(12):653 – 662, 2011.
- [93] J. Marks, J. Placone, K. Hristova, and W. C. Wimley. Spontaneous membrane-translocating peptides by orthogonal high-throughput screening. *J. Amer. Chem. Soc.*, 133:8995–9004, 2011.
- [94] S. J. Marrink, A. H. de Vries, and A. E. Mark. Coarse grained model for semi-quantitative lipid simulations. *J. Phys. Chem. B*, 108:750–760, 2004.

- [95] S. J. Marrink, S. Risselada, S. Yefimov, D. P. Tieleman, and A. H. de Vries. The martini forcefield: coarse grained model for biomolecular simulations. *J. Phys. Chem. B*, 111:7812–7824, 2007.
- [96] S. J. Marrink, R. M. Sok, and H. J. C. Berendsen. Free volume properties of a simulated lipid membrane. *J. Chem. Phys.*, 104:9090–9099, 1996.
- [97] Derek Marsh. Membrane water-penetration profiles from spin labels. *Eur. Biophys. J.*, 31:559–562, 2002.
- [98] J. C. Mathai, S. Tristram-Nagle, J. F. Nagle, and M. L. Zeidel. Structural determinants of water permeability through the lipid membrane. *J. Gen. Physiol.*, 131:69–76, 2008.
- [99] D. L. Mobley, A. E. Barber, C. J. Fennell, and K. Dill. Charge asymmetries in hydration of polar solutes. *J. Phys. Chem. B*, 112:2405–2414, 2008.
- [100] D. Mohammad-Aghaie, E. Mace, C. A. Sennoga, J. M. Seddon, and F. Bresme. Molecular dynamics simulations of liquid condensed to liquid expanded transitions in dppc monolayers. *J. Phys. Chem. B*, 114:1325–1335, 2010.
- [101] H. Mohwald. Phospholipid and phospholipid-protein monolayers at the air/water interface. *Annu. Rev. Phys. Chem.*, 41:441–476, 1990.
- [102] L. Monticelli, S. Kandasamy, X. Periole, R. Larson, D. P. Tieleman, and S. J. Marrink. The martini coarse grained force field: extension to proteins. *J. Chem. Theory Comput.*, 4:819–834, 2008.
- [103] C. P. Moon and K. G. Fleming. Side-chain hydrophobicity scale derived from transmembrane protein folding into lipid bilayers. *PNAS*, 108:10174–10177, 2011.
- [104] P. B. Moore, C. F. Lopez, and M. L. Klein. Dynamical properties of a hydrated lipid bilayer from a multianosecond molecular dynamics simulation. *Biophys. J.*, 81(5):2484–2494, 2001.
- [105] Wilfried J. Mortier, Karin Van Genechten, and Johann Gasteiger. Electronegativity equalization: Application and parametrization. *J. Am. Chem. Soc.*, 107:829–835, 1985.
- [106] Wilfried J. Mortier, Swapan K. Ghosh, and S. Shankar. Electronegativity equalization method for the calculation of atomic charges in molecules. *J. Am. Chem. Soc.*, 108:4315–4320, 1986.
- [107] Roman F. Nalewajski, Jacek Korchiwicz, and Zhongxiang Zhou. Molecular hardness and softness parameters and their use in chemistry. *Int. J. Quantum Chem.: Quantum Chemistry Symposium 22*, 22:349–366, 1988.

- [108] S. Nosé. A molecular dynamics methods for simulations in the canonical ensemble. *Mol. Phys.*, 52:255–268, 1984.
- [109] Dorte Otten, Michael F. Brown, and Klaus Beyer. Softening of membrane bilayers by detergents elucidated by deuterium nmr spectroscopy. *J. Phys. Chem. B*, 104:12119–12129, 2000.
- [110] S. A. Pandit, D. Bostick, and M. L. Berkowitz. Complexation of phosphatidylcholine lipids with cholesterol. *Biophys. J.*, 86(3):1345–1356, 2004.
- [111] Sagar A. Pandit, David Bostick, and Max L. Berkowitz. Mixed bilayer containing dipalmitoylphosphatidylcholine and dipalmitoylphosphatidylserine: Lipid complexation, ion binding, and electrostatics. *Biophys. J.*, 85:3120–3131, 2003.
- [112] Sagar A. Pandit, David Bostick, and Max L. Berkowitz. Molecular dynamics simulation of a dipalmitoylphosphatidylcholine bilayer with nacl. *Biophys. J.*, 84:3743–3750, 2003.
- [113] R. G. Parr and W. Yang. *Density-Functional Theory of Atoms and Molecules*. Oxford University Press, Oxford, 1989.
- [114] R. W. Pastor and A. D. MacKerell Jr. Development of the charmm force fields for lipids. *J. Phys. Chem. Lett.*, 2:1526–1532, 2011.
- [115] S. Patel and C. L. Brooks III. CHARMM fluctuating charge force fields for proteins: I parameterization and application to bulk organic liquid simulations. *J. Comp. Chem.*, 25:1–15, 2004.
- [116] S. Patel and C. L. Brooks III. A nonadditive methanol force field: Bulk liquid and liquid-vapor interfacial properties via molecular dynamics simulations using a fluctuating charge model. *J. Chem. Phys.*, 122:024508, 2005.
- [117] S. Patel and C. L. Brooks III. Structure, thermodynamics, and liquid-vapor equilibrium of ethanol from molecular dynamics simulations using nonadditive interactions. *J. Chem. Phys.*, 123:164502, 2005.
- [118] S. Patel and C. L. Brooks III. Revisiting the hexane-water interface via molecular dynamics simulations using nonadditive alkane-water potentials. *J. Chem. Phys.*, 124:204706, 2006.
- [119] S. Patel, J. E. Davis, and B. A. Bauer. Exploring ion permeation energetics in gramicidin a using polarizable charge equilibration force fields. *J. Am. Chem. Soc.*, 131:13890–13891, 2009.
- [120] S. Patel, A. D. MacKerell Jr., and C. L. Brooks III. CHARMM fluctuating charge force fields for proteins: II- protein/solvent properties from molecular dynamics simulations using a nonadditive electrostatic model. *J. Comp. Chem.*, 25:1504–1514, 2004.

- [121] Horia I. Petrache, Steven W. Dodd, and Michael F. Brown. Area per lipid and acyl length distributions in fluid phosphatidylcholines determined by 2h nmr spectroscopy. *Biophys. J.*, 79:3172–3192, 2000.
- [122] J-P. Piquemal, L. Perera, G. A. Cisneros, P. Ren, L. G. Pedersen, and T. A. Darden. Towards accurate solvation dynamics of divalent cations in water using the polarizable amoeba force field: From energetics to structure. *J. Chem. Phys.*, 125:054511, 2006.
- [123] J. W. Ponder, C. Wu, P. Ren, V. S. Pande, J. D. Chodera, M. J. Schnieders, I. Haque, D. L. Mobley, D. S. Lambrecht, R. A. DiStasio Jr., M. Head-Gordon, G. N. I. Clark, M. E. Johnson, and T. Head-Gordon. Current status of the amoeba polarizable force field. *J. Phys. Chem. B*, 114:2549–2564, 2010.
- [124] A. K. Rappe and W. A. Goddard. Charge equilibration for molecular dynamics simulations. *J. Phys. Chem.*, 95:3358–3363, 1991.
- [125] T. D. Rasmussen, P. Ren, J. W. Ponder, and F. Jensen. Force field modeling of conformational energies. the importance of multipole moments and intramolecular polarization. *Int. J. Quant. Chem.*, 107:1390–1395, 2006.
- [126] S. W. Rick and B. J. Berne. Dynamical fluctuating charge force fields: The aqueous solvation of amides. *J. Am. Chem. Soc.*, 118:672–679, 1996.
- [127] S. W. Rick and S. J. Stewart. *Reviews of Computational Chemistry*. John Wiley & Sons, New York, 2002.
- [128] S. W. Rick, S. J. Stuart, J. S. Bader, and B. J. Berne. Fluctuating charge force fields for aqueous solutions. *J. Mol. Liq.*, 65/66:31, 1995.
- [129] S. W. Rick, S. J. Stuart, and B. J. Berne. Dynamical fluctuating charge force fields: Application to liquid water. *J. Chem. Phys.*, 101:6141–6156, 1994.
- [130] B. Roux, H.-A. Yu, and M. Karplus. Molecular basis for born model of solvation. *J. Phys. Chem.*, 94:4684–4688, 1990.
- [131] Benoit Roux, Toby Allen, Simon Berneche, and Wonpil Im. Theoretical and computational models of ion channels. *Q. Rev. Biophys.*, 37:15–103, 2004.
- [132] R. T. Sanderson. An interpretation of bond lengths and a classification of bonds. *Science*, 114:670–672, 1951.
- [133] R. T. Sanderson. *Chemical Bonds and Bond Energy*. Academic Press, New York, 1976.
- [134] J. Schamberger and R. J. Clarke. Hydrophobic ion hydration and the magnitude of the dipole potential. *Biophys. J.*, 82:3081–3088, 2002.

- [135] Michael J. Schnieders, Nathan A. Baker, Pengyu Ren, and Jay W. Ponder. Polarizable atomic multipole solutes in a poisson-boltzmann continuum. *J. Chem. Phys.*, 126(12):124114, 2007.
- [136] E. V. Schow, J. A. Freites, P. Cheng, A. Bernsel, G. von Heijne, S. H. White, and D. J. Tobias. Arginine in membranes: the connection between molecular dynamics simulations and translocon-mediated insertion experiments. *J. Membr. Biol.*, 239:35–48, 2011.
- [137] L. D. Schuler, X. Daura, and W. F. van Gunsteren. An improved gromos96 force field for aliphatic hydrocarbons in the condensed phase. *J. Comput. Chem.*, 22(11):1205–1218, 1996.
- [138] R. Schurhammer, E. Engler, and G. Wipff. Hydrophobic ions in tip5p water and at a water-chloroform interface: The effect of sign inversion investigated by md and fep simulations. *J. Phys. Chem. B*, 105:10700–10708, 2001.
- [139] R. Schurhammer and G. Wipff. Are the hydrophobic asph4+ and bph4- ions equally solvated? a theoretical investigation in aqueous and nonaqueous solutions using different charge distributions. *J. Phys Chem. A*, 104:11159–11168, 2000.
- [140] Y. Shao, A. A. Stewart, and H. H. Girault. Determination of the half-wave potential of the species limiting the potential window. measurement of gibbs transfer energies at the water/1,2-dichloroethane interface. *J. Chem. Soc., Faraday Trans.*, 87:2593–2597, 1991.
- [141] K. Shimizu, H. Chaimovich, J. P. S. Farah, L. G. Dias, and D. L. Bostick. Calculation of the dipole moment for polypeptides using the generalized born-electronegativity equalization method: results in vacuum and continuum-dielectric solvent. *J. Phys. Chem. B*, 108:4171–4177, 2004.
- [142] M. R. Shirts and V. S. Pande. Solvation free energies of amino acid side chain analogs for common molecular mechanics water models. *J. Chem. Phys.*, 122:134508, 2005.
- [143] P. L. Silvestrelli and M. Parrinello. Structural, electronic, and bonding properties of liquid water from first principles. *J. Chem. Phys.*, 111(8):3572–3580, 1999.
- [144] P. L. Silvestrelli and M. Parrinello. Water molecule dipole in the gas and in the liquid phase. *Phys. Rev. Lett.*, 82:3308–3311, 1999.
- [145] S. W. I. Siu, R. Vacha, P. Jungwirth, and R. A. Bockmann. Molecular simulations of membranes: Physical properties from different force fields. *J. Chem. Phys.*, 128:125103, 2008.

- [146] J. M. Smaby and H. L. Brockman. Surface dipole moments of lipids at the argon-water interface: similarities among glycerol-ester-based lipids. *Biophys. J.*, 58:195–204, 1990.
- [147] P. J. Somerharju, J. A. Virtanen, K. K. Eklund, P. Vainio, and P. K. J. Kinnunen. 1-palmitoyl-2-pyrenedecanoyl glycerophospholipids as membrane probes: Evidence for regular distribution in liquid-crystalline phosphatidylcholine bilayers. *Biochemistry*, 24:2773–2781, 1985.
- [148] M. M. Sperotto and O. G. Mouritsen. Monte carlo simulation studies of lipid order parameter profiles near integral membrane proteins. *Biophys. J.*, 59:251–270, 1991.
- [149] M. Sprik. Hydrogen bonding and the static dielectric constant in liquid water. *J. Chem. Phys.*, 95:6762–6769, 1991.
- [150] G. Srinivas and M. L. Klein. Molecular dynamics simulations of self-assembly and nanotube formation by amphiphilic molecules in aqueous solution: a coarse-grain approach. *Nanotechnology*, 18:205703, 2007.
- [151] H. A. Stern and S. E. Feller. Calculation of the dielectric permittivity profile for a nonuniform system: Application to a lipid bilayer simulation. *J. Chem. Phys.*, 118:3401–3412, 2003.
- [152] S. Tanizaki and M. Feig. A generalized born formalism for heterogeneous dielectric environments: application to the implicit modeling of biological membranes. *J. Chem. Phys.*, 122:124706, 2005.
- [153] S. Tanizaki and M. Feig. Molecular dynamics simulations of large integral membrane proteins with an implicit membrane model. *J. Phys. Chem. B*, 110:548–556, 2006.
- [154] D. P. Tieleman, J. L. MacCallum, W. L. Ash, C. Kandt, Z. Xu, and L. M. Monticelli. Membrane protein simulations with a united atom lipid and all atom protein model: side chain transfer free energies and model proteins. *J. Phys. Condens. Matter*, 18:S1221–S1234, 2006.
- [155] T. P. Trouard, A. A. Nevzorov, T. M. Alam, C. Job, J. Zajicek, and M. F. Brown. Influence of cholesterol on dynamics of dimyristoylphosphatidylcholine bilayers as studied by deuterium nmr relaxation. *J. Chem. Phys.*, 110:8802–8818, 1999.
- [156] Kechuan Tu, Michael L. Klein, and Douglas J. Tobias. Constant-pressure molecular dynamics investigation of cholesterol effects in a dipalmitoylphosphatidylcholine bilayer. *Biophys. J.*, 75:2147–2156, 1998.

- [157] R. Vacha, P. Jurkiewicz, M. Petrov, M. L. Berkowitz, R. Bockmann, J. Barucha-Kraszewska, M. Hof, and P. Jungwirth. Mechanism of interaction of monovalent ions with phosphatidylcholine lipid membranes. *J. Phys. Chem. B*, 114:9504–9509, 2010.
- [158] Eric Vives, Julien Schmidt, and Andre Pelegrin. Cell-penetrating and cell-targeting peptides in drug delivery. *Biochimica et Biophysica Acta (BBA) - Reviews on Cancer*, 1786(2):126 – 138, 2008.
- [159] I. Vorobyov and T. W. Allen. The electrostatics of solvent and membrane interfaces and the role of electronic polarizability. *J. Chem. Phys.*, 132:185101, 2010.
- [160] I. Vorobyov, B. Bekker, and T. W. Allen. Electrostatics of deformable lipid membranes. *Biophys. J.*, 98:2904–2913, 2010.
- [161] I. Vorobyov, L. Li, and T. W. Allen. Assessing atomistic and coarse-grained force fields for protein-lipid interactions: the formidable challenge of an ionizable side chain in a membrane. *J. Phys. Chem. B*, 112:9588–9602, 2008.
- [162] I. V. Vorobyov, V. M. Anisimov, and Jr. MacKerell, A. D. Polarizable empirical force field for alkanes based on the classical drude oscillator model. *J. Phys. Chem B*, 109:18988–18999, 2005.
- [163] L. Wang, P. S. Bose, and F. J. Sigworth. Using cryo-em to measure the dipole potential of a lipid membrane. *PNAS*, 103:18528–18533, 2006.
- [164] G. L. Warren, J. E. Davis, and S. Patel. Origin and control of superlinear polarizability scaling in chemical potential equilization methods. *J. Chem. Phys.*, 128:144110, 2008.
- [165] G. L. Warren and S. Patel. Hydration free energies of monovalent ions in transferable intermolecular potential four point fluctuating charge water: An assessment of simulation methodology and force field performance and transferability. *J. Chem. Phys.*, 127:064509, 2007.
- [166] K. Watanabe and M. L. Klein. Effective pair potentials and the properties of water. *Chem. Phys.*, 131:157–167, 1989.
- [167] W. C. Wimley and K. Hristova. Antimicrobial peptides: Successes, challenges, and unanswered questions. *J. Membr. Biol.*, 239:27–34, 2011.
- [168] Z. Xu, H. H. Luo, and D. P. Tieleman. Modifying the opls-aa force field to improve hydration free energies for several amino acid side chains using new atomic charge and an off-plane charge model for aromatic residues. *J. Comput. Chem.*, 28:689–697, 2007.

- [169] Y. Yang, K. M. Mayer, N. S. Wickremasinghe, and J. H. Hafner. Probing the lipid membrane dipole potential by atomic force microscopy. *Biophys. J.*, 95:5193–5199, 2008.
- [170] J. Yoo and Q. Cui. Does arginine remain protonated in the lipid membrane? insights from microscopic pka calculations. *Biophys. J.*, 94:L61–L63, 2008.
- [171] H. Yu, T. W. Whitfield, E. Harder, G. Lamoureux, I. Vorobyov, V. M. Anisimov, A. D. MacKerell Jr., and B. Roux. Simulating monovalent and divalent ions in aqueous solution using a Drude polarizable force field. *J. Chem. Theory Comput.*, 6:774–786, 2010.
- [172] W. Zhang, Mikhail Bogdanov, J. Pi, A. J. Pittard, and William Dowhan. Reversible topological organization within a polytopic membrane protein is governed by a change in membrane phospholipid composition. *J. Biol. Chem.*, 278:50128–50135, 2003.
- [173] Y. Zhong, B. A. Bauer, and S. Patel. Solvation properties of *n*-acetyl- β -glucosamine: A molecular dynamics study incorporating electrostatic polarization. *J. Comp. Chem.*, 32:3339–3353, 2011.
- [174] Y. Zhong and S. Patel. Nonadditive empirical force fields for short-chain linear alcohols: methanol to butanol. Hydration free energies and Kirkwood-Buff analysis using charge equilibration models. *J. Phys. Chem. B*, 114:11076–11092, 2010.

Appendix A

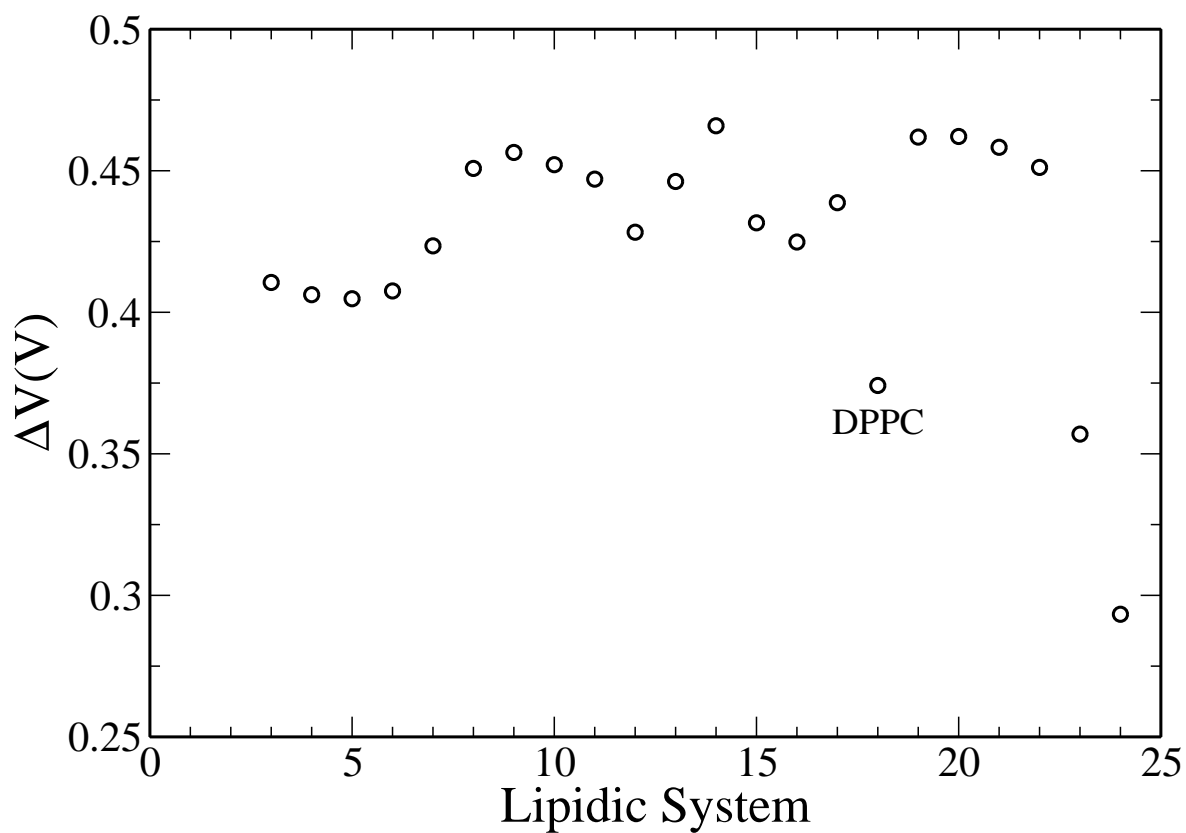


Figure A.1: Experimentally determined surface potential shifts for various phosphocholine lipid monolayer systems at the argon-water interface, as reported by Smaby and Brockman [Smaby, J. M.; Brockman, H. L. *Biophys. J.* **1990**, *58*, 195 - 204.] The lipidic system number designation corresponds to the row in which the lipid is presented in Table 1 of Smaby and Brockman with the experimentally comparable DPPC system explicitly labeled.

Appendix B

B.1 Lipid Force Field Reparameterization

The current charge equilibration (CHEQ) force field for phosphatidylcholine (PC) lipid bilayers predicts non-zero surface tension resulting in area per lipid values that are artificially low and the system contracts when run in the constant particle, pressure, and temperature (NPT) ensemble. In order to alleviate this contraction and improve the force field’s agreement with experimental area per lipid values, the interactions between lipid headgroups analogs are adjusted to better match the *ab initio* quantum mechanical gas-phase interaction energy and geometry. Small molecule analogs, dimethyl phosphate (DMP) and tetramethyl ammonium (TMA), were optimized at the MP2/6-31++g(2d,p) level and then interaction energy calculations were run at the same level with counterpoise correction. The force field interactions were modified by adjusting the specific non-bond (Lennard-Jones) interaction between the O2L oxygens atoms of dimethyl phosphate and the CTL carbon atoms of tetramethyl ammonium. Various sets of modified parameters were tested and the interaction energy was measured as:

$$E_{\text{interaction}} = E_{\text{dimer},ab} - (E_{\text{monomer},a} + E_{\text{monomer},b}) \quad (\text{B.1})$$

A summary of the modified parameters, corresponding geometry, and interaction energies, as well as the *ab initio* quantum mechanical values are shown in Table B.1.

As a test of the stability of the modified force field we have run a series of pure DPPC bilayer simulations in the NPT ensemble. The lipid-water interface systems are composed of 72 DPPC molecules (36 lipids per leaflet) hydrated with 2511 TIP4P-FQ water molecules and were run at a constant temperature and pressure of 323 K and 1

Model	ϵ (kcal/mol)	R_{min} (Å)	R_{P-N} (Å)	E_{int} (kcal/mol)
MP2/6-31++g(2d,p)	-	-	4.17	-95.4934
FQ	-0.114	3.78	4.028	-102.3194
1	-0.114	4.8	4.2046	-97.2246
2	-0.114	4.75	4.1849	-97.7777
3	-0.114	4.7	4.168	-98.2965
4	-0.114	4.6	4.1387	-99.2225

Table B.1: Non-bonded (Lennard-Jones) parameters, geometric separation, and interaction energy between lipid head group analogs DMP and TMA. R_{P-N} denotes the geometric separation between the two molecules measured as the distance between the phosphorus of DMP and the nitrogen of TMA. The first generation CHEQ force field parameters and interaction energy are labeled as FQ.

atm, respectively. The volume of the system was allowed to fluctuate with a tetragonal box geometry in which the fluctuation of the x and y -dimensions are coupled while the z -dimension fluctuates independently. In order to rate the quality of the force field in the NPT ensemble we monitor the area per lipid for each system over the course of the simulations with the results shown in Figure B.1. We find that that the modification with the weakest interaction energy (Model 1 in Table B.1) yields an area per lipid value that is consistent with the experimental value. However, early simulation results showed Model 3 as having the most stable area per lipid so these parameters were used in the mguanH⁺/bilayer simulations in the main and supporting texts. The various mguanH⁺/bilayer simulations were run in the $NPAT$ ensemble so the difference between the modified parameters sets, while still offering an improvement over the original unmodified force field, should be minimal.

Continuing the refinement of the deuterium order parameters (S_{CD}), we revised select torsional energy profiles as has been successfully implemented in the development of the CHARMM C36 lipid force field[66]. Using model compounds to mimic the relative torsions, we fit dihedral parameters for the CHARMM torsional function to *ab initio* values, as has been described previously[29, 28, 26]. The results of these fittings

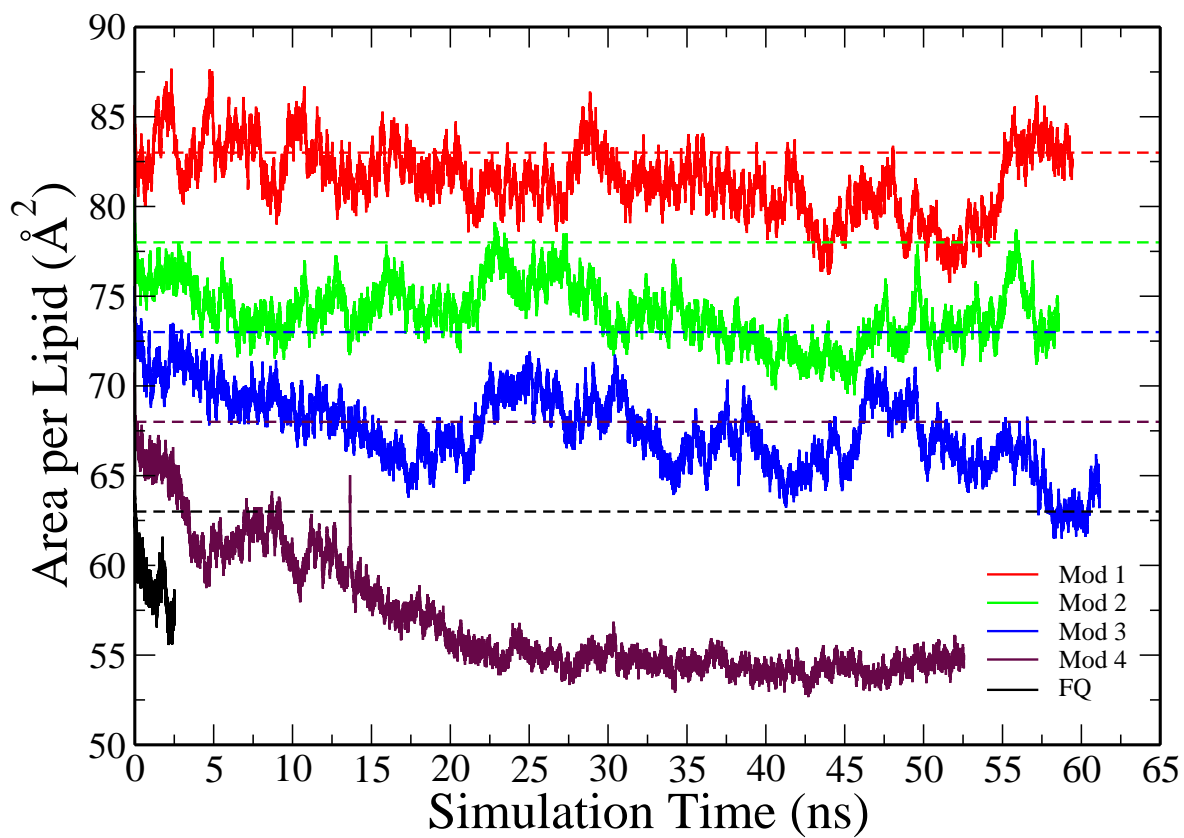


Figure B.1: Area per lipid as a function of simulation time for different parameter set modifications as well as the unmodified first generation (FQ) force field. The profiles are offset by 5 \AA^2 for clarity with the horizontal dashed lines corresponding to the experimental area per lipid value of 63 \AA^2 [69].

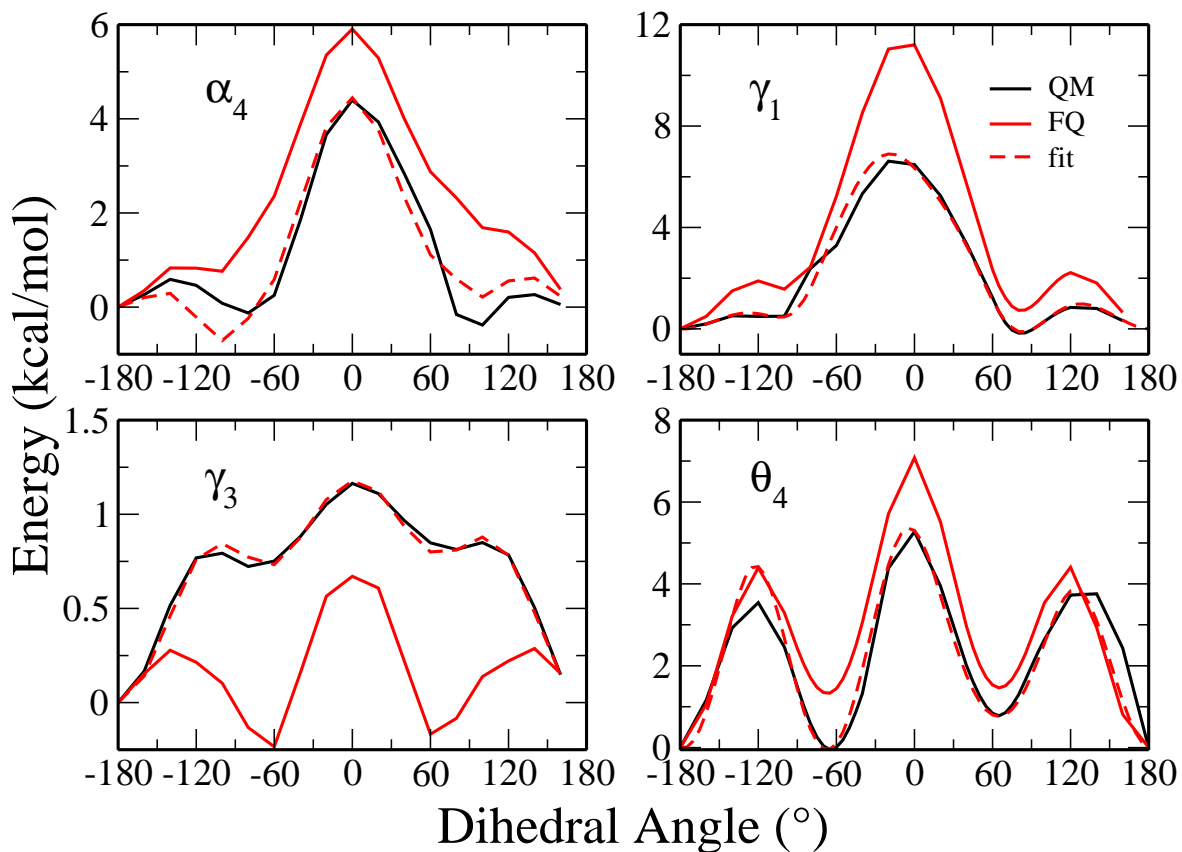


Figure B.2: Dihedral profiles based on model compounds propylmethylphosphate (PMP) and an esterified glycerol analog ((M)EGLY) and fit to ab initio data used in the most recent parameterization of the CHARMM nonpolarizable lipid force field[66].

are shown in Figure B.2. We note that only the α_4 , γ_1 , and γ_3 dihedral profiles were used for the force field reparameterization.

B.2 Unrestrained Methyl Guanidinium

In order to further validate the potential of mean force profiles we ran an additional simulation using the same bilayer-water interfacial system (1 M KCl Salt system) as in the main text but in which methyl guanidinium was not restrained to any distance from the lipid center of mass. Instead it was placed in the bulk and allowed to move freely throughout the system. We measure the z -component of the difference in the centers of mass of the free methyl guanidinium and the lipid in order to gauge where in the system mguanH^+ preferentially resides over the course of the simulation. Results of this analysis are shown in Figure B.3. We find that after a few nanoseconds methyl guanidinium travels out of the bulk solvent and moves into the bilayer. Initially mguanH^+ penetrates quite deeply into the membrane (around -15 \AA from the membrane center), past the head groups and into the carbonyl region, eventually migrating back toward the interface head group region of the lipid (-20 to -23 \AA from the membrane center), consistent with the potential of mean force calculations which show a global minimum around -22.5 \AA . The methyl guanidinium begins to move back further into the bilayer, near the carbonyl region, at a position in which the potential of mean force calculations predict a barrier of about 2.5 kcal/mol relative to the global minimum.

B.3 Lipid Structure

To test whether the lipid structure is dependent on the ion concentration of the system, we compare number density profiles of the Salt and No Salt systems at mguanH^+ -lipid center of mass separations of $z = -35 \text{ \AA}$ (bulk) and 0 \AA (membrane center) with results shown in Figure B.4. We find that the lipid structures are consistent between the two systems, with no large differences resulting from the presence or absence of ions.

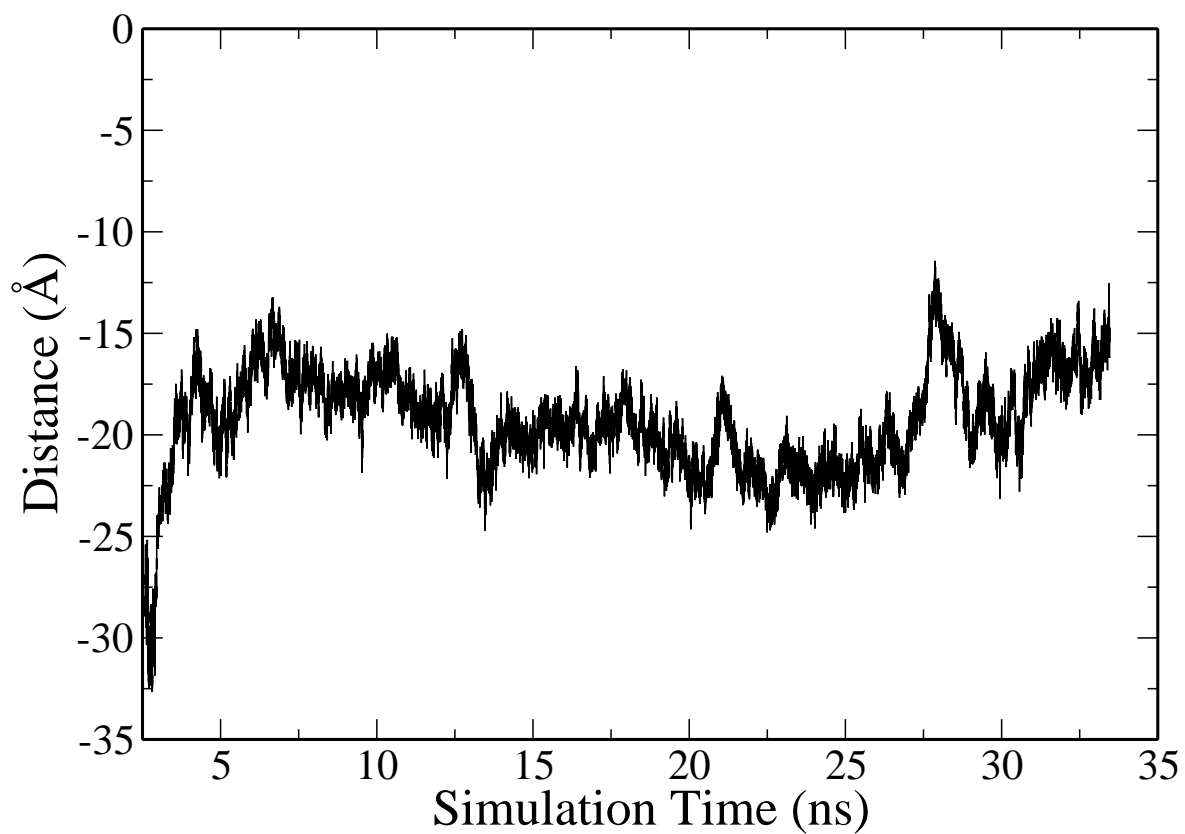


Figure B.3: Distance between the centers of mass of an unrestrained methyl guanidinium and the lipid membrane as a function of simulation time. The first 2.5 ns of simulation are not shown due to methyl guanidinium crossing the periodic boundary conditions and appearing in the bulk solution on either side of the membrane.

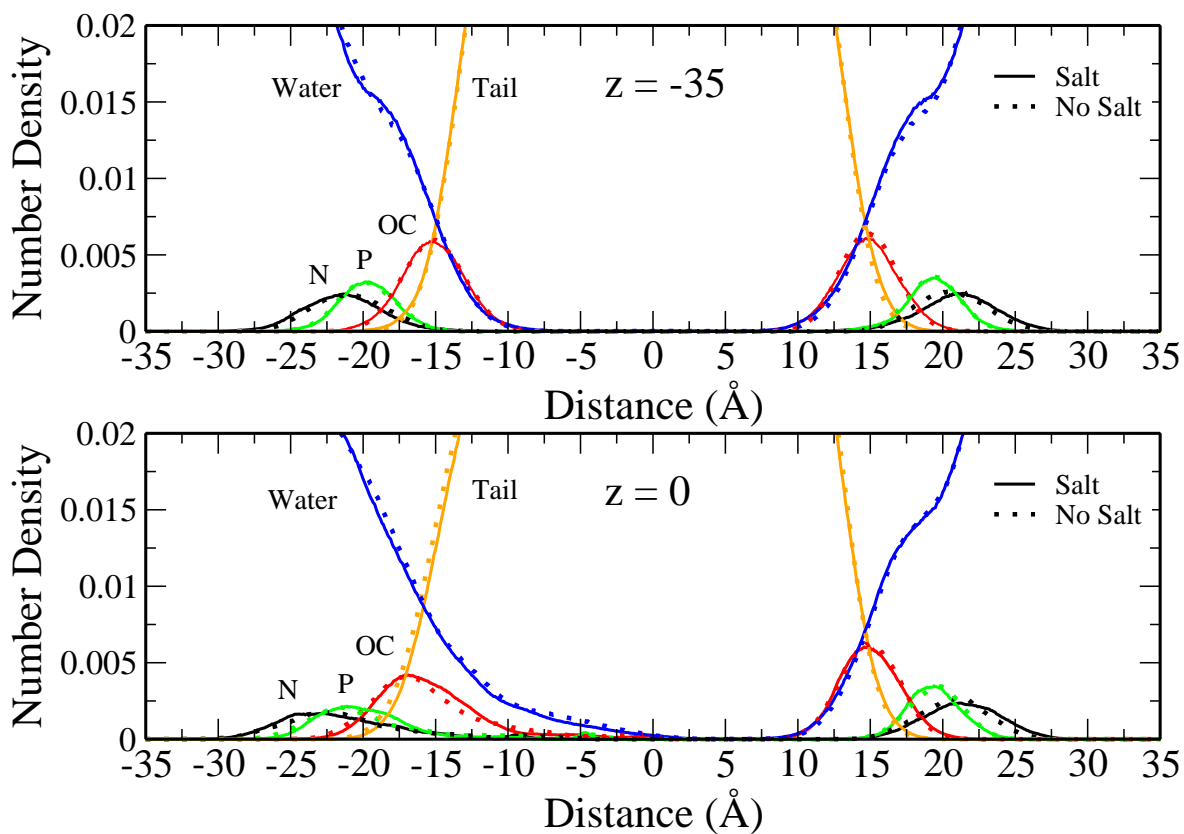


Figure B.4: Heavy atom number density profiles for select species (water oxygen, lipid head group phosphorus and nitrogen, carbonyl oxygens, and aliphatic tail carbons) in the Salt (solid curves) and No Salt (dotted curves) systems at mguanH⁺-lipid center of mass separations of -35 Å (top) and 0 Å (bottom).

B.4 Chloride Ion Position and Forces

In order to demonstrate that the force from the chloride ion on mguanH^+ in the No Salt is destabilizing, we measure the z -component of force from chloride as a function of the z -position of the chloride ion. A correction is included to account for the force of mguanH^+ on itself. Results are shown in Figure B.5 for several mguanH^+ -lipid center of mass separations. We find that when mguanH^+ is asymmetrically positioned on the negative side of the bilayer, in the bulk and as it permeates the membrane, the force from the chloride ion at z -positions that are more negative than that of mguanH^+ or are on the positive side of the bilayer will be destabilizing (force will be in the negative z -direction) and serve to “pull” mguanH^+ out of the membrane. The only stabilizing force (directed in the positive z -direction) arises when the chloride ion is between mguanH^+ and the membrane, “pulling” it towards the bilayer. When mguanH^+ is at the center of the membrane ($z = 0$) we find that the force from chloride on the negative side of the bilayer is destabilizing while the force from chloride on the positive side are stabilizing, except for a small number of positions near the edge of the simulation cell in which the force is destabilizing.

B.5 Asymmetric Water Solvation: Forces and Densities

We consider the effects of water molecules in close proximity to mguanH^+ (all water atoms within 10 Å of the center of mass of mguanH^+) by calculating the average z -component of the force from the local water molecules acting on mguanH^+ as a function of the water molecule position, as described in the main text section entitled Asymmetric Water Solvation. The results of the position-dependent force from local water molecules is shown in Figure B.6 for the Salt system and Figure B.7 for the No Salt system for several mguanH^+ -lipid center of mass separations. We also consider the density of water local to mguanH^+ (relative to the total number of water molecules sampled surrounding mguanH^+) with results shown in Figure B.8 for the Salt system and Figure B.9 for the No Salt system.

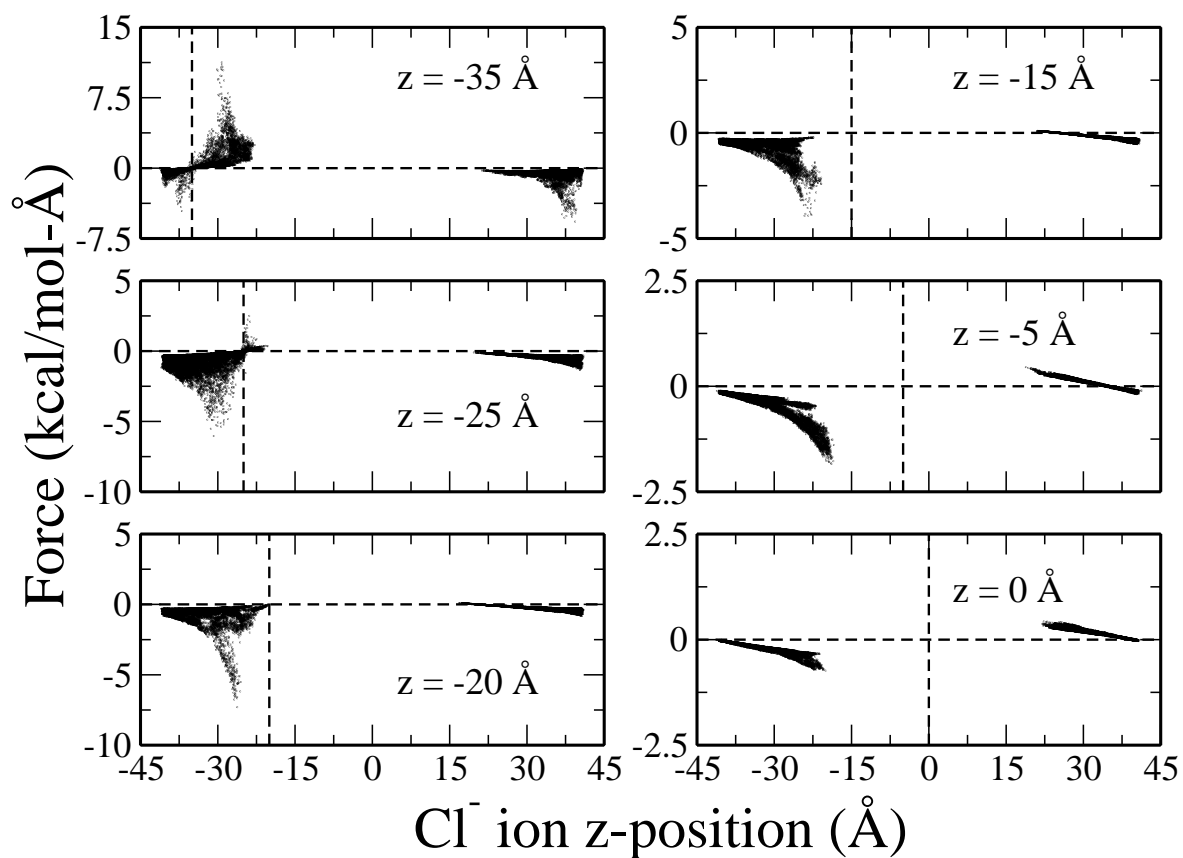


Figure B.5: Force (in the z -direction) of the chloride ion on methyl guanidinium for the No Salt system as a function of the z -position of the chloride ion. Results are shown for several PMF windows in which the mguanH⁺-lipid center of mass difference is -35, -25, -20, -15, -5, and 0 \AA . The vertical dashed line signifies the constrained position of mguanH⁺ in the membrane system while the horizontal dashed line represents a force value of 0.

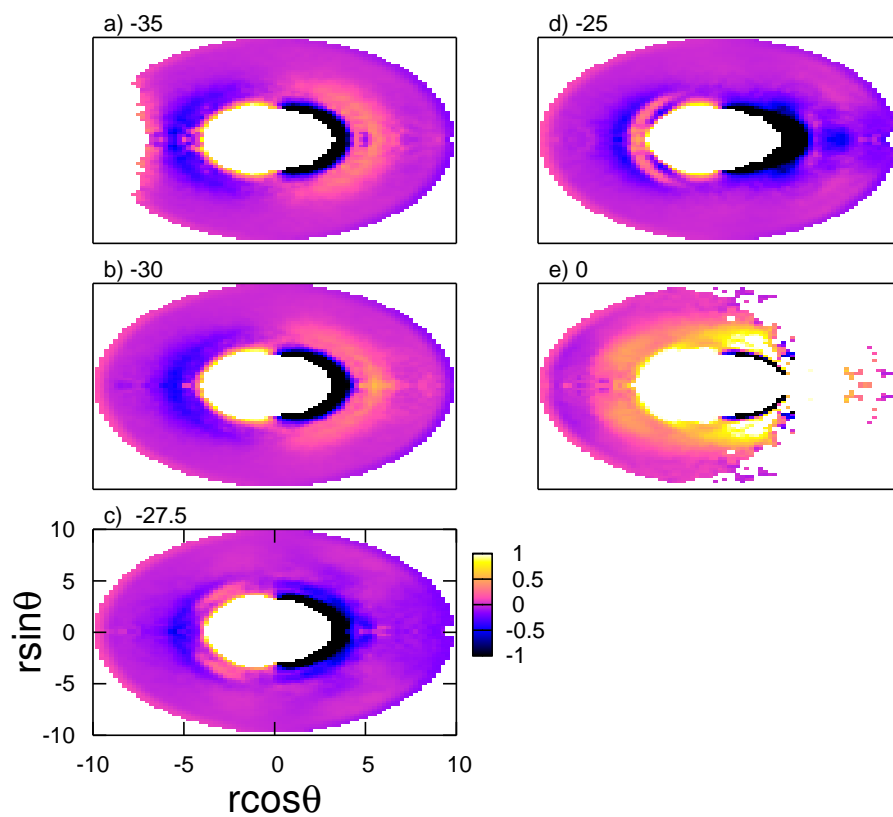


Figure B.6: Force in the z -direction from individual local water molecules (all atoms within 10 \AA of the center of mass of mguanH^+) acting on methyl guanidinium for the Salt system. Forces are calculated for mguanH^+ -lipid center of mass separations of a) -35 , b) -30 , c) -27.5 , d) -25 , and e) 0 \AA .

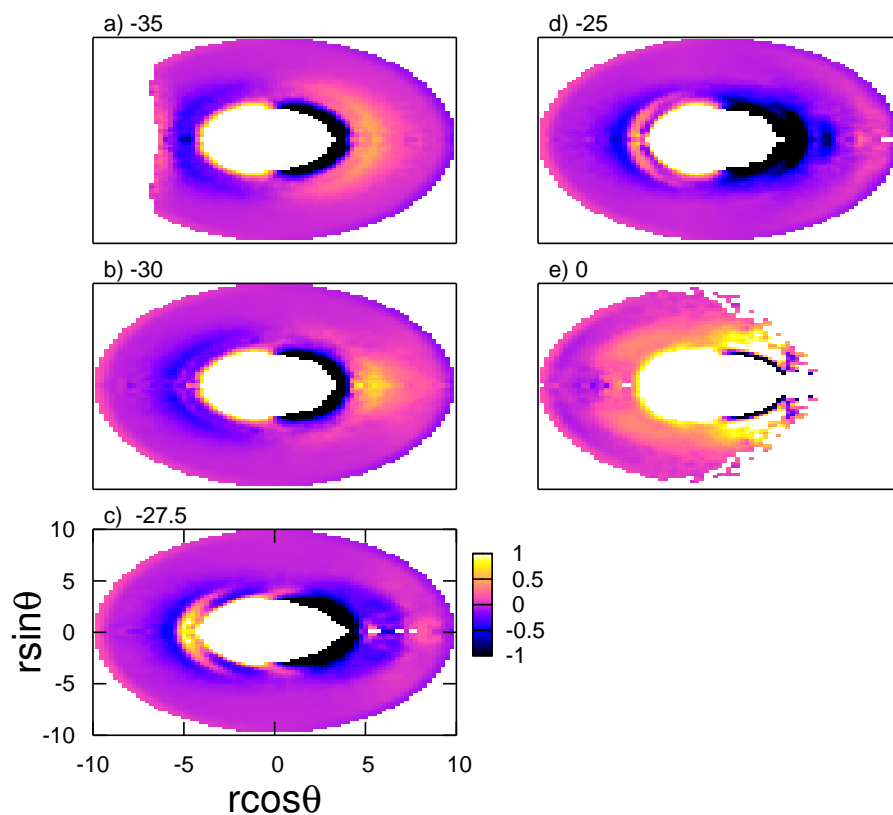


Figure B.7: Force in the z -direction from individual local water molecules (all atoms within 10 \AA of the center of mass of mguanH^+) acting on methyl guanidinium for the No Salt system. Forces are calculated for mguanH^+ -lipid center of mass separations of a) -35 , b) -30 , c) -27.5 , d) -25 , and e) 0 \AA .

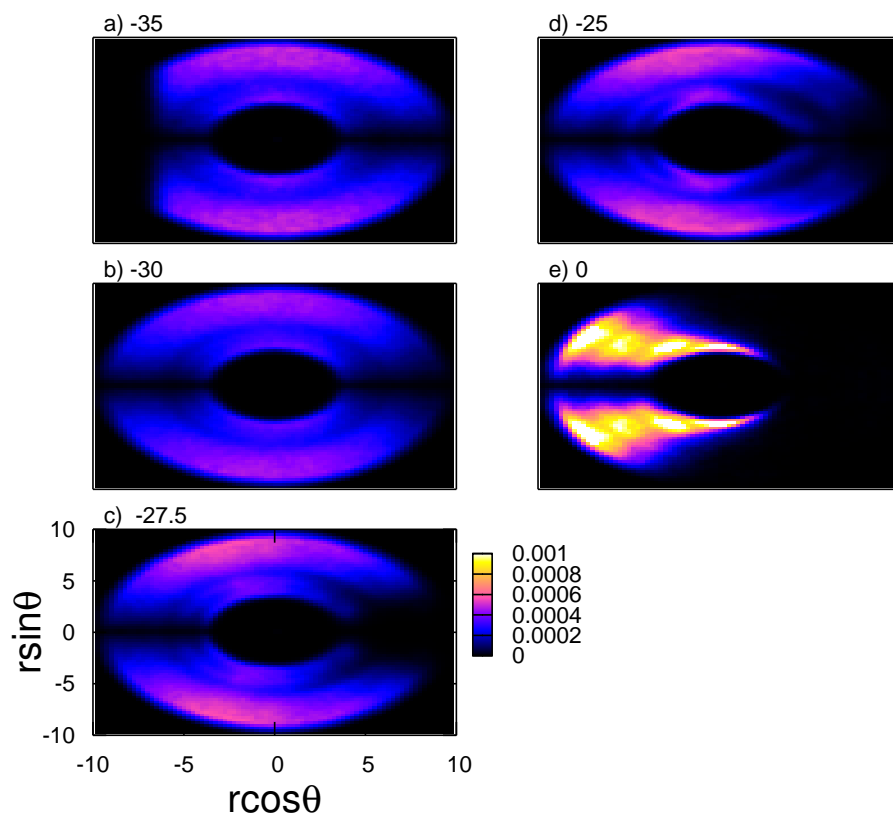


Figure B.8: Density of water molecules surrounding methyl guanidinium (all atoms within 10 Å of the center of mass of mguanH⁺) calculated for the Salt system. Densities are calculated for mguanH⁺-lipid center of mass separations of a) -35, b) -30, c) -27.5, d) -25, and e) 0 Å.

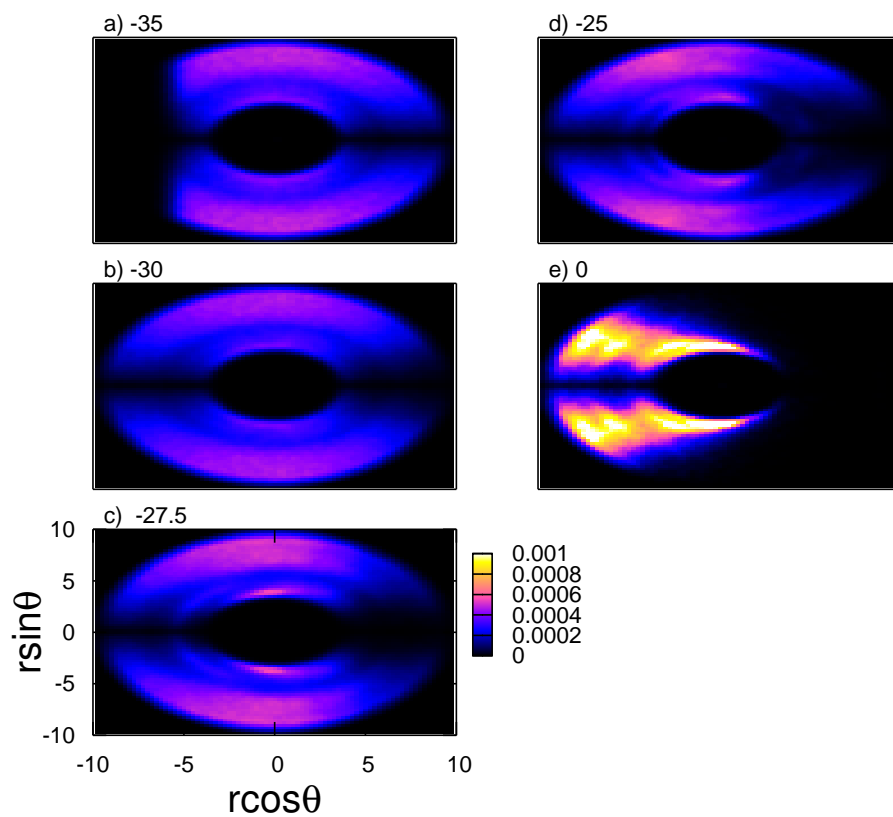


Figure B.9: Density of water molecules surrounding methyl guanidinium (all atoms within 10 Å of the center of mass of mguanH⁺) calculated for the No Salt system. Densities are calculated for mguanH⁺-lipid center of mass separations of a) -35, b) -30, c) -27.5, d) -25, and e) 0 Å.